Extreme fire weather in a changing climate: Projections for Europe based on bias-adjusted EURO-CORDEX simulations

Master's Thesis in
Meteorology and Climate Physics
by

Ali Serkan Bayar

July 2025

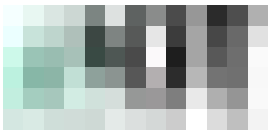

INSTITUTE OF METEOROLOGY AND CLIMATE RESEARCH
KARLSRUHE INSTITUTE OF TECHNOLOGY (KIT)

Supervisor:	Prof. Dr. Joaquim Pinto
Co-supervisor:	Prof. Dr. Andreas Fink

Abstract

The climate in Europe is warming faster than the global average, raising concerns about how climate change will affect extreme weather events. Among these, extreme wildfires have become an increasing concern, with recent events underscoring their severe societal, ecological, and economic impacts (e.g., California, Portugal, Australia). This thesis aims to investigate historical and projected changes in atmospheric conditions that could trigger and sustain wildfires, referred to as fire weather, across Europe. To quantify fire weather, the Canadian Forest Fire Weather Index (FWI) is used, a widely adopted measure that integrates the effects of temperature, precipitation, relative humidity, and wind speed on fuel dryness and fire potential.

To assess changes in extreme fire weather, a large ensemble of 34 high-resolution ($\sim$12.5 km) regional climate models (RCMs) following the RCP8.5 scenario from the EURO-CORDEX initiative was used, focusing on two global warming levels (GWLs): 2 °C and 3 °C above preindustrial levels. ERA5-Land reanalysis served both as a reference dataset and as a proxy for historical observations. All input fields of the RCMs were adjusted for biases using quantile delta mapping (QDM) to reduce systematic errors prior to the calculation of the FWI. Although some residual bias remained in the resulting FWI, QDM significantly improved its accuracy. Taking this into account, a multivariate bias adjustment method (MBCn) was tested and showed further potential to improve performance, albeit with greater computational cost.

Historical trends from 1950 to 2023 reveal statistically significant increases in both the frequency and intensity of extreme fire weather in regions such as the Iberian Peninsula, Central Europe, and parts of Eastern Europe. Projections based on the bias-adjusted EURO-CORDEX ensemble indicate that future extreme fire weather will become more frequent and more intense and will expand its geographic extent across Europe under climate change. The strongest signals are projected in southern Europe, with a northward expansion of fire-prone conditions under higher warming levels. At 3 °C GWL, the spatial extent of the robust change signal in extreme fire weather metrics nearly doubles compared to 2 °C GWL. These increases strongly coincide with an increase in the vapor pressure deficit, suggesting that thermodynamic processes play a key role through atmospheric drying.

Additionally to weather and climate factors investigated in this study, fire activity also depends on other critical factors, such as vegetation availability, ignition sources, land use, and forest management practices. Nevertheless, the projected intensification of extreme fire weather conditions highlights the growing need for coordinated climate action, along with proactive mitigation strategies that integrate climate adaptation with landscape and fire management across Europe.

Zusammenfassung

Das Klima in Europa erwärmt sich schneller als der globale Durchschnitt, was Besorgnis darüber auslöst, wie sich der Klimawandel auf extreme Wetterereignisse auswirken wird. Besonders extreme Waldbrände rücken zunehmend in den Fokus, da jüngste Ereignisse ihre gravierenden gesellschaftlichen, ökologischen und wirtschaftlichen Folgen verdeutlichen (z.B. in Kalifornien, Portugal, Australien). Ziel dieser Arbeit ist es, historische und projizierte Veränderungen atmosphärischer Bedingungen zu untersuchen, die sogenannte Feuerwetterlagen auslösen und begünstigen können. Zur Quantifizierung dieser Feuerwetterlagen wird der kanadische Fire Weather Index (FWI) verwendet – ein weit etablierter Index, der Temperatur, Niederschlag, relative Luftfeuchtigkeit und Windgeschwindigkeit kombiniert, um die Trockenheit des Brennmaterials und das Brandpotenzial zu erfassen.

Zur Analyse von Veränderungen extremen Feuerwetters wurde ein großes Ensemble von 34 hochauflösenden regionalen Klimamodellen ($\sim$12,5 km) aus der EURO-CORDEX-Initiative verwendet, die dem RCP8.5-Szenario folgen. Im Fokus standen zwei globale Erwärmungsniveaus (GWLs): 2 °C und 3 °C über relativ zum vorindustriellen Zeitraum. Die ERA5-Land-Reanalyse diente sowohl als Referenzdatensatz als auch als Ersatz für historische Beobachtungen. Alle Eingangsdaten der Klimamodelle wurden vor der Berechnung des FWI mittels Quantile Delta Mapping (QDM) bias-korrigiert, um systematische Fehler zu reduzieren. Obwohl einige systematischen Fehler im berechneten FWI bestehen blieben, konnte die Genauigkeit durch QDM deutlich verbessert werden. In diesem Zusammenhang wurde zusätzlich eine multivariate Bias-Korrekturmethode (MBCn) getestet, die weiteres Verbesserungspotenzial zeigte, jedoch mit einem höheren Rechenaufwand verbunden ist.

Historische Trends von 1950 bis 2023 zeigen statistisch signifikante Zunahmen sowohl in der Häufigkeit als auch in der Intensität von extremem Feuerwetter in Regionen wie der Iberischen Halbinsel, Mitteleuropa und Teilen Osteuropas. Projektionen auf Basis des bias-korrigierten EURO-CORDEX-Ensembles deuten darauf hin, dass extremes Feuerwetter unter zunehmender Erwärmung häufiger, intensiver und räumlich weiter verbreitet auftreten wird. Die stärksten Signale werden für Südeuropa prognostiziert, mit einer nordwärts gerichteten Ausdehnung feuergefährdeter Bedingungen bei höheren Erwärmungsniveaus. Bei einem GWL von 3 °C verdoppelt sich nahezu die räumliche Ausdehnung robuster Veränderungssignale in den Feuerwettermetriken im Vergleich zu 2 °C. Diese Zunahmen gehen stark mit einem erhöhten Dampfdruckdefizit einher, was auf die zentrale Rolle thermodynamischer Prozesse in Form atmosphärischer Austrocknung hinweist.

Zusätzlich zu den in dieser Studie untersuchten Wetter- und Klimafaktoren hängen Feueraktivitäten auch von anderen entscheidenden Faktoren ab, wie der Verfügbarkeit von Vegetation, Zündquellen, Landnutzung und Forstwirtschaft. Dennoch unterstreicht die gezeigte Intensivierung extremer Feuerwetterbedingungen die wachsende Notwendigkeit koordinierter Klimamaßnahmen sowie proaktiver Strategien zur Risikominderung, die Klimaanpassung mit Landschafts- und Feuerbewirtschaftung in Europa integrieren.

Preface

ChatGPT (https://chatgpt.com/) was used as a tool to correct grammatical errors and improve language clarity. It was also used for translating the German abstract. Initial spell checking was performed using Writefull (https://www.writefull.com/).

Special thanks to German Climate Computing Centre (DKRZ) for providing computing and storage resources.

Contents

1 Introduction

Wildfires have been part of Earth's history since the emergence of terrestrial plants more than 400 million years ago (Scott and Glasspool, 2006; Bowman et al., 2009). They are an essential component of the Earth system, shaping the evolution and distribution of plant and animal life, as well as influencing key biogeochemical processes (He et al., 2019; Bowman et al., 2020b). In fact, a large proportion of tropical grasslands would have been replaced by forests in a world without fire (Bond et al., 2005). Fires burn approximately 4 million km^2 area each year (Chuvieco et al., 2018) and have significant direct and indirect impacts on both global and regional climate through the emission of greenhouse gases and aerosols. For example, global mean carbon emissions from fires were estimated at 2.2 Pg of C $year^{-1}$ during the period 1997-2016 (van der Werf et al., 2017), which corresponds to roughly 21.6% of global CO_2 emissions from fossil fuels in 2024 (Bowman et al., 2020b; Friedlingstein et al., 2025). Fire-induced forest loss (e.g., in Amazonia) can also alter Earth's surface radiative budget by affecting evapotranspiration and surface albedo through land cover change (Liu et al., 2019). Additionally, intense heating from extreme fires can inject smoke aerosols into the lower stratosphere in quantities comparable to those produced by a moderate volcanic eruption, leading to short-term reductions in stratospheric temperatures (Peterson et al., 2018; Damany-Pearce et al., 2022).

Contrary to common perception, satellite-derived data show a nearly 25% decrease in global burned area between 1998 and 2015 (Andela et al., 2017), This decline is primarily concentrated in tropical savannas and grasslands and is largely attributed to agricultural expansion and changes in land cover (Andela et al., 2017). However, despite this decrease in global burned area, global fire emissions have remained relatively stable (Zheng et al., 2021), which is explained by an increase in forest fire emissions across North America and Eurasia where fires release more CO_2 per unit area burned (Zheng et al., 2021; Jones et al., 2024). Therefore, focusing solely on trends in global burned area can obscure important regional differences and changes in extreme events.

Extreme wildfires not only impact global and regional climate, but can also cause severe damage to ecosystems and result in significant socioeconomic consequences. Prominent examples from recent years, such as the Australian Black Summer in 2019-2020 (Filkov et al., 2020), the Canadian wildfires in 2023 (Jain et al., 2024), the Hawaii wildfires in 2023 (Marris, 2023), and the 2017 fire season in Portugal (Ramos et al., 2023) highlight the devastating effects fires can have on wildlife, human life, and the economy. For instance, the 2017 fire season in Portugal burned approximately 540,000 hectares, resulted in 114 fatalities, and led to insurance payouts nearing 300 million USD (Ramos et al., 2023). Wildfires may also occur outside of the typical fire season, such as the January 2025 Los Angeles fires, which caused at least 30 fatalities, destroyed more than 16,000 structures,

and incurred an estimated economic loss that could exceed 250 billion USD (Qiu et al., 2025). Wildfires are also associated with serious public health impacts; exposure to fire smoke is estimated to contribute to over 300,000 premature deaths globally each year (Johnston et al., 2012). Despite the global decline in burned area, the frequency and magnitude of these types of energetically extreme wildfires more than doubled between 2003 and 2023 (Cunningham et al., 2024), with a significant proportion of these events occurring under extreme fire weather conditions (Bowman et al., 2017).

Fire weather refers to atmospheric conditions that are conducive to triggering and propagating wildfires (Masson-Delmotte et al., 2021). It typically involves a combination of hot, dry and windy conditions, specifically high temperatures, low relative humidity, low precipitation totals, and strong winds. Numerous fire weather indices based on daily surface weather variables have been developed and applied across different regions (Jolly et al., 2015; Jones et al., 2022). These indices reflect the compound effects of atmospheric conditions on fuel moisture, vegetation stress (or flammability), and potential fire spread and they are strongly correlated with the magnitude and extent of wildfires, particularly in ecosystems with intermediate moisture availability (Carvalho et al., 2008; Jolly et al., 2015; Bedia et al., 2015; Abatzoglou et al., 2018; Jones et al., 2022).

Global surface temperatures have risen by approximately 1.1 °C since the preindustrial period (Masson-Delmotte et al., 2021). It is well established that climate change increases the frequency and intensity of certain weather and climate extremes (Masson-Delmotte et al., 2021; Capua and Rahmstorf, 2023). Over the past century, the occurrence of concurrent heatwaves and droughts has become more frequent, increasing the likelihood of extreme fire weather conditions, particularly in regions such as southern Europe, the United States, and Australia (Masson-Delmotte et al., 2021). Despite a global decline in burned area (Andela et al., 2017), 25.3% of the Earth's vegetated surface experienced a lengthening of the fire weather season length between 1979 and 2013, corresponding to an 18.7% increase in the global mean fire season length (Jolly et al., 2015). Using ERA5 reanalysis, Jones et al. (2022) found that between 1979 and 2013, the global annual fire weather season length increased by an average of 14 days (27%), while the frequency of annual extreme fire weather days rose by 10 days (54%). Climate change has also been shown to increase the likelihood of extreme fire weather conditions by at least a factor of four in 40% of the world's fire-prone regions between 1961 and 2018 (Liu et al., 2022). Under continued global warming, both the frequency and intensity of extreme fire weather are projected to increase further worldwide, according to climate model projections (Masson-Delmotte et al., 2021; Bowman et al., 2017; Abatzoglou et al., 2019; Jones et al., 2022).

Europe has warmed at twice the global average rate since the 1980s (Copernicus Climate Change Service (C3S), 2025), and approximately 70-90% of the continent's land area is projected to shift into different climate zones by the end of the century under high-emission scenario simulations (Bayar et al., 2023). This shift is primarily toward warmer summer climates across Europe, with a notable tendency toward warmer and drier conditions in southern and western regions (Bayar et al., 2023). Continued warming is also expected to increase the frequency and intensity of various extreme events, including heat extremes across the continent, floods in central and western Europe, drought in the Mediterranean, and compound hot and dry events (Masson-Delmotte et al.,

2021). Extreme fire weather is likewise projected to increase across much of Europe (Abatzoglou et al., 2019; Jones et al., 2022), with particularly pronounced changes in the Mediterranean region (Fargeon et al., 2020; Ruffault et al., 2020). In addition, growing concern surrounds the impacts of climate change on extreme fire weather in central Europe (Mozny et al., 2021; Carnicer et al., 2022; Miller et al., 2024).

Recently, two pan-European scale studies have been published (El Garroussi et al., 2024; Hetzer et al., 2024), and both projected widespread increases in extreme fire weather. Both studies relied on global climate models from the Coupled Model Intercomparison Project (CMIP) Phase 6 and applied statistical downscaling techniques to reach the desired resolution ($\sim$31 km in El Garroussi et al. (2024) and $\sim$9 km in Hetzer et al. (2024)). However, since statistically downscaled fields still inherit the climate change signal from driving global models and do not incorporate sub-GCM grid scale physical processes, they may not fully capture important regional scale phenomena, such as snow-albedo feedbacks in mountainous regions (Maraun et al., 2017), potentially leading to biased projections. To address this limitation, dynamically downscaled Regional Climate Model (RCM)s offer an alternative approach. RCMs refine the large-scale circulation response obtained from global climate models to finer scales by explicitly simulating sub-GCM grid-scale processes (Giorgi, 2019). This may result in more accurately simulated fields at regional scales, as demonstrated for extreme precipitation over complex topographical regions (Torma et al., 2015; Iles et al., 2020).

The Coordinated Regional Climate Downscaling Experiment (CORDEX) aims to coordinate dynamical downscaling efforts through a standardized set of experiments and protocols (Giorgi et al., 2009). As part of this framework, the EURO-CORDEX initiative (Jacob et al., 2014) provides RCMs by downscaling global climate models from the Fifth Phase of the Climate Model Intercomparison Project (CMIP5) (Taylor et al., 2012). In recent years, several studies have used EURO-CORDEX RCMs to assess fire weather danger projections in Europe. However, many of these studies relied on relatively small ensemble sizes (e.g., de Rigo et al. (2017); Galizia et al. (2023)), and were often limited to specific regions, such as Greece (Rovithakis et al., 2022), France (Varela et al., 2019; Fargeon et al., 2020), or the Iberian Peninsula (Bento et al., 2023). Recent progress has expanded the number of simulations available within the EURO-CORDEX framework to an unprecedented level (Vautard et al., 2021). This progress now enables the use of a larger RCM ensemble to more comprehensively assess projected changes and associated uncertainties in extreme fire weather across Europe in a changing climate.

However, dynamically downscaled RCMs can also inherit biases from their driving global climate models, as they are constrained by the boundary conditions imposed on them (Giorgi, 2019). For instance, EURO-CORDEX simulations have been found to be generally too wet, too cold, and too windy (Vautard et al., 2021). Since extreme fire weather is a multivariate phenomenon driven by the combined effects of multiple climate drivers, biases in the input fields can compound and amplify the overall bias in fire weather indices. This amplification can increase uncertainty in the outcomes and reduce confidence in the associated decision-making processes. Therefore, input fields need to be adjusted for biases before being used in impact studies aimed at comprehensively evaluating extreme fire weather under climate change.

Based on these developments and the identified research gaps, such as the limited use of large RCM ensembles and the absence of bias adjustment, there is a need to assess extreme fire weather danger at a pan-European scale under the influence of climate change using a large ensemble of dynamically downscaled, high-resolution, bias-adjusted RCMs. This study employs a large multi-model RCM ensemble from the EURO-CORDEX framework (Jacob et al., 2014) at ∼12.5 km resolution, to project extreme fire weather conditions across Europe under 2 °C and 3 °C Global Warming Level (GWL)s. Fire weather is quantified using the Canadian Forest Fire Weather Index (FWI) System (Van Wagner, 1987), as it relies solely on daily meteorological input fields and has been shown to perform well in Europe, especially in the Mediterranean (Viegas et al., 1999; Carvalho et al., 2008; San-Miguel-Ayanz et al., 2012; Jones et al., 2022). Prior to calculating projected fire weather danger, model input fields are bias adjusted using two different methodologies, with ERA5-Land reanalysis data serving as the reference. ERA5-Land is also used as a proxy for historical observations to assess trends in extreme fire weather across Europe since 1950. Accordingly, this thesis aims to address the following research questions:

- What is the observed climatology of the frequency and intensity of extreme fire weather across Europe and what are the associated trends since 1950?
- To what extent do bias adjustment methods improve model performance and spatial patterns of bias in the input meteorological fields and the FWI within the EURO-CORDEX multi-model ensemble?
- How do the frequency and intensity of extreme fire weather change at 2 °C and 3 °C GWLs, based on the bias-adjusted EURO-CORDEX multi-model ensemble? What are the potential drivers underlying these changes?

The thesis is organized as follows. Chapter 2 provides the necessary theoretical background. Chapter 3 outlines the datasets and methodologies employed. Chapter 4 examines the observed climatology and historical trends in extreme fire weather across Europe. Chapter 5 evaluates the performance of the EURO-CORDEX models and assesses the impact of bias adjustment on model performance. Chapter 6 investigates projected changes in extreme fire weather under different GWLs. Finally, Chapter 7 presents the discussion and key conclusions of the thesis.

2 Background Information

This chapter provides essential background information for understanding extreme fire weather in the context of a changing climate. Section 2.1 introduces extreme weather events and their relationship to climate change. Section 2.2 presents an overview of wildfires from multiple perspectives, including historical activity and key drivers. Section 2.3 defines fire weather conditions and examines how they evolve under changing climatic conditions. Section 2.4 offers a brief introduction to global and regional climate modeling, while Section 2.5 discusses the need for bias adjustment and outlines several available methods. A comprehensive review of all aspects of extreme events in the context of climate change can be found in Chapter 11 of Masson-Delmotte et al. (2021). Bowman et al. (2020b); Pausas and Keeley (2021); Jones et al. (2022) review the current literature and discuss several aspects of wildfires and fire weather. The historical context and the foundational concepts in global and regional climate modeling are provided by Edwards (2011) and Giorgi (2019), respectively. Maraun (2016) offers an overview of some of the bias adjustment techniques and discusses related methodological issues.

2.1 Extreme Weather Events in a Changing Climate

In a broad sense, climate is a description of the state of the climate system, which comprises five major components: the atmosphere, hydrosphere, cryosphere, lithosphere and biosphere - and encompasses the interactions among them (Masson-Delmotte et al., 2021). A more specific definition describes climate as the average weather or, more precisely, the statistical representation (e.g., mean, variance) of relevant variables over a defined period of time, ranging from months to millions of years (Masson-Delmotte et al., 2021). The standard time period for such averaging is 30 years, as defined by the World Meteorological Organization (WMO) (Masson-Delmotte et al., 2021).

The state of the climate changes due to natural internal processes, external forcings, and anthropogenic influences (Masson-Delmotte et al., 2021). Climate variability may arise from internal modes of variability, such as the El Niño Southern Oscillation in the Pacific Ocean, as well as from external forcings like changes in the solar cycle. However, the influence of natural variability diminishes when studying changes in climate over multiple decades. The global surface temperature increased by approximately 1.1°C in the last decade (2011-2020) relative to the pre-industrial period 1850-1900, while the contribution of natural variability remains within a range of -0.23°C to +0.23°C (Masson-Delmotte et al., 2021). According to the latest Intergovernmental Panel on Climate Change (IPCC) Assessment Report (AR6), human influence on the warming of the atmo-

sphere, ocean and land is unequivocal (Masson-Delmotte et al., 2021). Climate model simulations consistently show that the observed warming can only be reproduced when the anthropogenic contribution is included, especially the increase in greenhouse gas concentrations (Masson-Delmotte et al., 2021). As illustrated in Figure 2.1, models that incorporate both human and natural drivers accurately capture the observed temperature trend, whereas simulations that include only natural forcings fail to do so. The dominant warming effect of increasing greenhouse gas concentrations has been partially offset by the cooling effect of aerosols (Figure 2.1).

Figure 2.1: Global surface temperature from 1850 to 2019, from the observations and simulations. Changes in observations, compared to climate model simulations of the response to all human and natural forcings (grey band), greenhouse gases only (red band), aerosols and other human drivers only (blue band) and natural forcings only (green band). Solid coloured lines show the multi-model mean, and coloured bands show the 5–95% range of individual simulations. Figure and caption are reprinted and adapted from Masson-Delmotte et al. (2021).

The evidence of anthropogenic climate change extends beyond the increase in global surface temperature. The human influence on the climate system has also been detected in various other climate variables, including changes in the average precipitation distribution within latitudinal bands (Zhang et al., 2007), winter sea-level pressure patterns (Gillett et al., 2003), reductions in sea ice extent (Stroeve et al., 2007), and shifts in storm tracks (Shaw et al., 2016). Anthropogenic climate change not only impacts the mean state of the climate, but also affects the weather and climate extremes worldwide (Masson-Delmotte et al., 2021). It is now clear that global warming is contributing to an increase in the frequency and intensity of many extreme events (Capua and Rahmstorf, 2023), including heat extremes and heatwaves (Robinson et al., 2021; Perkins-Kirkpatrick and Lewis, 2020), heavy precipitation events (Zhang et al., 2013; Fischer and Knutti, 2015), and unprecedented wildfire activity (Descals et al., 2022). This rise in extreme weather events is driven by two primary mechanisms: a shift toward a warmer and moister atmosphere, which is known as the thermodynamic effect (Figure 2.2), and changes in atmospheric circulation patterns, known as the dynamical effect (Capua and Rahmstorf, 2023).

Figure 2.2: Schematic showing the effect on extreme temperatures when the mean temperature increases, for a normal temperature distribution. Figure and caption reprinted from Solomon et al. (2007).

2.2 Wildfires

2.2.1 Wildfire as a Multidimensional Phenomena

Wildfires or vegetation fires have been part of the history of Earth since the first appearance of terrestrial plants more than 400 million years ago (Scott and Glasspool, 2006; Bowman et al., 2009). They represent a fundamental component of the Earth system and influence the evolution of the history of plants, animals, and biogeochemical processes on Earth (Bowman et al., 2020b). The occurrence and prevalence of fire throughout Earth's history appear to be closely linked to fluctuations in atmospheric oxygen levels (Bowman et al., 2009). Previous studies suggest that self-sustaining wildfires begin to occur at atmospheric oxygen concentrations of approximately 16% (Belcher et al., 2010), while at levels around 30% even moist vegetation becomes flammable (Scott and Glasspool, 2006; Bowman et al., 2009). At today's typical oxygen concentration of nearly 21%, fire ignition and spread are readily possible.

Over the course of this evolutionary history, many plant species have developed specialized adaptations to fire events (Figure 2.3). Some plant species and biomes, such as the grasslands of tropical savannas, have expanded their spatial extent through fire-adaptive traits. These fire-dependent species possess characteristics that allow them to resprout from buried vegetative structures that survive fire and to disperse seeds following a fire event (Keeley and Fotheringham, 2000). Similarly, in fire-prone regions of the Mediterranean Basin, the seeds of certain woody species break dormancy after fire events and allow the establishment of seeds (Moreira and Pausas, 2012). Importantly, species are adapted to specific fire regimes rather than to fire itself, which includes factors such as fire frequency, intensity, duration, and fuel consumption patterns (Keeley et al., 2011). Species that have specific traits for a particular fire regime may be at risk when there is any departure from that regime (Keeley et al., 2011). For example, woody plants that regenerate

from their seeds could be threatened by a reduction in the length of fire-free periods needed for recovery, driven by warmer and drier conditions (Enright et al., 2015).

Wildfires not only shape the distribution of the Earth's biomes along with climatic factors, but also have significant direct impacts on global and regional climate and air quality through the emission of greenhouse gases and aerosols (Figure 2.3). The global mean carbon emissions resulting from fires were 2.2 Pg of carbon pear year from 1997 to 2016 (van der Werf et al., 2017), representing approximately 21.6% of global CO_2 emissions from fossil fuels in 2024 (Bowman et al., 2020b; Friedlingstein et al., 2025). About 65% of the total emissions from fires are due to savanna fires as they burn with a high frequency (Bowman et al., 2020b; van der Werf et al., 2017). Individual fire events can also release substantial amounts of CO_2 into the atmosphere. For instance, the 2023 Canadian forest fires are estimated to have emitted 647 Tg of carbon (Byrne et al., 2024). Generally, emissions from fires can be offset by post-fire vegetation recovery. However, if there is permanent deforestation or frequent combustion of organic soils such as peatlands, the emissions can become a net source of carbon in the atmosphere (Bowman et al., 2020b; Walker et al., 2019). When wildfires lead to net greenhouse gas emissions, they contribute to a positive climate feedback that further amplifies global warming.

Fires also influence the climate by emitting aerosols, which in turn affect Earth's radiative balance both directly and indirectly (Figure 2.3). A key aerosol emitted from biomass burning is black carbon, which absorbs incoming solar radiation, an example of a direct effect, and contributes to global warming (Bowman et al., 2009). Some high-intensity wildfires can trigger dense, towering vertical clouds known as pyrocumulonimbus, formed through strong convection generated by the fire's heat (Pausas and Keeley, 2021). These clouds share some characteristics with severe convective storms, such as lightning occurrence, hail, and downdraft wind hazards, but they typically do not produce a significant amount of precipitation (Fromm et al., 2022). Intense heating from extreme fires can cause smoke aerosols to be injected into the lower stratosphere at a mass comparable to that of a moderate volcanic eruption (Peterson et al., 2018). For example, stratospheric injection of biomass-burning aerosols during the 2019-2020 Australian wildfires caused the largest lower stratospheric temperature anomaly since the 1991 eruption of Mount Pinatubo (Damany-Pearce et al., 2022). Fires can also alter Earth's surface albedo by replacing forested areas with barren land. Globally, the total net radiative effect of fire emissions is estimated to be a reduction of approximately 0.56 Wm^{-2} at the top of the atmosphere (Tian et al., 2022).

Wildfires also impact air quality and human health due to their emissions of fine particulate matter ($PM_{2.5}$). Since $PM_{2.5}$ is associated with serious adverse health effects, many countries have implemented regulations to reduce its concentrations, such as the Clean Air Act in the United States (Aldy et al., 2022). However, recent increases in wildfire smoke have caused previously observed improvements in $PM_{2.5}$ levels in the U.S. to stagnate (Burke et al., 2023). Areas in close proximity to severe fires experience higher pollution levels, but wildfire smoke can also travel thousands of kilometers and affect distant regions. For instance, smoke from extreme wildfires in California in September 2020 reached Europe within 3-4 days and resulted in the highest aerosol optical thickness ever recorded in Leipzig, Germany (Baars et al., 2021).

Figure 2.3: Vegetation fire in the Earth system. Landscape perspective of the multiple factors that influence, interact with and are impacted by vegetation fire. Fires have numerous direct and indirect affects that impact the biosphere (including vegetation cover), geosphere (including soil erosion), hydrosphere (including fluvial sediment and nutrient transport), cryosphere (including soot fallout and changed albedo) and atmosphere (including smoke pollution). PyroCb, pyrocumulonimbus. Figure and caption are reprinted from Bowman et al. (2020b).

2.2.2 Historical Wildfire Activity

In a warming climate, there is a common perception that wildfire activity is increasing. Indeed, the global mean duration of the fire season increased by 18.7% between 1979 and 2013 (Jolly et al., 2015). However, in contrary to this perception, satellite-derived burned area data show a decrease of approximately 25% in global burned area between 1998 and 2015 (Andela et al., 2017). This decline is primarily concentrated in regions with low to intermediate levels of tree cover, particularly the tropical savannas of South America and Africa and the grasslands of the Asian steppe (Andela et al., 2017) (Figure 2.4). Fewer and smaller fires as a result of agricultural expansion and changes in land cover are suggested as the main reasons for the decline in global burned area (Andela et al., 2017), although there is some uncertainty surrounding this conclusion due to limitations in remote sensing land cover products (Zubkova et al., 2023). In Mediterranean Europe, burned area also shows a decreasing trend between 1985 and 2011 (with the exception of Portugal, where trends are mixed), partly due to improved fire management and prevention efforts (Turco et al., 2016).

Figure 2.4: Satellite observations show a declining trend in fire activity across the world's tropical and temperate grassland ecosystems and land-use frontiers in the Americas and Southeast Asia. (A) mean annual burned area and (B) trends in burned area (GFED4s, 1998 through 2015). Line plots (inset) indicate global burned area and trend distributions by fractional tree cover. Figure and caption are reprinted from Andela et al. (2017).

In contrast to the decreasing trend in global burned area, global fire emissions have been mostly stable (Zheng et al., 2021). This is explained by an increase in forest fire emissions which offsets the decline in emissions from grassland and shrubland fires, as forest fires emit more CO_2 per unit area burned (Zheng et al., 2021). The rise in forest fire emissions is particularly notable in boreal forests across North America and Eurasia, which is associated with increasingly severe fire weather conditions and reduced soil moisture (Jones et al., 2024). As a result, trends in global burned area alone are not sufficient to characterize contemporary fire behavior, especially given the substantial regional differences. For instance, as noted above, the increasing extent and severity of extratropical forest fires are strongly influenced by climatic factors, whereas the decline in fire activity in tropical grasslands is primarily driven by direct human activities, such as agricultural expansion (Jones et al., 2024).

Focusing solely on trends in average global burned area can also conceal important trends in extreme fire events. In fact, the frequency and magnitude of energetically extreme wildfires (defined as those with fire radiative power exceeding the 99.99^{th} percentile) have more than doubled during 2003-2023, with most of this increase occurring in boreal and temperate conifer forests of the Northern Hemisphere (Cunningham et al., 2024). Notably, 6 of the most extreme years in terms of fire intensity occurred within the last seven years of that period (Cunningham et al., 2024). The following are some examples of major global wildfire events and their impacts in recent years:

- Australian Black Summer (2019-2020): Fueled by Australia's hottest and driest year on record, 2019 (Abram et al., 2021), the fires burned nearly 19 million hectares, destroyed over 3000 homes and caused 33 fatalities (excluding those related to air pollution or post-traumatic stress) (Filkov et al., 2020).

- Canada 2023 wildfire season: This record-breaking fire season has burned approximately 15 million hectares, caused several fatalities, and significantly impacted air quality not only in Canada, but also in other parts of the northern hemisphere, including the United States and China (Jain et al., 2024; Wang et al., 2024). Preliminary estimates indicate that around 232,000 people were evacuated (Jain et al., 2024). The event was driven by several environmental factors, such as early snowmelt, multiannual drought conditions in western Canada and extreme fire weather conditions (Jain et al., 2024).

There have also been many extreme wildfires in Europe in recent years; for example, Portugal 2017 fires:

- Portugal 2017 fire season: Burned approximately 540,000 hectares, the highest total recorded in Portugal since 1980 (Ramos et al., 2023). The entire 2017 fire season resulted in the loss of 114 lives and the local insurance sector declared it the costliest natural disaster in Portugal with payouts of almost 300 million dollars (Ramos et al., 2023). The event that happened in October 2017 was responsible for almost half of the burned area and fatalities. A prolonged drought and the passage of Hurricane Ophelia off the coast of Portugal (Figure 2.5) were the main drivers of the event, along with a large number of ignitions (Ramos et al., 2023).

The number of historical wildfire examples is kept limited here, as a detailed review of individual events falls outside the scope of this thesis. Moreover, each wildfire event is shaped by a unique combination of contributing drivers that determine the final impact. In the following section, the focus shifts to a broader perspective on wildfire drivers, rather than focusing on specific case studies.

2.2.3 Drivers of the Wildfires

Wildfires occur within an ecosystem as a result of the simultaneous occurrence of at least four factors: continuous fuel availability, drought conditions, ignition sources, and appropriate fire weather conditions (Pausas and Keeley, 2021). Therefore, this complex interplay makes it challenging to isolate the specific causes of the major wildfire events. Pausas and Keeley (2021) propose to view wildfires through a threshold-based approach, wherein fires occur once certain thresholds are crossed for ignition, fuel availability, and drought. However, these thresholds are not fixed; extreme fire weather can lower them, thereby increasing the likelihood of fire occurrence from ignitions, intensifying vegetation stress that increases flammability, and enhancing the fire spread (Figure 2.6a). In this section, I will go through each of these drivers following the framework proposed by Pausas and Keeley (2021), except for fire weather, which is addressed in a dedicated section (see Section 2.3).

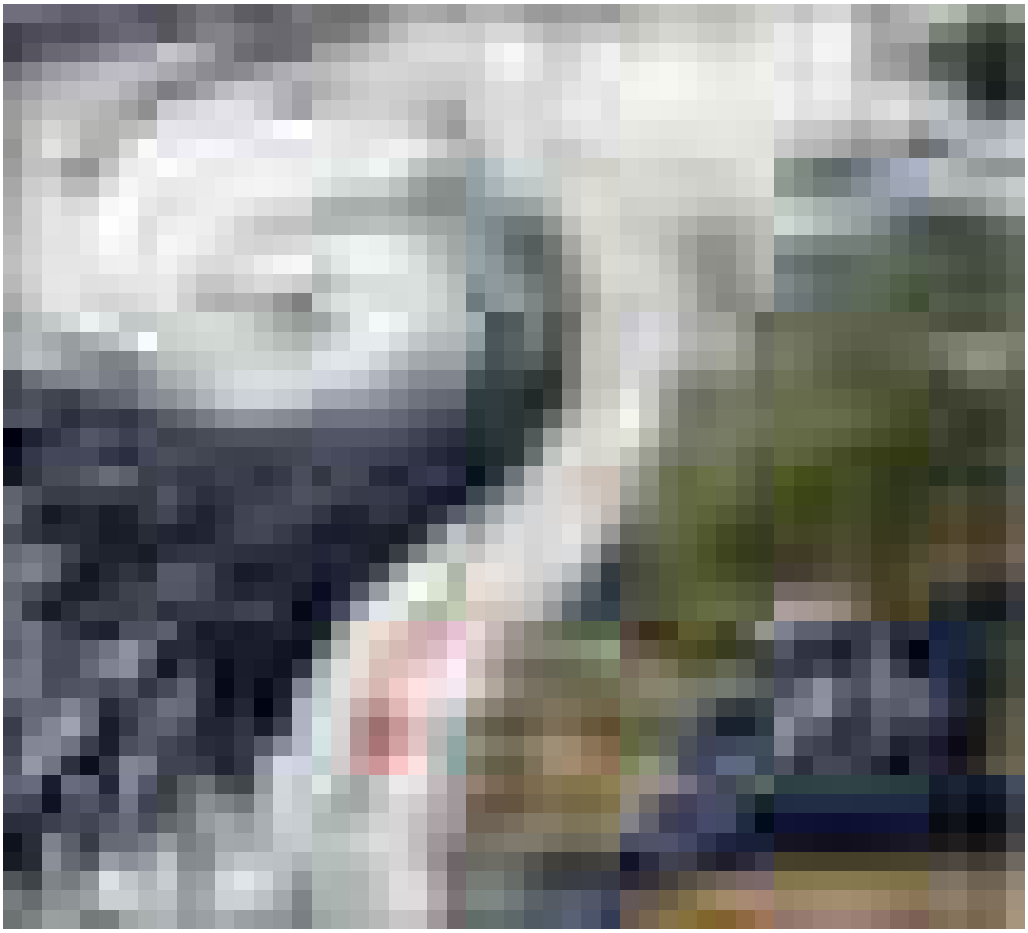

Figure 2.5: Hurricane Ophelia originated in the Caribbean and eventually reached Europe, where it fueled fires in Portugal and Spain, and covered the UK with smoke from those fires (16 Oct 2017). It is considered the easternmost Atlantic hurricane on record. Red circles are fires as detected by the Visible Infrared Imaging Radiometer Suite (VIIRS). Figure and caption are reprinted from Pausas and Keeley (2021).

Ignitions can result from either natural or anthropogenic sources. In many regions, lightning is the primary natural source of ignition. Lightning-ignited fires are generally dominant in sparsely populated areas of extratropical forests (Jones et al., 2022; Balch et al., 2017; Kharuk et al., 2011; Veraverbeke et al., 2017; Janssen et al., 2023). Jones et al. (2022) found strong correlations between monthly climatological burned area and lightning activity in boreal forest zones, suggesting that lightning is a major ignition source in these ecosystems. Although lightning-induced fires are less frequent on average than human-caused fires, they tend to be more intense and cover larger areas(Cattau et al., 2020), likely because they often occur in remote regions. The impact of global warming on lightning occurrence remains uncertain, varies by region, and is model-dependent (Finney et al., 2018; Murray, 2018), with a possible increase in the United States (Romps et al., 2014; Romps, 2019), extratropical forests (Janssen et al., 2023), and in the Arctic (Chen et al., 2021b). Recently, an increase in the occurrence of lightning in the Arctic is hypothesized to trigger a positive climate feedback, where more frequent burning of the Arctic tundra accelerates the northward shift of the treeline and decreases surface albedo, which results in a further increase in surface temperature (Chen et al., 2021b).

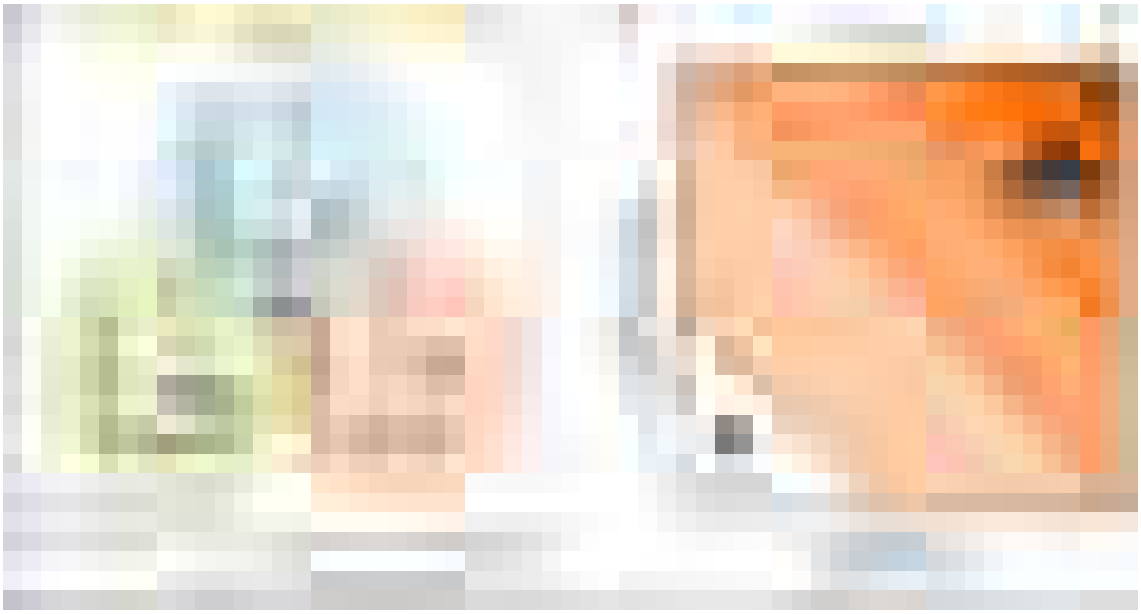

Figure 2.6: Conceptual model of relationships between fire parameters and their drivers. (a) Probability of fire occurrence versus ignitions, fire spread versus landscape fuel continuity, and fuel flammability versus drought. In these graphs, dashed vertical lines indicate thresholds. In all cases, fire weather (strong wind, high temperature, or low humidity) shifts the curve and the threshold toward lower values (thick red arrows; ie saturation is reached at lower values along the x-axis), consequently increasing the probability of an ignition resulting in a fire, fire spread (for a given landscape configuration), and vegetation flammability (fuel dries faster). The flow chart shows the main factors affecting the fire drivers, including human population growth in or near wildlands, altered fuel loads (fragmentation, oldfields, fire exclusion, among others), and climate change. Arrows indicate positive interactions, with the exception of changes in fuel, which can increase or decrease fuel continuity depending on the system (eg fragmentation versus fire exclusion or increasing oldfields). (b) Once all thresholds have been crossed, the size of the fire is determined by the duration of the extreme fire weather and the availability of continuous fuels in the landscape. Figure and caption are reprinted from Pausas and Keeley (2021).

Although natural ignitions, primarily from lightning, are possible, the majority of fire ignitions are anthropogenic in origin (Pausas and Keeley, 2021; Balch et al., 2017). For example, in Europe, an overwhelming 97.1% of all fires with a known cause between 2006 and 2010 were attributed to human activity (Ganteaume et al., 2013). Anthropogenic ignitions can occur accidentally (e.g., cigarettes, campfires, powerlines) or intentionally (arson) (Pausas and Keeley, 2021). Humans also use fire for land clearing purposes for agriculture, especially in tropical forests for the so-called slash-and-burn practice (Jones et al., 2022). Generally, the number of human-caused ignitions increases with expansion of the Wildland-Urban Interface (WUI) - areas where settlements encroach into rural landscapes (Radeloff et al., 2018; Silva et al., 2019), as well as with proximity to roads (Clarke et al., 2019). However, it is important to note that high population density can also decrease fire activity, due to faster detection and closer access to suppression resources (Pausas and Keeley, 2021). Furthermore, WUI expansion may reduce fire risk through human practices such as grazing or gathering wood, which lower fuel availability (Pausas and Keeley, 2021).

The relationship between ignitions and the probability of fire occurrence is not linear; rather, it exhibits a threshold-like behavior, where the probability increases sharply once a critical point is reached (Pausas and Keeley, 2021) (Figure 2.6a). As discussed above, fire weather reduces this

threshold and shifts the curve, thereby substantially increasing the likelihood of fire. This implies that under mild fire weather conditions, a few ignitions are unlikely to lead to fire outbreaks. In contrast, even a relatively small number of ignitions can result in large wildfires when coupled with extreme fire weather conditions (Pausas and Keeley, 2021).

Another essential driver of wildfire occurrence is fuel availability and continuity. Higher fuel loads and greater continuity across the landscape increase the likelihood of fire spread (Figure 2.6). This relationship also exhibits a threshold-like behavior due to the spatial nature of fire propagation (Pausas and Keeley, 2021). As with ignition, this threshold is modulated by fire weather conditions, which, when extreme, allow fires to spread rapidly across the landscape (Pausas and Keeley, 2021). There are also many ways in which anthropogenic factors affect fuel continuity. For instance, agricultural expansion disrupts fuel continuity across the terrain and contributes to the global decline in total burned area, as discussed in 2.2.2 (Andela et al., 2017). Fire suppression efforts have also been shown to decrease the burned area in the Mediterranean in recent decades (Turco et al., 2016; Urbieta et al., 2019). However, aggressive fire suppression can contribute to fuel accumulation over time and can lead to larger, more severe, and more difficult to control fires during extreme fire weather conditions (Curt and Frejaville, 2018; Moreira et al., 2020). Additionally, rural depopulation has led to increased fuel loads and connectivity and has resulted in a greater burned area in regions such as the Western Mediterranean Basin (Pausas and Fernández-Muñoz, 2012).

Drought is another key factor in wildfire occurrence, as it directly influences vegetation flammability. However, the relationship between droughts and fires is not uniform in all ecosystems. In fact, fire occurrence depends on a delicate balance between vegetation productivity and fuel moisture, such that fires occur most frequently in regions with intermediate moisture availability (Jones et al., 2022). In woody ecosystems, such as Mediterranean and boreal forests, drought increases fire risk by drying vegetation, raising plant mortality, and enhancing fuel connectivity (Pausas and Keeley, 2021). Like other wildfire drivers, the relationship between drought and fire spread is nonlinear and exhibits threshold behavior that is further modulated by fire weather conditions. Conversely, in grass-dominated ecosystems, droughts can reduce vegetation productivity and inhibit fuel accumulation, resulting in reduced fire activity (Pausas and Keeley, 2021; Jones et al., 2022). For instance, the 2019-2020 Australian wildfires disproportionately affected forests rather than savannas, largely due to the prolonged drought that preceded the event (Pausas and Keeley, 2021; Bowman et al., 2020a).

2.3 Fire Weather

2.3.1 Definition & Indices

Fire weather refers to weather conditions that are conducive to triggering and sustaining wildfires (Masson-Delmotte et al., 2021). This consists of a combination of hot, dry, and windy weather. In other words, these conditions include high temperatures, low relative humidity, low precipitation (or droughts), and strong winds. In this context, fire weather can be seen as a compound event,

where multiple climate drivers contribute to the resulting environmental risk (Zscheischler et al., 2020). As discussed in Section 2.2.3, fire weather acts to reduce the ignition, fuel and drought thresholds, and to shift the response curves. This results in a higher likelihood of fire resulting from a certain number of ignitions and enhanced vegetation desiccation that increases its flammability (Figure 2.6a) (Pausas and Keeley, 2021). Once all thresholds are crossed and a fire is triggered, the size, duration, and spread of the fire are primarily determined by the duration and intensity of extreme fire weather conditions, in combination with the availability of continuous fuel (Figure 2.6b) (Pausas and Keeley, 2021).

High temperature and low relative humidity intensify the evapotranspiration rates and dry out the fuels. This lowers the threshold values for ignition and fuels, due to the fact that warm and dry fuels ignite more easily and burn more rapidly because they require less heat energy to combust (Pausas and Keeley, 2021). In addition, in the absence of short- or long-term precipitation, fuel moisture is not replenished, further increasing vegetation stress and flammability. Wind is another critical component of extreme fire weather. Strong winds enhance combustion by supplying oxygen, accelerate vegetation desiccation through increased evapotranspiration, and facilitate fire spread by dispersing embers (Pausas and Keeley, 2021).

Numerous indices have been developed to quantify fire weather with varying degrees of use in the literature (Jones et al., 2022). Some prominent examples include the Nesterov Index (Nesterov, 1949), the Fosberg Fire Weather Index (Fosberg, 1978), the Australian McArthur Forest Fire Danger Index (Noble et al., 1980), and the Canadian Forest Fire Weather Index (FWI) System (Van Wagner, 1987). Among these, Fire Weather Index (FWI) is arguably the most widely used, as it integrates all major influencing factors and provides detailed information on fuel dryness and fire risk through its subcomponents. In addition, the FWI calculation relies solely on meteorological inputs, namely temperature, precipitation, relative humidity, and wind speed, which makes it broadly applicable across regions. In this study, FWI is used to quantify extreme fire weather danger, due to its widespread adoption in both global and regional studies (Bedia et al., 2015; Abatzoglou et al., 2019; Jones et al., 2022; Ramos et al., 2023). It is also employed by The European Forest Fire Information System (EFFIS) for real-time fire danger forecasting (San-Miguel-Ayanz et al., 2012) and has been shown to be particularly suitable for southern Europe (Viegas et al., 1999). A detailed introduction to the FWI system is provided in Section 3.2.3.

It is important to note that fire weather indices provide the greatest insight in regions where fire activity is limited by fuel dryness, as opposed to areas where fires are limited by vegetation productivity (Jones et al., 2022). In fact, a significant proportion of the global land area exhibits a strong relationship between FWI and burned area. However, this relationship weakens in regions with low vegetation productivity, such as deserts and xeric shrublands, where burned area is relatively insensitive to the variability of FWI (Bedia et al., 2015; Jones et al., 2022). The strongest relationships between FWI and burned area are typically observed in mesic ecosystems, including boreal forests and evergreen temperate forests (Bedia et al., 2015; Abatzoglou et al., 2018). In addition, a strong relationship between FWI and burned area has also been documented in Mediterranean Europe (Carvalho et al., 2008; Urbieta et al., 2015; Fox et al., 2018; Jones et al., 2022).

2.3.2 Extreme Fire Weather under Climate Change

In a warmer climate, concurrent heatwaves and droughts have become more frequent, which, in turn, makes fire weather conditions more probable, especially in regions such as Southern Europe, the United States and Australia (Masson-Delmotte et al., 2021). Between 1979 and 2013, the fire weather seasons have lengthened on 25.3% of the vegetated Earth's surface, leading to an increase of 18.7% in the global mean fire weather season length (Jolly et al., 2015). Similarly, (Jones et al., 2022) reported that between 1979 and 2019, the annual fire weather season length increased by an average of 14 days per year (27%), while the frequency of extreme fire weather days rose by 10 days per year (54%) based on ERA5 reanalysis data. The most pronounced increases were observed in central and boreal Asia, South America, temperate North America and Europe (Figure 2.7). Rising temperatures and decreasing relative humidity are identified as the dominant drivers responsible for the increase in extreme fire weather conditions (Jain et al., 2022).

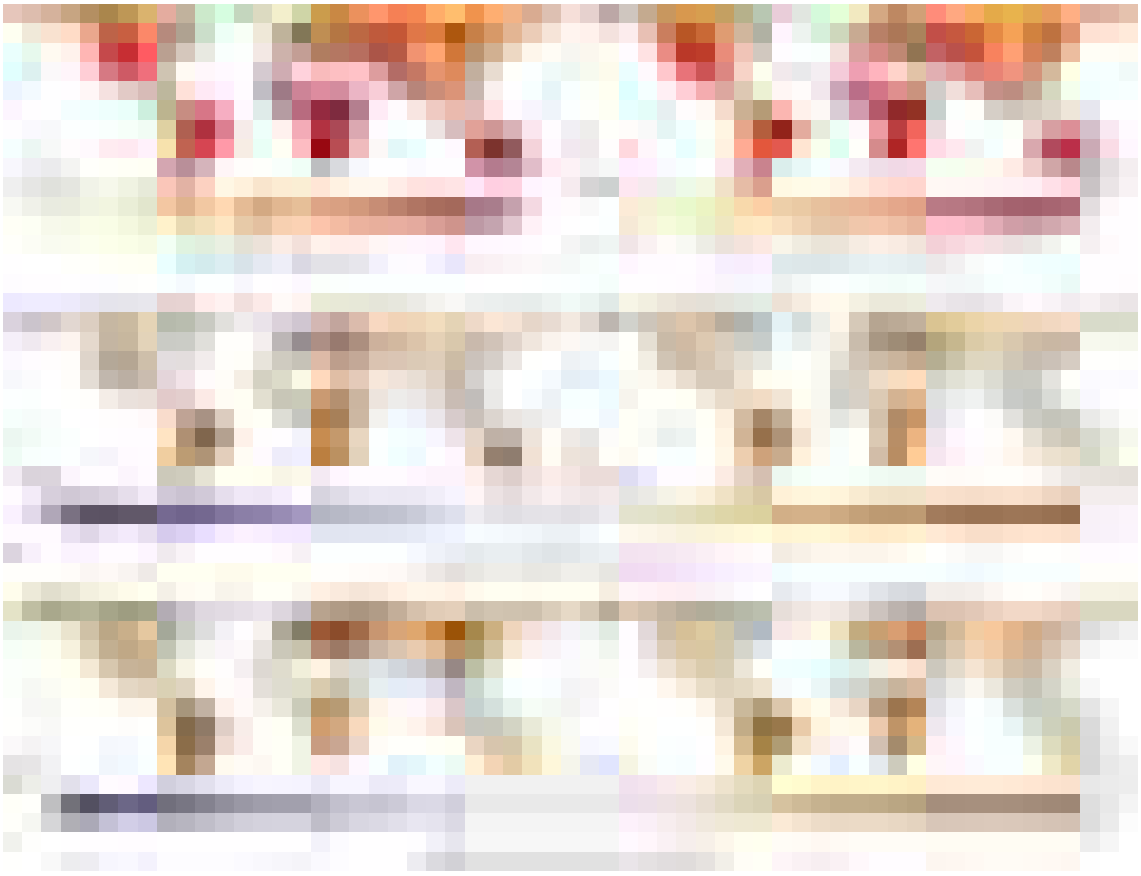

Figure 2.7: Global patterns and trends in fire weather during 1979–2019 based on ERA5 reanalysis data. (Left panels) include (top) mean, (middle) absolute change and (bottom) relative change in annual fire weather season length (FSWL) during 1979–2019. (Right panels) include (top) the 95th percentile daily value of FWI threshold value during 1979–2019, (middle) the absolute change in annual days with FWI values exceeding the 95th percentile and (bottom) the relative change. Absolute change (days year^{-1}) is calculated as the trend (days year^{-2}) multiplied by the length of the time series (41 years). The relative change is the absolute change divided by the mean. Figure and caption are reprinted from Jones et al. (2022).

Although it is challenging to attribute the effects of climate change on individual extreme fire events due to the complex interactions among weather, vegetation, ignition sources, land use, human

management and suppression efforts, many studies have sought to estimate the influence of climate change on fire weather. Liu et al. (2022) found that climate change increased the likelihood of extreme fire weather conditions (as represented by components of the FWI system) by at least a factor of four in 40% of the world's fire-prone regions. Several regional studies have also attributed the influence of climate change on extreme fire weather seasons with varying degrees of impact. Examples include Canada (Kirchmeier-Young et al., 2019), Australia (van Oldenborgh et al., 2021), France (Barbero et al., 2020), and the western United States (Hawkins et al., 2022). More recently, some studies attributed changes in global burned area to climate change, using methods such as logistic regression between FWI and burned area (Feng et al., 2025) or process-based fire modeling (Burton et al., 2024).

As global surface temperatures rise, the frequency of extreme fire weather conditions is expected to increase, primarily due to the projected increase in compound hot and dry conditions (Masson-Delmotte et al., 2021). Using a pseudo-climate change experiment, Bowman et al. (2017) estimated a 20-50% increase in the number of days with high fire danger by the mid-21st century with larger increases in the European Mediterranean Basin and subtropical regions of the Southern Hemisphere. Abatzoglou et al. (2019) and Jones et al. (2022) also found that the anthropogenic signal in fire weather is projected to emerge from internal variability as global warming intensifies. Regional studies similarly project an increase in future fire weather conditions in a warming world across several regions, including Canada (Wang et al., 2015), the United States (Barbero et al., 2015), Australia (Herold et al., 2021), and the Mediterranean (Ruffault et al., 2020).

2.4 Climate Models

Climate models are essential tools for studying Earth's climate, as the global climate system cannot be studied through experimental methods due to its massive size and the long time scales involved (Edwards, 2011). These models are theory-based representations designed to simulate the key processes and mechanisms that govern Earth's climate, including interactions among the various components of the climate system (Edwards, 2011). All climate models consist of a dynamical core that simulates large-scale fluid motion by solving the primitive equations, which represent the conservation of mass, momentum, and energy, along with the equation of state. In addition, models incorporate a set of model physics for processes such as convection, radiative transfer, or turbulence, which usually occur at subgrid-scale and cannot be explicitly resolved at the model grid scale; hence, they are parameterized. Many models use a rectangular grid to solve the horizontal and vertical exchanges between neighboring grid cells (Figure 2.8), although some adopt alternative grid structures such as icosahedral grids (e.g., ICON) or employ spectral modeling techniques.

After decades of development ranging from simple conceptual models to energy balance and radiative convective models, efforts eventually turned into General Circulation Model (GCM)s. The first attempt to develop a computerized GCM was made by Norman A. Phillips in 1956 (Phillips, 1956). In the late 1960s, Manabe and Bryan (1969) introduced the first coupled atmosphere-ocean GCM (Edwards, 2011). Since the 1980s, model complexity steadily increased to incorporate more

Figure 2.8: Schematic representation of the Cartesian grid structure used in finite-difference GCMs. Figure and caption are reprinted from Edwards (2011).

processes in the Earth system, such as the land surface, cryosphere, and hydrology, which can be considered as predecessors to today's Earth System Model (ESM)s (Edwards, 2011). Following the establishment of the IPCC in 1988, the CMIP was launched by the World Climate Research Programme (WCRP) in 1995. The main objective of CMIP is to provide a database of coupled GCM simulations, enabling the scientific community to better understand past, present and future climate change through a standard experimental protocol (Eyring et al., 2016). These standardized protocols (boundary conditions) allow for meaningful intercomparison of models developed by different institutions and help identify model biases and limitations by comparing outputs against observations. In addition, CMIP simulations serve as a key input for IPCC assessment reports to provide information about the state-of-the-art in climate science.

In addition to a common set of experiments (e.g., pre-industrial control run or abrupt CO_2 quadrupling), modeling groups participating in CMIP phases also follow a common set of future greenhouse gas concentration scenarios for climate projections. In the fifth phase of CMIP (CMIP5), the Representative Concentration Pathway (RCP) were used (van Vuuren et al., 2011), which describe different levels of radiative forcing that could be reached by the end of the 21st century. There are four RCP scenarios that span a range of radiative forcing values from 2.6 to 8.5 W/m^2 (e.g., RCP8.5 represents a scenario with 8.5 W/m^2 radiative forcing by 2100). In the latest phase, CMIP6, the scenario framework incorporates alternative pathways for socioeconomic development in addition to the radiative forcing component, hence called Shared Socioeconomic Pathway (SSP) (Riahi et al., 2017).

Although GCMs can provide information on a global scale, their resolution is typically insufficient to capture processes that shape regional climates, such as orography or mesoscale dynamical processes. To address this limitation, regional climate models (RCMs) have been developed to provide climate fields at finer spatial scales, making them suitable for regional impact studies (e.g., water resources or renewable energy production). The underlying approach is that GCMs can simulate the general circulation response to large-scale forcings (e.g., greenhouse gases), while RCMs can refine this information at finer scales by incorporating sub-GCM grid-scale processes (Giorgi, 2019). The primary technique for generating RCM outputs is generally referred to as dynamical downscaling or nested regional climate modeling (Figure 2.9) (Giorgi, 2019; Giorgi and Jr, 2015). This involves running a regional model (limited area RCM) that is driven by initial and time-dependent lateral boundary conditions obtained from driving GCM simulations (Giorgi, 2019). As shown in Figure 2.9, the boundary conditions obtained from the GCMs can be incorporated into the model using a relaxation term in the prognostic equations, which nudges the model toward the imposed boundary conditions in the buffer zone (Giorgi, 2019).

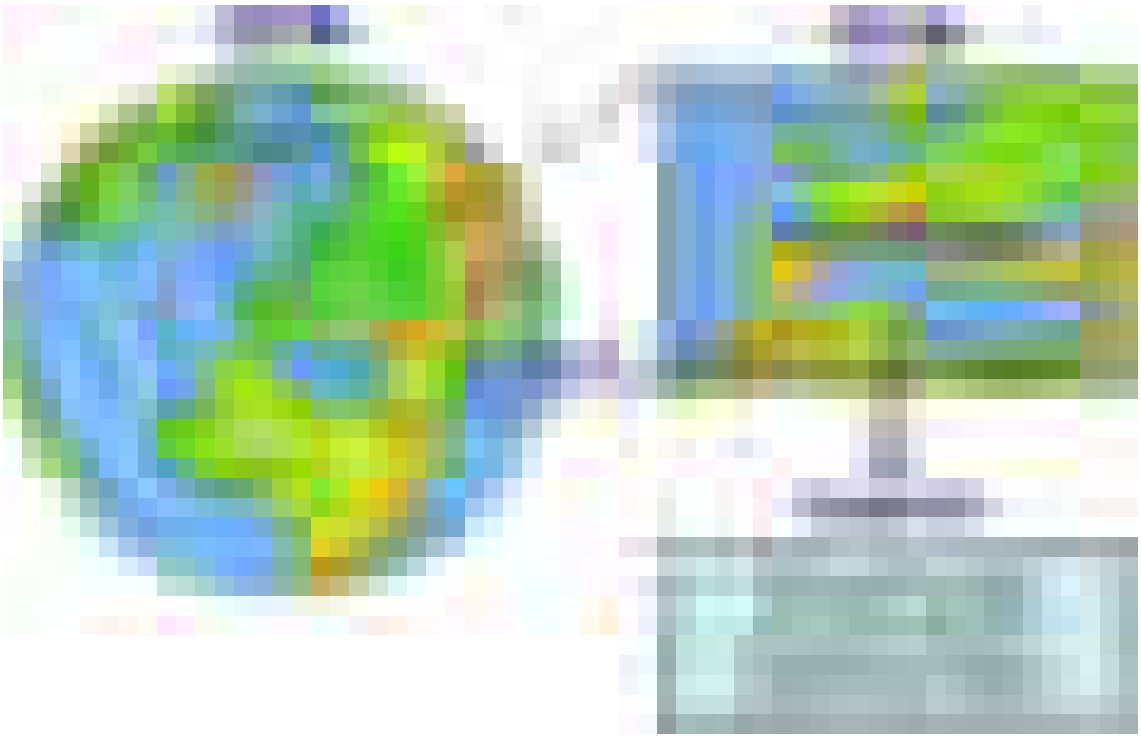

Figure 2.9: Schematic depiction of regional climate modeling and application to VIA studies. VIA = vulnerability, impacts, and adaptation; RCM = regional climate model; GCM = global climate model. Figure and caption are reprinted from Giorgi (2019).

Similar to the CMIP framework for coordinating global climate modeling, the CORDEX aims to coordinate downscaling and regional climate modeling efforts by designing a set of experiments and protocols (Giorgi et al., 2009). The main objectives of the CORDEX framework are to improve the understanding of regional and local climate phenomena, to evaluate and improve regional climate modeling, and to generate large ensembles of downscaled projections to characterize projected changes and associated uncertainties (Giorgi, 2019). The final product is a set of GCM-RCM matrix that consists of multiple GCMs and RCMs for multiple scenarios, covering all land regions of the world (e.g., EURO-CORDEX or CORDEX-Africa, etc.) (Giorgi, 2019).

2.5 Bias Adjustment of Climate Model Outputs

Climate model bias is defined as the systematic deviation of a model-simulated climate statistic from the corresponding observed climate statistic (Maraun, 2016). GCMs are known to have systematic biases due to various factors, such as discretization and spatial averaging within grid cells (Teutschbein and Seibert, 2012), inadequate representation of thermodynamic processes (Wehrli et al., 2018), or inaccuracies in simulating atmospheric dynamics (Shepherd, 2014). Since the nested downscaled model cannot deviate too much from the imposed boundary conditions, RCMs also often inherit the biases of driving GCMs, such as incorrect placement of storm tracks (Giorgi, 2019). As a result, it is common practice to adjust biases in climate model outputs, particularly before using them in climate change assessments and impact studies (Muerth et al., 2013; Hakala et al., 2018; Dosio and Paruolo, 2011; Chen et al., 2021a).

Bias adjustment refers to a set of statistical methods used to adjust systematic biases in climate model outputs. The primary goal of bias adjustment is to align the simulated statistical properties (e.g., mean temperature or variance of precipitation) with those observed during a defined calibration period (Maraun, 2016). A key assumption underlying most bias adjustment methods is that the driving model provides an adequate representation of the physical system, since bias adjustment techniques are purely statistical and cannot compensate for misrepresentations of the dynamical and physical processes (Haerter et al., 2011; Maraun, 2016).

Numerous methods have been developed for bias adjustment. Here, linear scaling (simple mean bias correction) and quantile mapping will be introduced first, as they are arguably the most commonly used univariate bias adjustment methods in the literature.

Linear scaling is likely the simplest bias adjustment method. It adjusts future simulations by subtracting the present-day model bias from the future time series (Maraun, 2016). The present-day bias is calculated as the difference between historical raw model simulations and reference observations. The additive version of the method is typically applied to adjust non-stochastic variables, such as temperature:

$$x^f_{i,cor} = x^f_{i,raw} - (\overline{x^h_{i,raw}} - \overline{y_i}) \tag{2.1}$$

The multiplicative version of the method can be used to adjust stochastic variables, such as precipitation:

$$x^f_{i,cor} = x^f_{i,raw} \times \frac{\overline{y_i}}{\overline{x^h_{i,raw}}} \tag{2.2}$$

where $x^f_{i,cor}$ represents the corrected simulated future time series, $x^f_{i,raw}$ represents the raw simulated future time series, $\overline{x^h_{i,raw}}$ represents the mean of the raw simulated historical time series, and $\overline{y_i}$

represents the mean of the observed reference data. The subscript i corresponds to the calendar month, as the adjustment is usually applied to monthly pooled data.

Quantile-based methods are also widely used in the literature because they allow for the adjustment of the entire distribution of a variable, unlike linear scaling, which only adjusts the mean biases. Simple quantile mapping (Figure 2.10) adjusts the future simulated time series by aligning the quantiles of the historical simulations with those of the reference observations (Maraun, 2016):

$$x^f_{cor}(i) = F^{-1}_{h,obs}\{F_{h,raw}[x^f_{raw}(i)]\} \tag{2.3}$$

where $x^f_{cor}(i)$ represents the corrected simulated future time series, $F^{-1}_{h,obs}$ is the inverse of the empirical or parametric Cumulative Distribution Function (CDF) of the reference observations, $F_{h,raw}$ is the empirical or parametric CDF of the historical simulated time series and $x^f_{raw}(i)$ is the raw simulated future time series to be corrected.

Figure 2.10: Quantile mapping. A simulated value, a quantile of the simulated distribution, is replaced by the quantile of the observed distribution corresponding to the same probability. Figure and caption are reprinted from Maraun (2016).

These univariate methods are designed to adjust the marginal distribution of each variable independently. However, for multivariate hazard assessments, such as fire weather, not only the marginal distributions of individual variables but also their interdependencies are important. If the dependence structure between variables is not accurately represented by climate models, univariate bias adjustment methods may be insufficient to reliably estimate the impacts of multivariate hazards (Zscheischler et al., 2019). To address this limitation, several multivariate bias adjustment methods have been developed in recent years (for a review of commonly used methods, see François et al. (2020)). These methods aim to adjust both the marginal distributions and the dependence structure between variables (e.g., Pearson or rank correlation). The performance improvement achieved through these multivariate bias adjustment methods is case-specific and should be carefully eval-

uated before applying them indiscriminately. Moreover, these methods can vary significantly in performance, especially in high-dimensional contexts (see François et al. (2020) for discussion). It is also important to note that they are generally more computationally demanding than univariate approaches.

3 Data and Methods

This chapter introduces the ERA5-Land reanalysis and the EURO-CORDEX simulations used throughout the thesis (Section 3.1). Then, a description of the methodology followed is given (Section 3.2), including the calculation of global warming levels, the bias adjustment process, FWI calculation and related metrics, as well as the statistical methods used to assess trends, significance and robustness.

3.1 Data

3.1.1 ECMWF ERA5-Land Reanalysis

In this study, hourly atmospheric fields, including 2-meter temperature, precipitation, 10 meter u (zonal) and v (meridional) components of wind speed and 2-meter dew point temperature from the ERA5-Land reanalysis have been used (Muñoz-Sabater et al., 2021). ERA5-Land is produced by the European Centre for Medium-Range Weather Forecast (ECMWF) through numerical integration of the ECMWF land surface model driven by downscaled meteorological fields from the ERA5 reanalysis (Muñoz-Sabater et al., 2021). Therefore, ERA5-Land and ERA5 share most of their parameterizations for their physics schemes (Muñoz-Sabater et al., 2021). The main advantage of ERA5-Land is its enhanced horizontal grid resolution of 9 km, compared to 31 km for ERA5 (Muñoz-Sabater et al., 2021). The dataset covers the period from 1950 to the present, with data up to 2023 used in this study. ERA5-Land reanalysis data were used for several purposes throughout the study:

- to estimate the best proxy input combination for computing FWI at daily resolution
- to evaluate the performance of the climate model outputs
- and to adjust the biases in atmospheric fields derived from climate model outputs.

3.1.2 EURO-CORDEX Simulations

A set of 34 GCM-RCM pairs from the EURO-CORDEX framework (Jacob et al., 2014) has been used to evaluate historical model performance and project future changes in extreme fire weather in Europe. The variables used include daily maximum temperature, accumulated precipitation, mean relative humidity, and maximum wind speed (details on variable selection are provided in Section

4.1). The EURO-CORDEX models are dynamically downscaled from GCMs participating in CMIP5 (Taylor et al., 2012) to provide high-resolution regional climate simulations across Europe.

All models share a common grid resolution of 12.5 km (see Figure 3.1 for the model domain). Both historical simulations (covering the period from 1950 or 1970, depending on the model, to 2005) and scenario simulations (covering 2006 to 2100) have been used. The scenario simulations follow the RCP 8.5 (van Vuuren et al., 2011), which represents a high-end greenhouse gas emission scenario with a radiative forcing of 8.5 W m^{-2} by the end of the century. A single model realization (r1i1p1) has been used for each model. All simulations have been regridded to the ERA5-Land grid resolution of 9 km using first-order conservative remapping (Jones, 1999). The list of models used in this study is provided in Table 3.1.

All model data were downloaded from the Earth System Grid Federation (ESGF) node at DKRZ and are publicly accessible at https://esgf-metagrid.cloud.dkrz.de.

Figure 3.1: EURO-CORDEX model domain. The simulations are performed on a rotated grid and the domain covers approximately the region from 22°W to 45°E in longitude and 27°N to 72°N in latitude. Figure and caption adapted from the Climate Limited-area Modelling (CLM) community (Keuler et al., 2016)

3.2 Methodology

3.2.1 Global Warming Levels

Many drivers of global and regional climate impacts are closely linked to GWLs (Masson-Delmotte et al., 2021). Therefore, this study follows the IPCC AR6 concept of GWLs to quantify changes in extreme fire weather (Masson-Delmotte et al., 2021). Each GCM may follow a different trajectory and reach a given GWL at a different time due to differences in climate sensitivity between models. However, the GWL approach enables the estimation of impacts independently of the specific scenario or timing of when a given GWL is reached. This study focuses on +2 °C and +3 °C

Table 3.1: List of the 34 GCM-RCM pairs used in this study. All scenario simulations follow RCP8.5, as all models reach the 3 °C GWL during the 21st century. All models belong to the same ensemble member r1i1p1.

GCM	RCM
CNRM-CERFACS-CNRM-CM5	CLMcom-ETH-COSMO-crCLIM-v1-1
	DMI-HIRHAM5
	GERICS-REMO2015
	IPSL-WRF381P
	KNMI-RACMO22E
	SMHI-RCA4
ICHEC-EC-EARTH	CLMcom-ETH-COSMO-crCLIM-v1-1
	DMI-HIRHAM5
	KNMI-RACMO22E
	SMHI-RCA4
IPSL-IPSL-CM5A-MR	DMI-HIRHAM5
	GERICS-REMO2015
	IPSL-WRF381P
	KNMI-RACMO22E
	SMHI-RCA4
MOHC-HadGEM2-ES	CLMcom-ETH-COSMO-crCLIM-v1-1
	DMI-HIRHAM5
	IPSL-WRF381P
	KNMI-RACMO22E
	MOHC-HadREM3-GA7-05
	SMHI-RCA4
MPI-M-MPI-ESM-LR	CLMcom-ETH-COSMO-crCLIM-v1-1
	DMI-HIRHAM5
	IPSL-WRF381P
	KNMI-RACMO22E
	MOHC-HadREM3-GA7-05
	SMHI-RCA4
NCC-NorESM1-M	CLMcom-ETH-COSMO-crCLIM-v1-1
	DMI-HIRHAM5
	GERICS-REMO2015
	IPSL-WRF381P
	KNMI-RACMO22E
	MOHC-HadREM3-GA7-05
	SMHI-RCA4

GWLs relative to the preindustrial reference period 1881-1910 as in Moemken et al. (2022) and Hundhausen et al. (2024). The methodology is based on the time sampling approach (James et al., 2017) as implemented by Vautard et al. (2014) and Teichmann et al. (2018) for regional climate change signals in Europe.

First, the 30-year running average of global mean temperature is calculated from the scenario simulations of the GCMs. The observed global warming from 1881-1910 to 1971-2000 has already been estimated as 0.46 °C (Vautard et al., 2014). The average global mean temperature of the GCMs during 1971-2000 is then used as the present-day reference, so that an increase of 1.54 °C (2.54 °C) from that value corresponds to +2 °C (+3 °C) GWL relative to the preindustrial period. Next, 30-year time periods are identified based on when the relevant GWLs are reached for the first time in the running average (as listed in Table 3.2). Note that although the GWLs are defined relative to the preindustrial period, the change signals presented in this study are expressed relative to the present-day reference period (1971-2000). This is a deliberate choice, as RCM simulations only begin after 1950.

Table 3.2: Thirty-year time periods when the specified global warming level is reached for the first time by the GCMs used as boundary conditions for the RCMs used in this study (scenario: RCP8.5). Note that each model follows a different trajectory to reach the relevant GWLs due to differences in climate sensitivity.

GCM	+2 °C GWL Period	+3 °C GWL Period
CNRM-CERFACS-CNRM-CM5	2029-2058	2052-2081
ICHEC-EC-EARTH	2028-2057	2052-2081
IPSL-IPSL-CM5A-MR	2020-2049	2039-2068
MOHC-HadGEM2-ES	2016-2045	2037-2066
MPI-M-MPI-ESM-LR	2029-2058	2052-2081
NCC-NorESM1-M	2031-2060	2057-2086

3.2.2 Bias Adjustment of the EURO-CORDEX Model Outputs

As explained in Section 2.5, it is common practice to adjust biases in climate model outputs before using them in impact and climate change assessment studies. In this study, the Quantile Delta Mapping (QDM) method is applied to adjust biases in the EURO-CORDEX simulations as described by Cannon et al. (2015) due to its ability to adjust biases in each quantile while preserving the relative change signal of the underlying climate model, as demonstrated for precipitation- and temperature-based indices (Cannon et al., 2015; Xavier et al., 2022; Tong et al., 2021; Casanueva et al., 2020). First, the non-exceedance probabilities of the simulations are calculated over the projected time window:

$$\tau(t) = F^{d}_{s,p}[x_{s,p}(t)] \tag{3.1}$$

where $x_{s,p}(t)$ is the projected simulation value of the variable of interest at time step t, $F^{d}_{s,p}$ is the empirical CDF for the time period being corrected (in this case, decades) and $\tau(t)$ is the non-exceedance probability associated with the time step that has a range between 0 and 1.

Next, the relative change signal between the projected and historical simulations is calculated:

$$\Delta(t) = \frac{x_{s,p}(t)}{F^{-1}_{s,h}[\tau(t)]} \tag{3.2}$$

where $\Delta(t)$ is the relative change signal at time step t and $F^{-1}_{s,h}$ is the inverse CDF of the simulation during the calibration period.

Finally, the calculated climate change signal is multiplied by the corresponding reference observation value (from ERA5-Land) at the same quantile during the calibration period:

$$x_{ba}(t) = F^{-1}_{r,h}[\tau(t)]\,\Delta(t) \tag{3.3}$$

where $x_{ba}(t)$ is the bias adjusted variable at time step t and $F^{-1}_{o,h}$ is the inverse CDF of the reference data (ERA5-Land) during the calibration period (1971-2000).

Note that the described multiplicative approach has been applied to precipitation, mean relative humidity, and maximum wind speed. An additive version of the same method was used for maximum temperature.

Quantile-based methods can inherently correct the so-called drizzle effect (Van de Velde et al., 2021; Argüeso et al., 2013; Gutowski et al., 2003), where models simulate too many rainy days compared to the reference data, by multiplying the lower end of the distribution by zero. To address cases where modeled dry days are more frequent than in the reference data, Cannon et al. (2015) replaced dry days in both modeled and observed data with uniformly distributed non-zero values below a specified threshold prior to bias adjustment. This also prevents division by zero issues when applying the QDM. After the bias adjustment, values below the threshold are returned to zero. This approach has later been referred to as Singularity Stochastic Removal (SSR) (Vrac et al., 2016; Lehner et al., 2023). SSR is applied here using a threshold of 0.05 mm/day to adjust occurrence biases in the EURO-CORDEX precipitation simulations, and a more conservative threshold of 0.1 mm/day is used to reset values to zero after the bias adjustment.

The biases in the seasonal cycle of each atmospheric field were adjusted using a three-month running window centered on the month of interest (Cannon et al., 2015). Future simulation periods were adjusted in separate 10-year batches to preserve climate change signals and reduce computational demands.

The QDM implementation is based on the Python package 'cmethods' (Schwertfeger et al., 2023). SSR, seasonal cycle correction, and relative change signal adjustments were implemented on top of this package specifically for the purposes of this thesis.

Spatial correlations between selected input field metrics and the 95$^{\text{th}}$ percentile of FWI were also calculated to identify the dominant drivers of FWI biases before and after bias adjustment with QDM. For that purpose, Pearson's correlation coefficient was computed between the corresponding grid cells of the two fields.

$$\rho = \frac{\text{cov}(Bias^{95}_{FWI}, Bias_{input})}{\sigma_{Bias^{95}_{FWI}} \cdot \sigma_{Bias_{input}}} \tag{3.4}$$

Since FWI is a multivariate index, bias adjustment methods that adjust only the marginal distributions of individual variables may not be sufficient. Therefore, a multivariate bias adjustment method (MBCn) which is able to adjust the full multivariate distribution (Cannon, 2018) is also used here, albeit as a proof of concept, applied to a single model over a smaller domain to reduce computational cost. The MBCn algorithm (Cannon, 2018) extends the N-pdft algorithm originally developed for image processing (Pitié et al., 2007) to climate applications by replacing RGB channels with multiple climate variables. In the first step, a random orthogonal rotation matrix (R) is multiplied with the reference observation (X_O), historical (X_H) simulations and scenario/projection (X_P) simulations, which provides linear combinations of the input fields:

$$\begin{aligned} \tilde{X}^j_O &= X^j_S R^j \\ \tilde{X}^j_H &= X^j_H R^j \\ \tilde{X}^j_P &= X^j_P R^j \end{aligned} \tag{3.5}$$

In the next step, an additive version of QDM is applied to $\tilde{X}^j_H$ and $\tilde{X}^j_P$ using $\tilde{X}^j_O$ as the reference. Then, these matrices are rotated back by multiplying with the inverse of the rotation matrix (R^{-1}):

$$\begin{aligned} \tilde{X}^{j+1}_O &= X^j_S R^{-1,j} \\ \tilde{X}^{j+1}_H &= X^j_H R^{-1,j} \\ \tilde{X}^{j+1}_P &= X^j_P \end{aligned} \tag{3.6}$$

These steps are repeated until the multivariate distributions of the reference (X_O) and the adjusted historical simulation (X^{j+1}_H) converge. The algorithm has been shown to converge after multiple iterations and can be measured using energy distance (Pitié et al., 2007; Cannon, 2018). In this study, 20 iterations were used. The MBCn implementation is based on the Python package 'xclim' (Bourgault et al., 2023).

3.2.3 FWI Calculation

The widely used Canadian Forest Fire Weather Index (FWI) System (Van Wagner, 1987) is employed in this study to calculate the historical and future distribution of extreme fire weather across Europe. As the system consists of many empirical equations, the full calculation scheme is not repeated here; details can be found in Van Wagner (1987). Figure 3.2 provides a schematic overview of the calculation flow and the required atmospheric input fields.

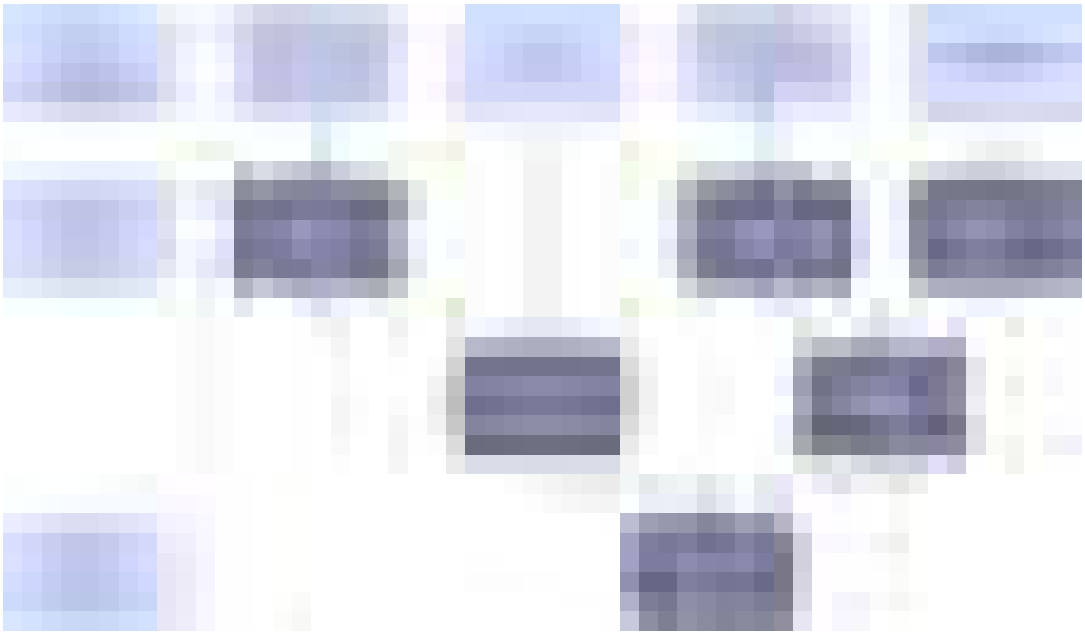

Figure 3.2: Schematic representation of the Canadian Forest Fire Weather Index System, showing the input variables and its six components, adapted from Ramos et al. (2023)

.

The FWI system consists of six components in total. These components are unitless, and increasing values indicate higher levels of fire danger for all of them. Each component is described in detail in Wotton (2009); and a brief overview is provided below following that framework. The first three components are fuel moisture codes that represent the dryness of fuel at different layers of the forest floor:

- Fine Fuel Moisture Code (FFMC): Requires all input variables, that is, temperature, relative humidity, wind and precipitation. It describes the dryness of fine surface fuels and litters. It is an indication of ease of ignition. It responds quickly to changing conditions and does not retain long-term memory.

- Duff Moisture Code (DMC): Requires temperature, relative humidity, and precipitation. It reflects the fuel dryness at medium depth layers, located just below the surface litter.

- Droght Code (DC): Requires temperature and precipitation. It represents the fuel dryness of the deep, compact organic layers. It serves as an indicator of seasonal drought effects on fuel dryness. At a temperature of 25 °C, the response time is approximately 50 days, indicating a strong seasonal memory.

The final three components of the FWI system represent fire behavior. A summary, following Wotton (2009), is provided below:

- Initial Spread Index (ISI): Combines FFMC and wind speed to give an indication of the rate of potential fire spread.
- Buildup Index (BUI): Combines DMC and DC to give an indication of the potential fuel available for consumption.
- Fire Weather Index (FWI): The final output of the system. It combines ISI and BUI and is a measure of the potential fire intensity.

It is important to understand the final calculation step of FWI to see how ISI and BUI influence the final output. The function that incorporates BUI was designed as a piecewise function, as BUI needs to saturate at a value due to the fact that there is a physical limit to the amount of fuel that can burn in a fire (Van Wagner, 1987):

$$f(D) = \begin{cases} 0.626\,BUI^{0.809} + 2 & \text{BUI} \leq 80 \\ \dfrac{1000}{25 + 108.64\,e^{-0.023\,BUI}} & \text{BUI} > 80 \end{cases} \tag{3.7}$$

Then, $f(D)$ is combined with ISI to obtain FWI:

$$FWI = 0.1\,ISI\,f(D) \tag{3.8}$$

Therefore, FWI is linearly correlated with ISI, but its relationship with BUI follows a piecewise nonlinear function that saturates at higher values.

By definition, the FWI calculation requires temperature, relative humidity, and wind speed at local noon (12:00), as well as accumulated precipitation from the previous day's noon to the current day's noon. All input data required for FWI calculation are directly available from the ERA5-Land reanalysis product, as explained in Section 3.1.1, except for relative humidity. Therefore, relative humidity was calculated using the 2-meter temperature and 2-meter dewpoint temperature outputs from ERA5-Land, applying the Magnus formula (Alduchov and Eskridge, 1996). FWI was then computed for the ERA5-Land reanalysis from 1950 to 2023 using these four atmospheric fields as input.

To account for dry conditions outside the fire season (fall and winter), overwintering was applied to the DC (McElhinny et al., 2020). The overwintering calculation requires a definition of the fire season, outside of which FWI is not calculated. The definition used here follows Wotton and Flannigan (1993), where the fire season begins when the maximum temperature exceeds 12 °C for at least three consecutive days and ends when it drops below 5 °C for at least three consecutive days (Quilcaille et al., 2023). The purpose of overwintering the DC is to capture dry fall and winter

conditions, which can lead to more severe fire weather conditions at the beginning of the fire season compared to the default DC value (McElhinny et al., 2020). FWI calculations were performed using a Python script provided by Quilcaille et al. (2023).

3.2.4 Concatenation of the Reanalysis Data and Sensitivity Analysis

In order to account for the variation in local noon times across Europe, three different time zones were used to extract atmospheric fields at the corresponding local noon: UTC+1 for grids west of 0° longitude, UTC+2 for those between the 0° and 20° longitudes and UTC+3 for grids east of 20° longitude. These three regions were then concatenated into a single product to represent the original FWI calculation.

Table 3.3: FWI input combinations tested in this study to approximate the original FWI calculation.

Combination	Temperature	Precipitation	Relative Humidity	Wind Speed
Original	at noon	accumulated at noon	at noon	at noon
Comb-1	daily maximum	accumulated daily	daily mean	daily maximum
Comb-2	daily maximum	accumulated daily	daily mean	daily mean
Comb-3	daily maximum	accumulated daily	daily minimum	daily maximum
Comb-4	daily maximum	accumulated daily	daily minimum	daily mean

Even though FWI can be computed using observational or reanalysis products at local noon, many climate models do not provide sub-daily information. Therefore, the best proxy input combination at daily resolution to approximate the typical noon-time FWI calculation was investigated. To do this, first, hourly ERA5-Land data were first aggregated to daily resolution (e.g., maximum temperature). A summary of the daily aggregated variable combinations tested in this study is provided in Table 3.3. Then, FWI estimates derived from these combinations were compared with the original noon-time FWI product described above. Specifically, the relative percentage bias in the 95$^{\text{th}}$ percentile of FWI at each grid cell was used to evaluate the performance of each proxy input combination:

$$Bias = \frac{FWI^{95}_{comb} - FWI^{95}_{original}}{FWI^{95}_{original}} \times 100 \tag{3.9}$$

where $FWI^{95}_{original}$ is the FWI 95$^{\text{th}}$ percentile value obtained from the original calculation scheme, FWI^{95}_{comb} is the 95$^{\text{th}}$ percentile FWI value obtained using the input combination being tested. The time period covered is 1950 to 2023.

Finally, the combination that resulted in the lowest spatially weighted average relative bias was selected. Since some daily resolution atmospheric fields may not be available for some models (e.g., minimum relative humidity), obtaining a sufficiently large climate model ensemble was also considered in the selection process.

3.2.5 FWI Metrics to Evaluate the Fire Weather Characteristics

In this study, four annual FWI metrics were used to analyze extreme fire weather behavior at each grid cell for the reference period (1971-2000) and at +2K and +3K GWLs, following Abatzoglou et al. (2019) and Quilcaille et al. (2023):

- Days exceeding the 95th percentile of FWI relative to the reference period 1971-2000 (FWI_{95d}): Represents days with potentially high fire danger at the local scale and can be interpreted as a frequency metric.

  The calculation involves determining the 95^{th} percentile FWI value from the reference period (1971-2000), and counting the total number of days that exceed this value during the reference period, as well as during the +2 °C and +3 °C GWL periods.

- Days exceeding the mid-range value of FWI (FWI_{fwsl}): Serves as an indicator of the duration of the fire season.

  The mid-range is defined as the average of the 30-year mean annual maximum and minimum values during the reference period (1971-2000). Then, the total number of days that exceed this value is counted for the reference period, as well as for the +2 °C and +3 °C GWL periods.

- Annual maximum FWI (FWI_{max}): It gives an indication of the magnitude of the local extreme fire danger.

  This metric is calculated as the 30-year average of annual maximum FWI values during the reference period, as well as during the +2 °C and +3 °C GWL periods.

- Annual peak 90-day average FWI (FWI_{fs}): Represents average fire weather conditions during the peak fire season and can be interpreted as a measure of seasonal fuel aridity (Abatzoglou et al., 2019).

  This metric is calculated as the 30-year average of the annual peak 90-day running mean FWI values during the reference period, as well as during the +2 °C and +3 °C GWL periods.

To shed light on the potential drivers underlying changes in extreme fire weather, atmospheric Vapor Pressure Deficit (VPD) was also calculated. VPD is defined as the difference between the saturation vapor pressure (e_s) and the actual vapor pressure (e_a) and it serves as an indicator of atmospheric aridity (Seager et al., 2015). It is an essential metric for understanding how atmospheric conditions influence fuel dryness (He et al., 2025) and has been shown to be closely linked to wildfire activity, for example, in western U.S. forests (Abatzoglou and Williams, 2016; Williams et al., 2019). VPD can be calculated using temperature and relative humidity:

$$VPD = e_s(T_a)\,(1 - RH/100) \tag{3.10}$$

where RH is the relative humidity and $e_s(T_a)$ is the saturation vapor pressure as a function of air temperature T_a, calculated using the Clausius-Clapeyron equation:

$$e_s(T_a) = e_s(T_0) \cdot \exp\left(\frac{L_v}{R_v}\left(\frac{1}{T_0} - \frac{1}{T_a}\right)\right) \tag{3.11}$$

where $e_s(T_0) = 6.112$ hPa is the saturation vapor pressure at the reference temperature $T_0 = 273.15$ K, $L_v = 2.5 \times 10^6$ J kg^{-1} is the latent heat of vaporization for water and $R_v = 461$ J kg^{-1} K$_{-1}$ is the specific gas constant for water vapor. Note that daily maximum temperature and relative humidity are used here to estimate VPD, which leads to a possible overestimation. However, the focus of this study is not on absolute VPD values, but rather on deviations from the baseline.

In order to better understand regional differences in extreme fire weather behavior across Europe, the above metrics have also been spatially averaged over the so-called PRUDENCE regions (Christensen and Christensen, 2007). In addition to the eight regions that have been previously defined, Turkey has been included as an additional subregion, as it has been shown to be particularly sensitive to extreme climate events (Gumus et al., 2023).

3.2.6 Trends, Significance and Robustness

To calculate trends in the historical period, the non-parametric Theil-Sen slope estimator was used, as it is relatively insensitive to outliers (Theil, 1950; Sen, 1968). The significance of these trends was tested using the non-parametric Mann-Kendall test (Mann, 1945; Kendall, 1955) at a significance level $p < 0.05$.

To assess the robustness of the future climate change signal in the FWI indices, a criterion based on model agreement in both the significance and direction of the reported change was applied. Specifically, the climate change signal is considered robust only when at least 66% of the models agree on both the sign and the statistical significance of the change. The significance of the simulated change was evaluated using a paired t-test at a significance level of $p = 0.05$.

3.2.7 A Note on Computational Demand

Since this study uses four atmospheric fields at daily resolution from 34 RCMs at relatively high spatial resolution and over a large domain with a long simulation period, and includes the bias adjustment for each input field, the computational demand was substantial. This work would not have been possible without the extensive resources provided by the DKRZ, especially given the time constraints of this thesis.

Figure 3.3: PRUDENCE regions used in the study. BI = British Isles, FR = France, IP = Iberian Peninsula, MD = Mediterranean, AL = Alps, ME = Mid-Europe, EA = Eastern Europe. Note that Turkey (TR) is also included, defined by coordinates 26-45°E longitude and 36-42°N latitude. Figure and caption adapted from Bellprat et al. (2012)

.

4 Observed Trends and Climatology of Extreme Fire Weather

This chapter explores the sensitivity of FWI to proxy input data (Table 3.3) and identifies the combination with the smallest bias that could replace typical noon-time variables on a daily scale. Then, it examines the historical climatology and observed trends of extreme fire weather in Europe based on the ERA5-Land reanalysis as a reference.

4.1 Sensitivity to Different Input Data

The typical calculation of FWI is performed using noon-time atmospheric fields, as explained in Sections 3.2.3 and 3.2.4. However, since many RCMs do not provide subdaily scale information, daily fields need to be identified in such a way that they can replace the typical noon-time calculation with minimal bias. Figure 4.1 shows the distribution of the relative percentage bias in the 95$^{\text{th}}$ percentile FWI calculated using the four different input combinations (Table 3.3) relative to the typical noon-time 95$^{\text{th}}$ percentile FWI ($FWI^{95}_{original}$) across Europe based on ERA5-Land reanalysis. At the European scale, combinations that include mean relative humidity generally underestimate extreme fire weather danger (Figures 4.1a,b), while those that include minimum relative humidity tend to overestimate it (Figures 4.1c,d). Since maximum temperature and daily precipitation are common to all combinations, using mean values for both relative humidity and wind leads to a substantial underestimation of $FWI^{95}_{original}$ with a mean absolute relative bias of 34.5% (Figure 4.1b). In contrast, using daily extremes, i.e., minimum relative humidity and maximum wind speed, considerably overestimates $FWI^{95}_{original}$, resulting in a mean absolute relative bias of 43.8% (Figure 4.1c). Thus, using the daily extreme for one variable and the mean for the other appears to offer a balanced compromise. The mean absolute biases for these combinations are similar: 21% for Comb-1 and 20.5% for Comb-4 (Figures 4.1a,d). Selecting Comb-4 would significantly reduce the number of models in the EURO-CORDEX ensemble, as minimum relative humidity is not an available output for most simulations. Therefore, Comb-1 is selected to calculate the FWI projections using the EURO-CORDEX ensemble, that is, daily maximum temperature, daily accumulated precipitation, mean relative humidity, and daily maximum wind speed. The remainder of the analysis in this study uses these atmospheric fields, for both ERA5-Land reanalysis and EURO-CORDEX models to ensure consistency.

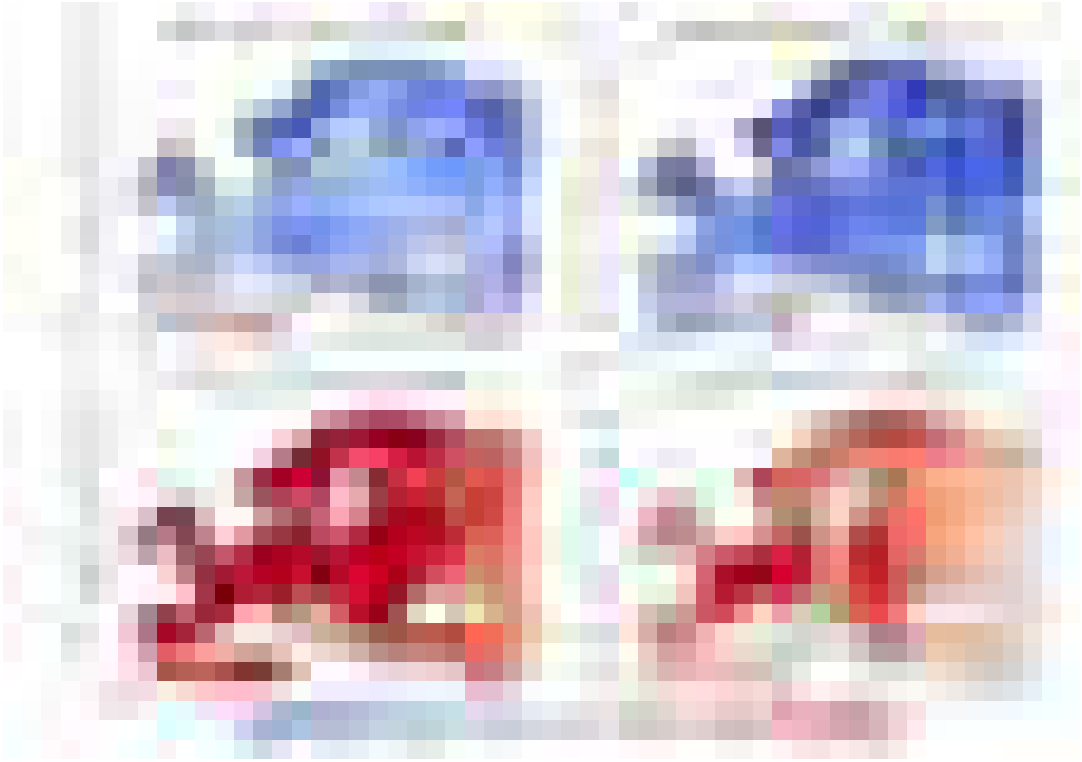

Figure 4.1: Relative percentage bias of the 95th percentile FWI calculated using the four input variable combinations compared to the original noon-time FWI calculation based on ERA5-Land reanalysis data. Daily maximum temperature and daily precipitation are common to all combinations. The time period analyzed is 1950-2023. Note that the artifacts near 0° and 20° latitude result from to the concatenation operation described in Section 3.2.4.

4.2 Extreme Fire Weather Climatology

In order to understand how extreme fire weather evolves under the influence of climate change, it is important to first establish a baseline understanding of the observed climatology. Figure 4.2 shows the observed climatology of the 95th percentile FWI (FWI^{95}) in Europe during the period 1950-2023, based on ERA5-Land. As expected, extreme FWI values in the Mediterranean Basin are much higher than in the rest of Europe as this region is characterized by hot and dry summers. A latitudinal gradient in FWI^{95} is evident throughout Europe, although there are some exceptions, particularly in mountainous regions where FWI values tend to be lower. Given that EFFIS classifies FWI values above 38 as representing very high fire danger (San-Miguel-Ayanz et al., 2012), it is reasonable to conclude that many southern European countries are frequently exposed to very high danger conditions (Figure 4.2). However, it is important to note that the extremeness of FWI values does not always directly correspond to fire danger, and this relationship may vary significantly from region to region. Globally, higher FWI values (around 50) often represent extreme fire danger in warmer and drier climates, while lower values (around 25) can signal extreme danger in cooler and moister climates (Kudláčková et al., 2024). Since FWI reflects fuel dryness but not fuel quantity, it can be hypothesized that cooler and moister regions may require less extreme FWI values to produce a fire intensity comparable to that seen in warmer and drier regions, where fuel loads tend to be lower (Kudláčková et al., 2024). Therefore, FWI values and their relationship to fire danger

should be interpreted with caution taking into account the climate and biome of each region in regional studies.

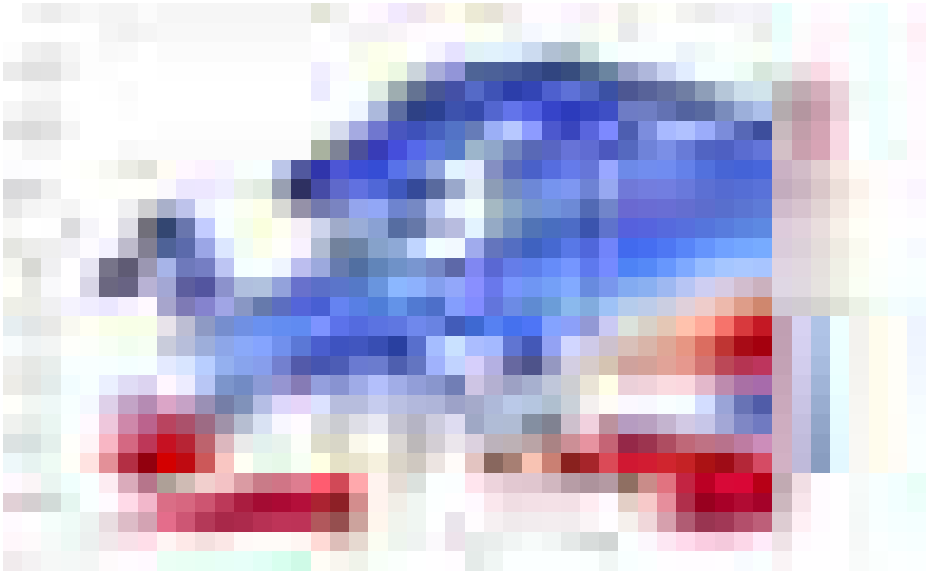

Figure 4.2: Observed climatology of the 95th percentile FWI (FWI^{95}, unitless) based on ERA5-Land reanalysis data for the period 1950-2023.

4.3 Observed Trends

The global average surface temperature was observed to be approximately 1 °C warmer during the period 2001-2020 compared to the 1851-2000 average (Masson-Delmotte et al., 2021). In Europe, a consistent warming trend of 0.04 °C year^{-1} to 0.05 °C year^{-1} has been observed since 1980 (Masson-Delmotte et al., 2021). Additionally, there has been a decreasing trend in relative humidity across many global land areas (Masson-Delmotte et al., 2021). However, this trend is not spatially uniform, relative humidity has a decreasing trend in mid-latitudes and subtropics, while increasing trends have been observed in high latitudes and the tropics (Masson-Delmotte et al., 2021). A likely weakening of surface wind speeds has also been observed over land since the 1970s, particularly in the Northern Hemisphere, with partial recovery noted since 2010 (Masson-Delmotte et al., 2021). Finally, while global average annual precipitation has shown an increasing trend since the 1980s, there is considerable regional heterogeneity (Masson-Delmotte et al., 2021), making it difficult to generalize trends specifically for Europe.

Given the observed trends in the variables that comprise the FWI, it is reasonable to expect corresponding trends in extreme fire weather metrics. In this context, Figure 4.3 presents the trends in the annual maximum FWI FWI_{max} and the number of days per year that exceed the 95th percentile FWI FWI_{95d} based on ERA5-Land reanalysis data for the period 1950-2023. Approximately 29% of Europe's land area shows a significant trend in FWI_{max}, while nearly 37% exhibits a significant trend in FWI_{95d}. In both cases, almost all grid cells with significant trends indicate an increase, with only a small number of grid cells in the Eastern Mediterranean displaying significant negative trends in these extreme fire weather metrics.

Figure 4.3 indicates a significant intensification of fire weather both in magnitude and frequency in several regions, including the Iberian Peninsula, France, Germany, and Ukraine. In these areas, the trend in FWI_{95d} exceeds 0.3 days year^{-1}, corresponding to more than 20 additional days of extreme fire weather conditions over the 74-year study period. In particular, some parts of the Iberian Peninsula exhibit trends greater than 0.5 days year^{-1}, amounting to nearly 40 additional days of extreme fire weather conditions. Conversely, certain regions such as a large part of Scandinavia display negative trends in FWI_{95d}, however, these changes are not statistically significant. Other areas that are climatologically prone to fire weather conditions, such as Italy, the Balkans, and the eastern Mediterranean, show mixed and generally non-significant trends, reflecting the high interannual variability of extreme fire weather conditions in these regions.

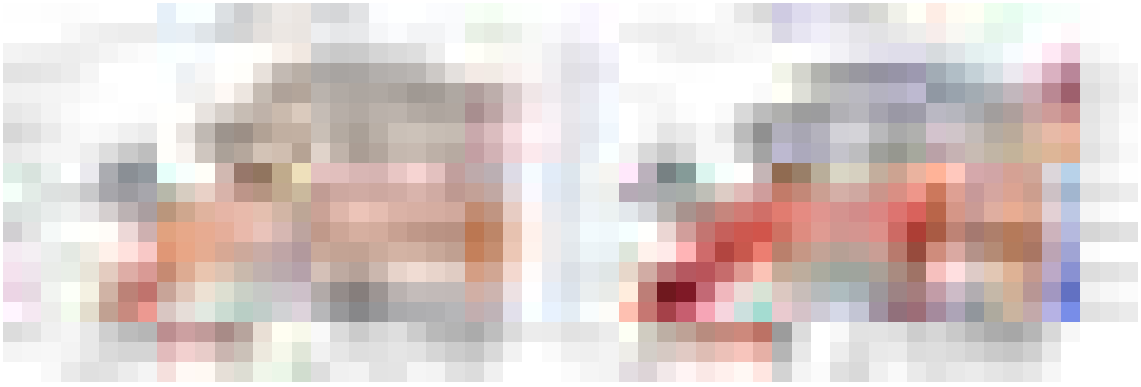

Figure 4.3: **(Left)** Observed trends (unitless year^{-1}) in annual maximum FWI (FWI_{max}), **(right)** observed trends (days year^{-2}) in the number of days per year when FWI exceeds the 95th percentile (FWI_{95d}) relative to the reference period 1971-2000 based on ERA5-Land reanalysis data. Trends are calculated using the Theil-Sen slope estimator. Hatched areas indicate regions where the trend is not statistically significant ($p < 0.05$), according to the Mann-Kendall test. The analysis covers the period 1950-2023. Note that a single colorbar is used for both panels although the units differ.

5 Model Evaluation and Bias Adjustment

In this chapter, the performance of the RCMs is evaluated for the atmospheric fields that are used in the calculation of the FWI, as well as for the resulting FWI itself. The impact of bias adjustment on model performance is then assessed for both the input variables and the FWI. Finally, the added value of the multivariate bias adjustment is explored in a smaller subdomain where model performance was initially poor, offering insights and suggestions for future research.

5.1 Evaluation of the Historical Performance of EURO-CORDEX Models

GCMs are known to exhibit systematic biases for various reasons (as discussed in Sections 2.5 and 3.2.2) and RCMs often inherit these biases because they use GCM outputs as boundary conditions for downscaling. Therefore, it is essential to evaluate the performance of RCMs before using their outputs in impact studies. In this study, the input variables required for FWI calculation, namely, daily maximum temperature, accumulated precipitation, mean relative humidity and maximum wind speed, along with the resulting FWI, are evaluated for the EURO-CORDEX ensemble relative to the reference ERA5-Land reanalysis product. For daily maximum temperature and maximum wind speed, the 95^{th} percentile is used for comparison, as higher values of these variables are positively associated with extreme fire weather. For the daily mean relative humidity, the 5^{th} percentile is used for performance assessment, as lower values are more likely to influence the FWI. To evaluate the performance of precipitation outputs, the number of dry days (defined as days with precipitation < 1 mm/day), given that wildfire occurrence favors prolonged dry conditions. Lastly, the 95^{th} percentile of the FWI is used for comparison because extreme fire weather is highly associated with high-impact wildfire events, as discussed in Section 2.3.1. All figures in this section show the percentage bias of the respective variable in the selected percentile relative to its ERA5-Land counterpart. The evaluation period spans 1971-2000.

Figure 5.1 presents the distribution of bias in the 95^{th} percentile of daily maximum temperature for each GCM-RCM chain. Overall, a gradient from warm biases in Southern Europe to cool biases in Northern Europe is evident in many models. However, individual models exhibit varying behaviors. The spatial mean absolute percentage bias across the 34 models is 8%, with individual mean model biases varying from 5.4% to 13.1%. By visual inspection, bias patterns appear to be more strongly influenced by the choice of RCM (columns) than by the driving GCM (rows) as the

bias distributions tend to be more consistent along the columns, indicating less variability among simulations that share the same RCM. However, a quantitative assessment, such as the analysis of variance (ANOVA) across the GCM and RCM dimensions of the GCM-RCM matrix, would be required to confirm this observation, which is beyond the scope of this study. Nevertheless, a recent study looking at this bias partition between the GCMs and the RCMs found that both contribute to the overall model bias with shared responsibility (Vautard et al., 2021).

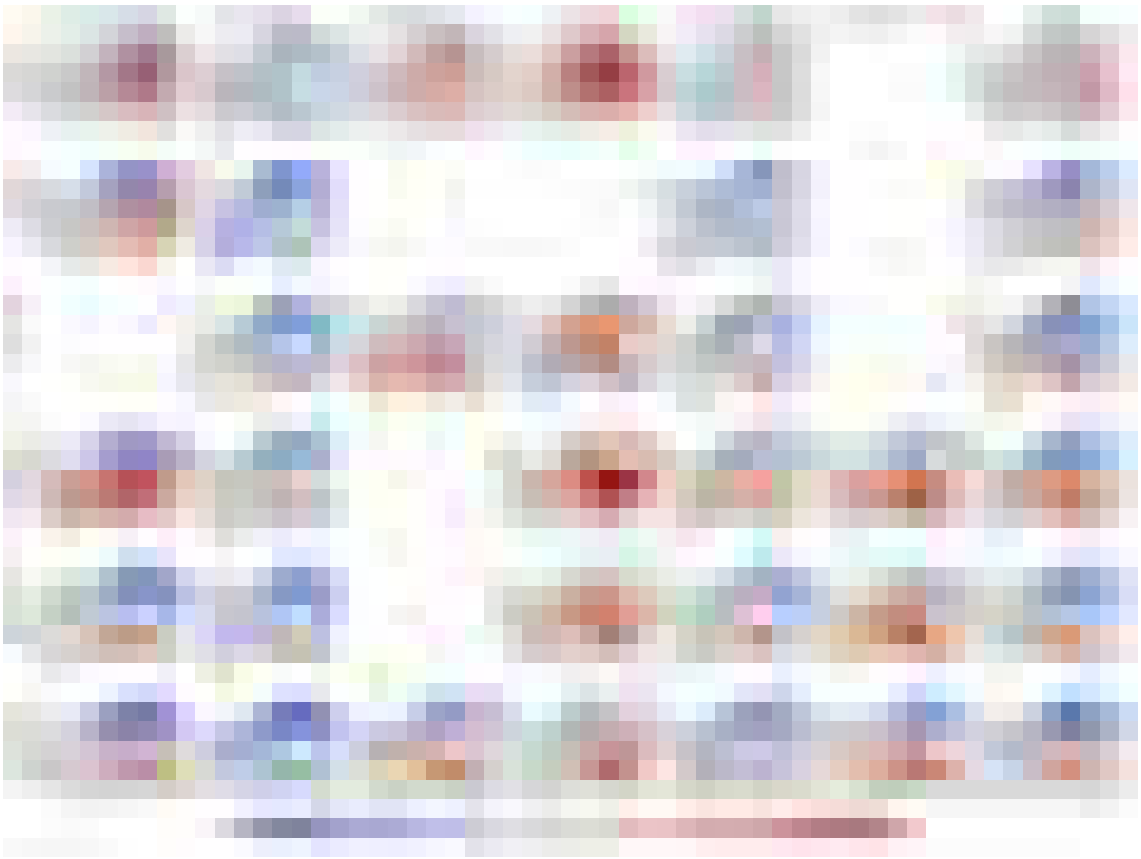

Figure 5.1: Relative percentage bias (%) of EURO-CORDEX models in the 95th percentile daily maximum temperature, relative to ERA5-Land for the period 1971-2000.

The distribution of percentage bias in the number of dry days simulated by each GCM-RCM chain relative to ERA5-Land is shown in Figure 5.2. Although it is more difficult to identify a consistent pattern for the number of dry day biases as for maximum temperature, the total bias still appears to be more strongly influenced by the choice of RCM (e.g., particularly evident in the case of the DMI-HIRHAM5 RCM). Most models tend to overestimate the number of dry days, especially in Southern and Central Europe, which could lead to an overestimation of the FWI. The spatial mean absolute percentage bias across all models is 8.1% averaged for all models, with individual model means ranging from 4.7% to 12.4%.

Figure 5.3 reveals a pronounced overestimation of the 95th percentile of daily maximum wind speed across all models in the ensemble. As with maximum temperature, the bias patterns appear to be primarily influenced by the choice of RCM. The spatial mean absolute percentage bias across the 34 models is 63.4%, with individual model biases ranging from 35.2% up to 131.6%. A large evaluation study of EURO-CORDEX models similarly reported that these models tend to

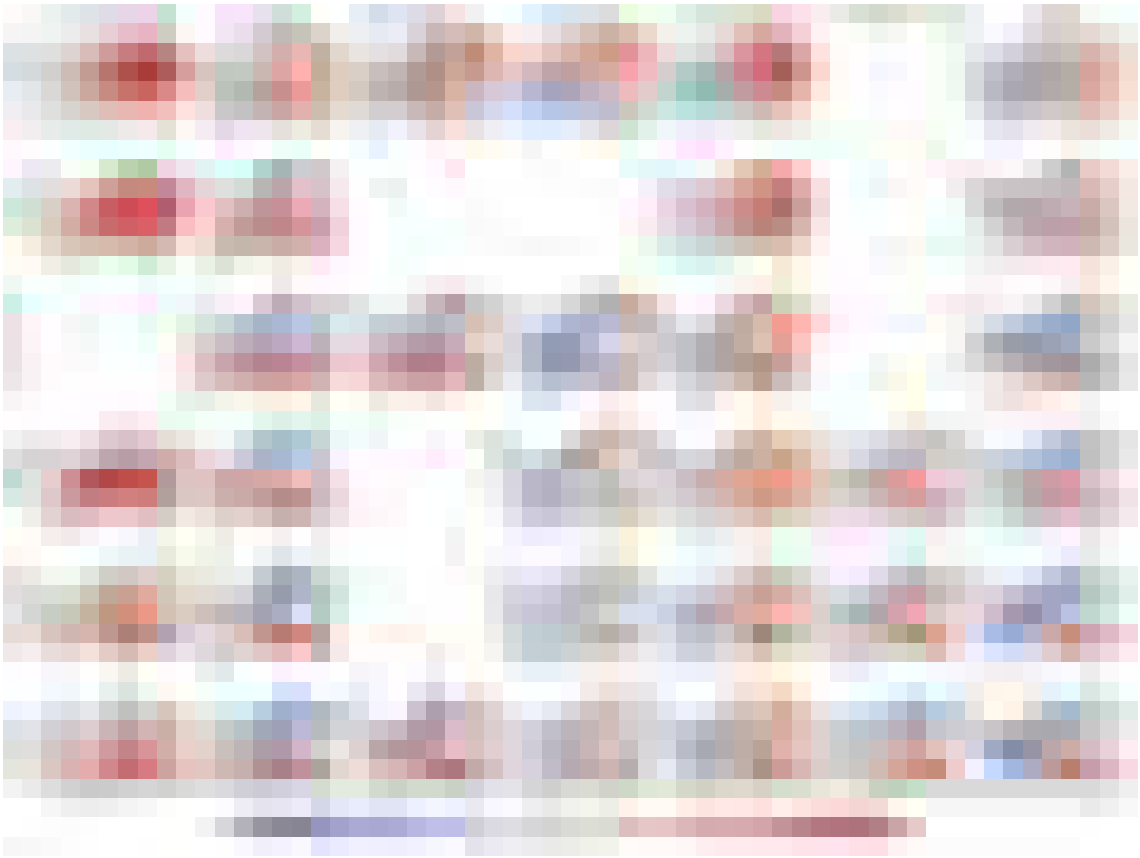

Figure 5.2: Same as in Figure 5.1, but for the number of dry days (defined as days with precipitation < 1 mm/day).

simulate wind speeds that are too strong compared to ERA5 surface winds (Vautard et al., 2021). However, Alifdini et al. (2025) found a negative bias over mountainous regions when evaluating daily maximum wind gusts.

The distribution of the bias in the 5th percentile of daily mean relative humidity for each GCM-RCM pair is shown in Figure 5.4. Most models exhibit a bias gradient from negative in the south to positive in the north, which suggests that drying conditions may be overestimated in southern and southeastern Europe. This could lead to an overestimation of FWI in these regions. The spatial mean absolute percentage bias across the 34 models for relative humidity is 14.3%, with individual model biases ranging from 9% to 22%.

Figure 5.5 shows the distribution of the bias in the 95th percentile of the FWI, calculated for each GCM-RCM chain using the relevant input fields (daily maximum temperature, accumulated precipitation, mean relative humidity, and maximum wind speed). The spatial mean absolute percentage bias across the 34 models is remarkably high: 100.9% averaged across all models, ranging from 50.2% for the model with the least bias to 199.8% for the model with the greatest bias. This implies that the bias in the final multivariate index, FWI in this case, can be substantially larger than the individual biases of its component variables. Unfortunately, it is challenging to trace how each input variable contributes to the overall bias, as the FWI involves several nonlinear relationships in its formulation (Van Wagner, 1987). Here, as an approximation, the spatial

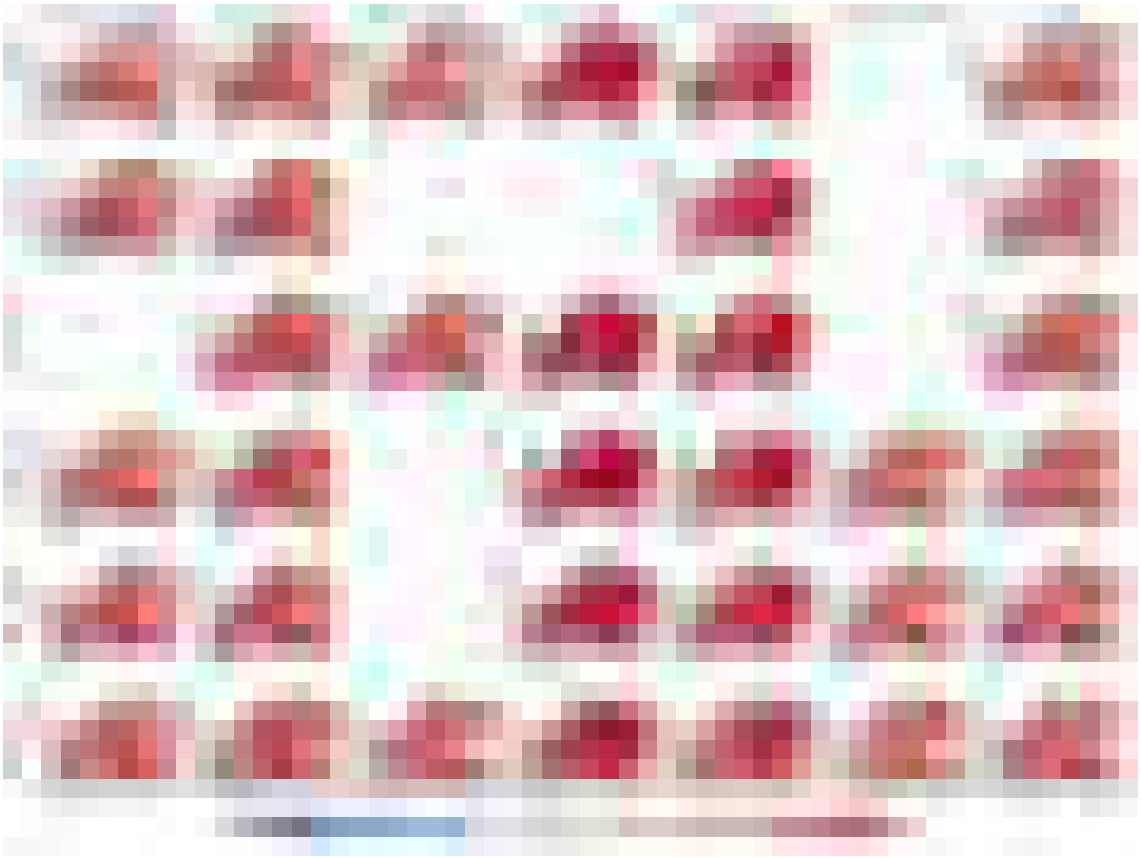

Figure 5.3: Same as in Figure 5.1, but for the 95th percentile of daily maximum wind speed.

correlation between the FWI bias at the 95th percentile and the biases of the four individual input fields was calculated for each model. Pearson correlation coefficients (ρ) summarizing these relationships are given in Table 5.1.

The Pearson spatial correlation coefficients (ρ) presented in Table 5.1 show that the biases in the 95th percentile of the maximum temperature, the number of dry days, and the 95th percentile of the maximum wind speed are positively correlated with the bias in the 95th percentile of FWI, while the bias in the 5th percentile of relative humidity is negatively correlated. The direction of these statistical relationships supports the physical understanding that extreme fire weather is associated with hot, dry, and windy conditions. However, disentangling the specific contributions of each variable to the overall FWI bias remains a challenge. On average, the bias in the number of dry days shows the strongest positive correlation with the FWI bias, with a mean correlation of 0.58 across all models. This is followed by the bias in the 5th percentile of relative humidity, which shows a mean negative spatial correlation of -0.5. Importantly, the range of spatial correlation values is wide, and individual models display different patterns. For some models, the FWI bias correlates most strongly with maximum wind speed, while for some others it aligns more closely with the number of dry days and relative humidity, with minor contributions from wind speed.

It is important to emphasize that these are spatial correlations across Europe and pertain only to extreme values; different results may be observed for other percentiles or at local scales. For example, Bedia et al. (2012) found that relative humidity and temperature have the highest influence

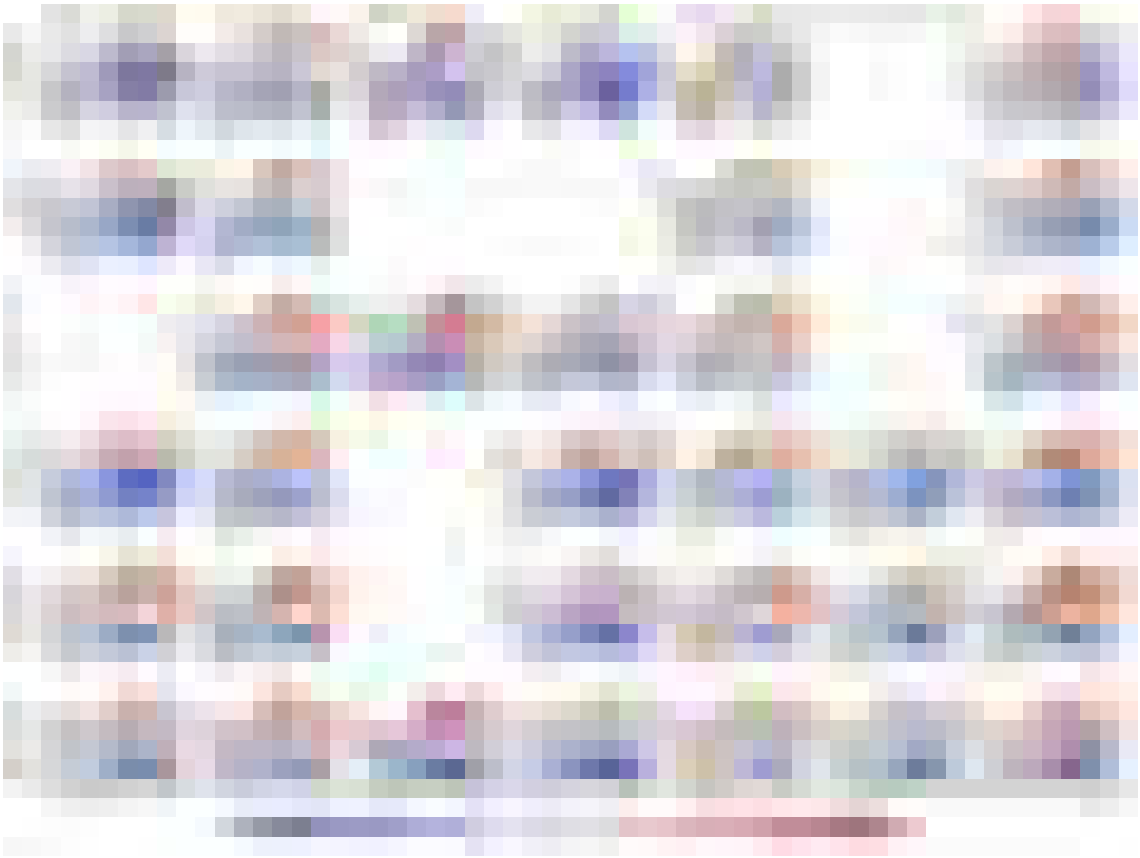

Figure 5.4: Same as in Figure 5.1, but for the 5th percentile of daily mean relative humidity.

on mean FWI in the Iberian Peninsula. In contrast, Dowdy et al. (2010) reported that the FWI was sensitive to wind speed in Australia. Note that the Pearson coefficients shown in Table 5.1 capture only linear spatial correlations and should be considered a first-order approximation of the actual complex relationships between FWI bias and biases in its input fields (consider that FWI bears a series of non-linear calculations in its formulation). Also note that the variables assessed here are selected indicators of the extremes and do not represent the full distributions.

Spatial correlation between	Mean ρ across all models [min. model, max. model]
FWI^{95} bias & tasmax^{95} bias	0.38 [0.14, 0.69]
FWI^{95} bias & no. of dry days bias	0.58 [0.33, 0.74]
FWI^{95} bias & hurs^{5} bias	-0.5 [-0.4, -0.68]
FWI^{95} bias & sfcWindmax^{95} bias	0.43 [0.01, 0.68]

Table 5.1: Spatial correlation between the bias in FWI 95th percentile of FWI and metrics representing the input fields. The variable names from the CMIP framework are used here: tasmax = daily maximum temperature, sfcWindmax = daily maximum wind speed, hurs = daily mean relative humidity.

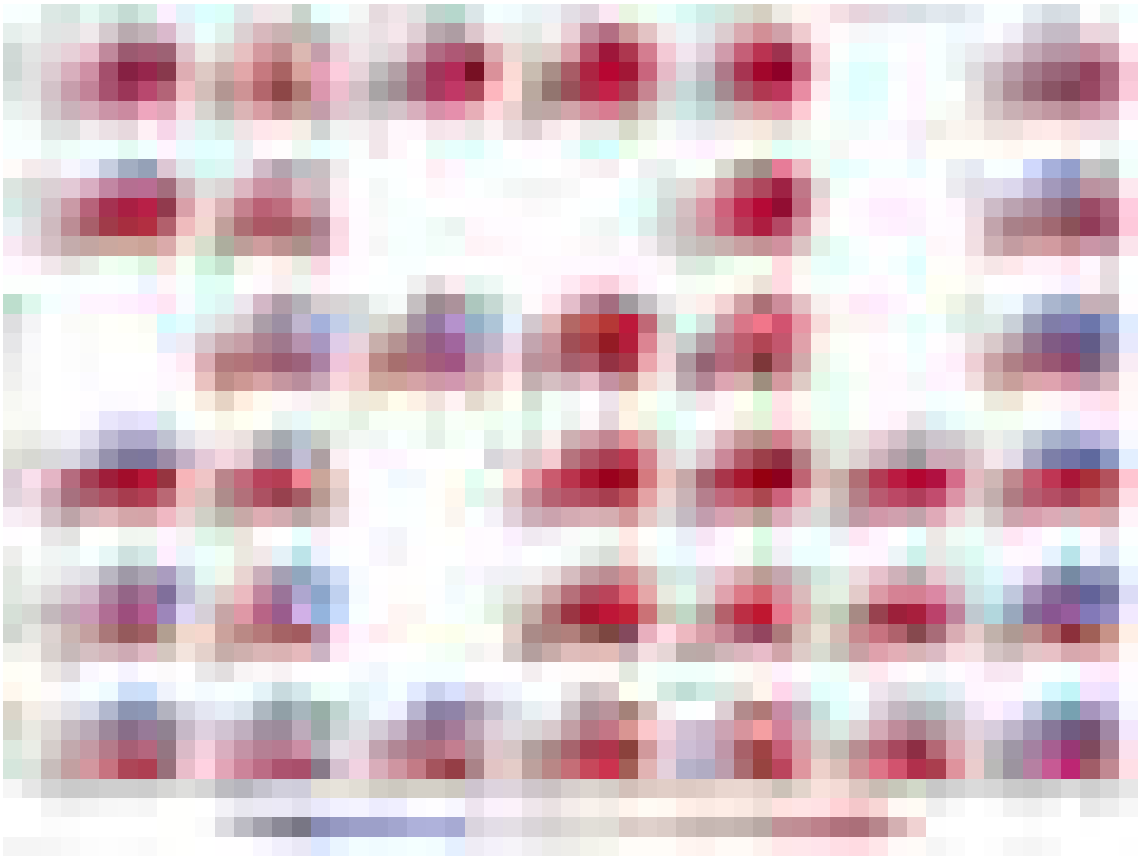

Figure 5.5: Same as in Figure 5.1, but for the 95th percentile of the FWI.

5.2 Evaluation of the Effect of Bias Adjustment on Model Performance

In this section, the effect of bias adjustment on model performance is discussed for the FWI and the input variables used in its calculation. All figures shown in this section represent the relative biases as in Section 5.1 but after the bias adjustment. The time period covered is the same as in Section 5.1, which also serves as the calibration period (1971-2000) for the bias adjustment. Although the performance of bias adjustment methods is typically evaluated using a separate validation period (e.g. Cannon et al. (2015)), this study focuses on evaluating model performance during the calibration period. There are two main reasons for this: 1) the historical simulations are not long enough to allocate a separate validation period for most of the EURO-CORDEX models, considering that 30 years of data have already been used for calibration; 2) the effect of bias adjustment on the FWI input fields is less critical than its effects on the FWI itself for the purposes of this study. Moreover, improvements in FWI performance may not match those of its components due to interdependencies and the non-linear nature of the FWI calculation. Therefore, demonstrating a significant improvement in FWI performance during the calibration period is also essential. In addition, a cross-validation strategy may not always provide reliable results when evaluating bias adjustment performance (Maraun and Widmann, 2018). This is because the internal variability of the climate system can dominate the differences between calibration and validation

periods, potentially leading to misleading evaluations, particularly in mid-latitudes, where dominant modes of variability can be as long as several decades (Maraun and Widmann, 2018).

Figure 5.6 shows the distribution of bias in the 95th percentile of daily maximum temperature for each GCM-RCM chain after bias adjustment. The bias adjustment substantially reduces the bias in the raw model outputs across Europe: the spatial mean absolute percentage bias across the 34 models is reduced to 0.5% (compared to 8% before bias adjustment), with inter-model variability also reduced to a range of 0.4% to 0.7%.

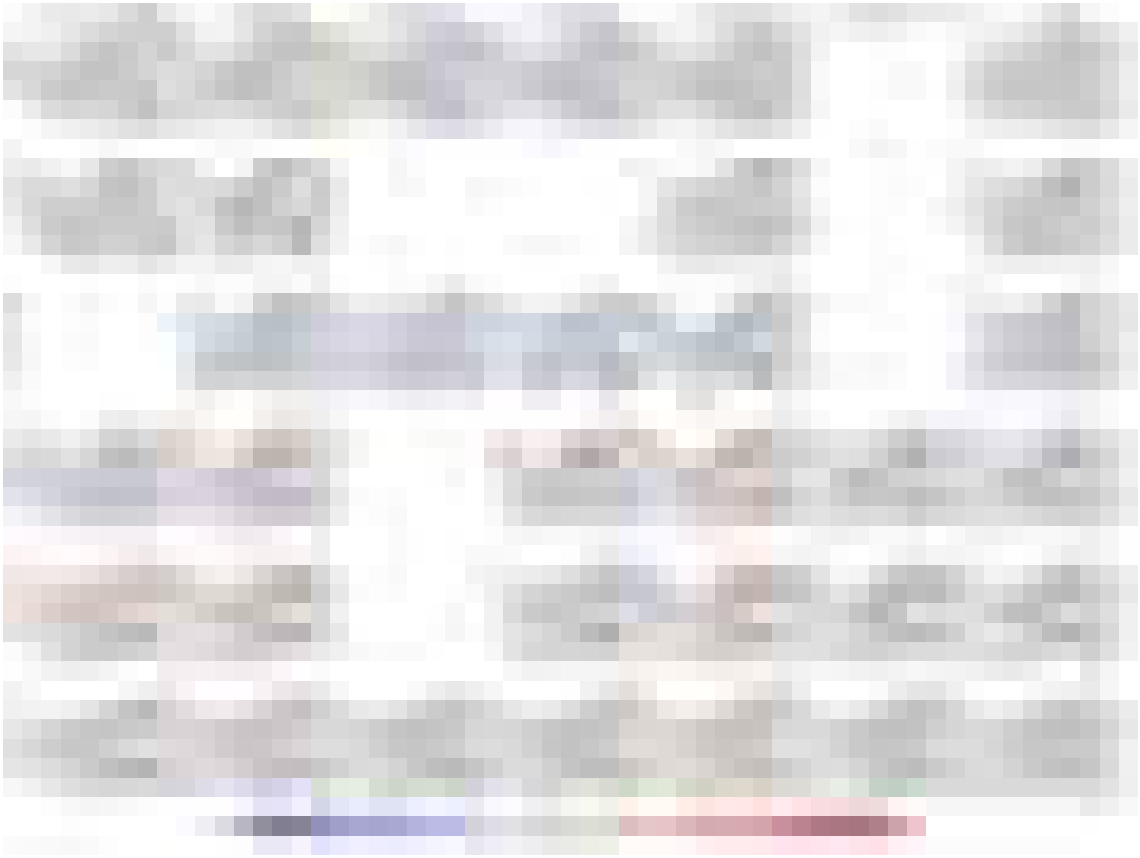

Figure 5.6: Relative percentage bias (%) in the 95th percentile of daily maximum temperature for EURO-CORDEX models after bias adjustment. Biases are relative to ERA5-Land for the period 1971-2000.

The distribution of bias in the number of dry days for each GCM-RCM pair after bias adjustment is shown in Figure 5.7. The bias adjustment performs well for precipitation - specifically, the number of dry days: the spatial mean absolute percentage bias across the ensemble is reduced from 8.1% to 0.7%. The spread of individual model biases is also narrower, ranging from 0.2% to 1.8%. It is also worth noting that the bias adjustment appears to smooth the fields, as the regional variability seen in the raw model outputs becomes less apparent after adjustment. However, this is partly due to the use of a fixed colorbar, which is deliberately selected to match that of the raw models to emphasize the improvement, though this comes at the expense of depicting less regional variability, particularly for the higher biases in Eastern Europe.

Figure 5.8 shows that biases in the 95th percentile of maximum daily wind speed are substantially reduced after bias adjustment. As shown in 5.3, the raw models were generally too windy, with

Figure 5.7: Same as in Figure 5.6, but for the number of dry days (defined as days with precipitation < 1 mm/day).

some exhibiting biases as high as 131.6%. The QDM method performs well in adjusting these biases, reducing the average spatial mean bias across models to just 0.3%. The inter-model spread is also significantly narrowed, ranging from 0.2% to 0.5%.

Figure 5.9 shows the distribution of bias in the 5th percentile of daily mean relative humidity for each GCM-RCM chain after bias adjustment. While the initial raw model biases were relatively low, they are further reduced after bias adjustment: the ensemble average drops to 0.5%, with individual model biases ranging from 0.3% to 0.9%.

In summary, the QDM method performs well, at least for the extreme climate metrics presented, in adjusting biases in the input variables used to compute FWI. However, the more important question for the purpose of this study is whether the improvements in the biases of individual variables are also reflected in the multivariate output: the FWI itself. To address this question, Figure 5.10 shows the distribution of bias in the 95th percentile of FWI for each bias-adjusted GCM-RCM chain. The raw ensemble exhibited an average bias of 100.9% (Figure 5.5), which is drastically reduced to 12.3% after bias adjustment of the input variables. The range of individual model biases is also significantly narrowed - from 50.2% - 199.8% before adjustment to 7% - 24.4% afterward.

Although the improvement in FWI bias is substantial, it still does not match the performance seen in the univariate components, where the average absolute biases are much lower. This discrepancy is particularly noticeable for the CLMcom-ETH-COSMO RCM (first column in Figure 5.10) in

Figure 5.8: Same as in Figure 5.6 but for the 95th percentile of daily maximum wind speed.

Eastern Europe. Spatial correlation analysis reveals that the remaining FWI biases for this model chain are primarily driven by the residual biases in the number of dry days, with spatial Pearson correlation coefficients ranging from 0.48 to 0.70. The spatial correlation coefficients for the other variables are mostly negligible. It is also worth noting that, although the bias in the number of dry days for these models in Eastern Europe is generally below 10%, the FWI exhibits biases as high as 100%. This highligts that despite the high spatial correlation, a single variable alone cannot predict the total impact on the output variable. Instead, there is a compounding bias effect that is difficult to trace back to individual variables. This is due in part to the complex structure of the FWI, which includes multiple subcomponents which are themselves calculated by the atmospheric input fields (e.g., DC is calculated using temperature and precipitation).

The compounding bias effect may also stem from the fact that QDM does not account for biases in the inter-variable dependencies among the components. To address this, a multivariate bias adjustment method could be used to adjust these dependencies (François et al., 2020), which could theoretically lead to reduced bias in FWI. As a proof of concept, a multivariate bias adjustment method (MBCn) was applied to a smaller domain in Eastern Europe (Figure 5.10), where significant FWI bias remained after QDM adjustment. Due to the higher computational cost of MBCn, and because a full evaluation of different methods is beyond the scope of this thesis, it was applied only to the first model chain, CNRM-CM5-CLMcom-ETH-COSMO, which still exhibited residual bias after QDM.

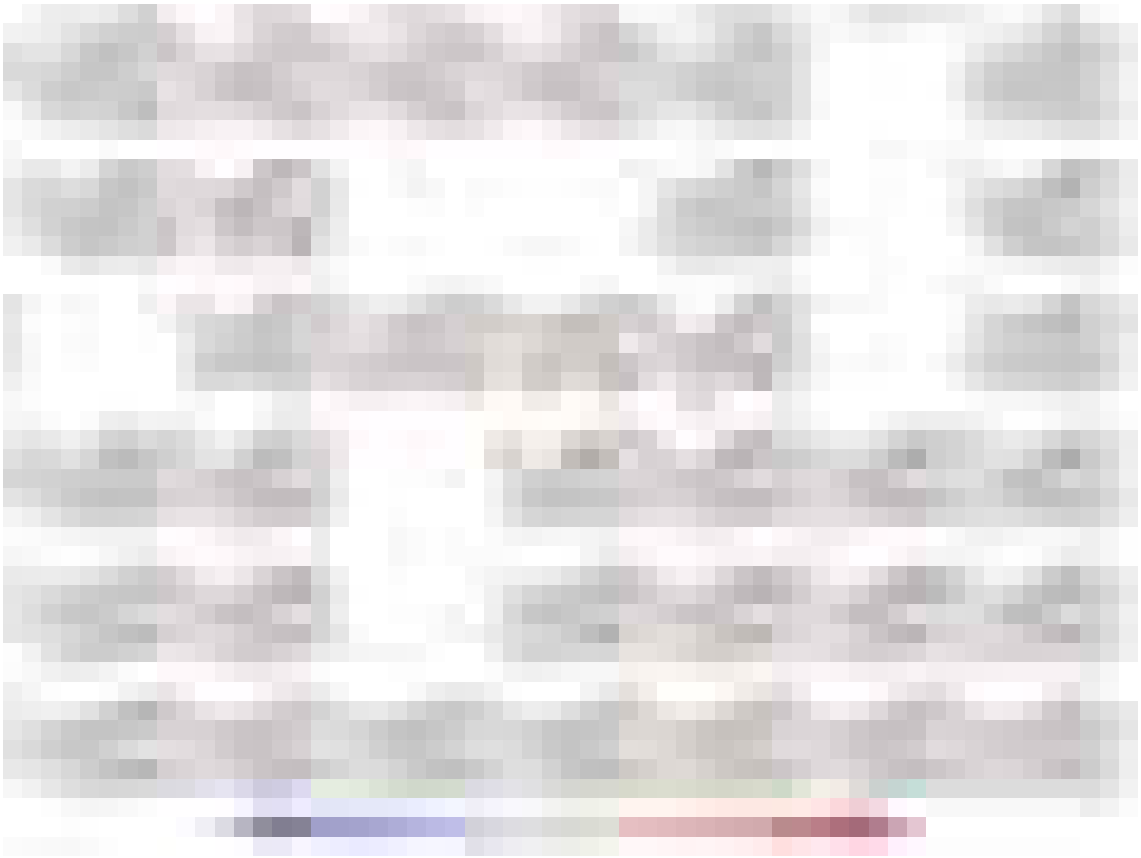

Figure 5.9: Same as in Figure 5.6, but for the 5th percentile of daily mean relative humidity.

Figure 5.11 compares the bias in the 95th percentile of FWI relative to ERA5-Land over the smaller domain, using the QDM and MBCn bias adjustment methods. For this model chain, QDM shows a significant bias in the region, exceeding 100% in some areas, particularly over the Carpathian Mountains. MBCn reduces the bias substantially, yet it still struggles to fully adjust it over the mountainous region. It is important to note, however, that FWI values in the mountains are already quite low even at the 95th percentile (below 10). As a result, even small absolute differences can lead to large relative biases. Additionally, the MBCn implementation used here does not include a correction for the seasonal cycle as QDM does; hence, there is still a possibility to further improve the performance. Nevertheless, as previously discussed, the higher computational cost of MBCn limits its practical application over a larger domain and for a large ensemble. Therefore, for the purposes of this study, the significant bias reduction achieved by QDM across the larger domain is considered sufficient to perform the rest of the study, and all subsequent analysis shown in the later sections are based on the QDM-adjusted simulations.

To summarize the results of the univariate QDM approach, Figure 5.12 presents the biases in the 95th percentile of FWI for both the raw and bias adjusted ensemble medians. Consistent with the individual model results shown in Figure 5.10, the ensemble median bias is also substantially reduced. The spatial mean of the absolute relative percentage bias is 78.2% before adjustment, with particularly large biases found south of the 50° latitude and in Norway. After bias adjustment, this spatial mean bias of the ensemble median is reduced to 8.6%, with significant improvements observed in regions where the raw ensemble median previously exhibited large biases. However,

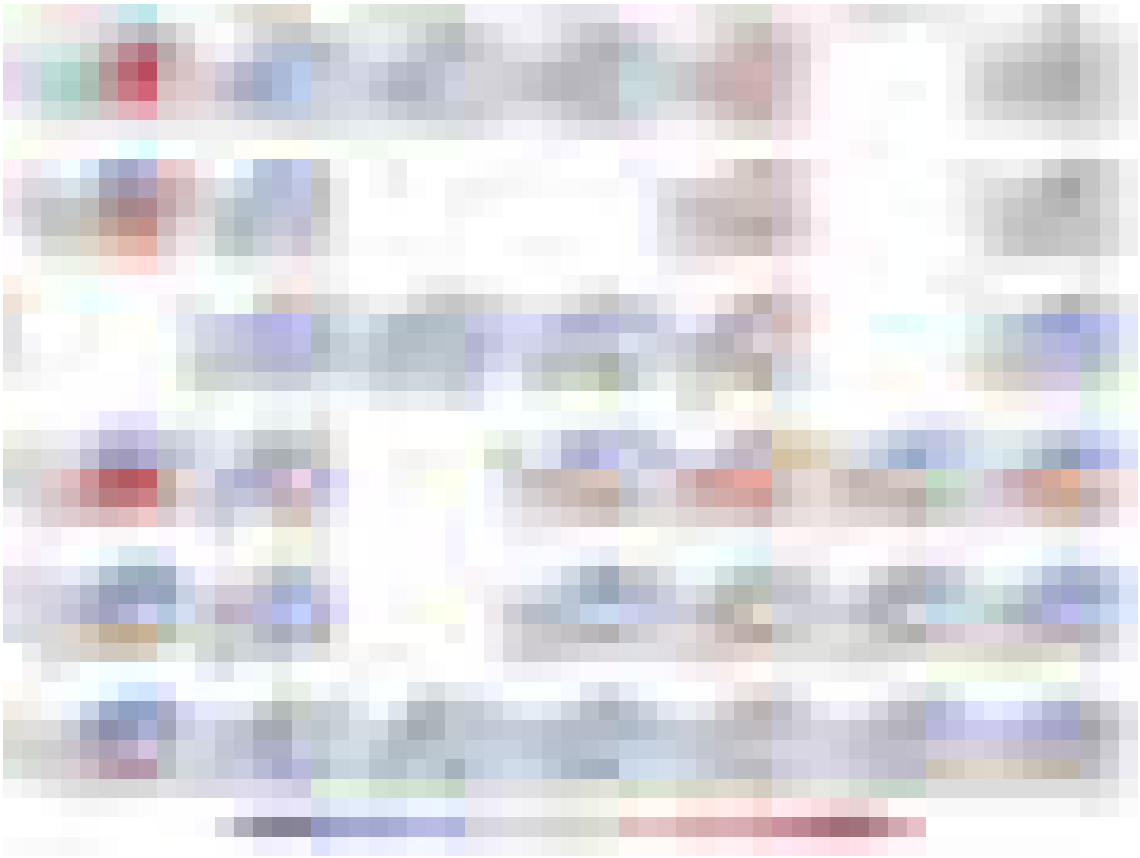

Figure 5.10: Same as in Figure 5.6, but for the 95th percentile of the FWI.

some grids still exhibit high biases, especially in mountainous areas, such as parts of the Alps, Carpathians and Caucasus Mountains. This requires further investigation, though one possible explanation is the limited number of iterations (20) used in this study, which may not have been sufficient to ensure convergence in those complex regions. Also,it is important to note that the FWI values in mountainous regions are already quite low, so expressing biases in relative percentage terms makes the situation appear worse than it actually is.

Figure 5.11: Relative percentage bias (%) in the 95th percentile of daily maximum temperature for the model chain CNRM-CM5-CLMcom-ETH-COSMO. Biases are relative to ERA5-Land and for the period 1971-2000. Note that this is a smaller domain compared to the rest of the study.

Figure 5.12: Relative percentage bias (%) in the 95th percentile of FWI for EURO-CORDEX models after bias adjustment.

6 Projections of Exteme Fire Weather in Europe

This chapter explores the evolution of FWI metrics in Europe at 2 °C and 3 °C GWLs based on the bias-adjusted EURO-CORDEX simulations. It then provides insights into the significance and robustness of these changes, regional differences across Europe, and potential drivers based on the subcomponents of the FWI system.

6.1 Evolution of FWI Metrics under Climate Change

Europe is projected to experience warmer summer climates across all regions, with a particular tendency towards increased drying in the southern and western regions (Bayar et al., 2023). The observed trends in extreme fire weather, as discussed in Section 4.3, make it reasonable to expect further changes under these amplified global warming conditions. Therefore, the changes in FWI metrics introduced in Section 3.2.5 are explored in this section under different GWLs in Europe.

Figure 6.1 shows the number of days per year that exceed the 95th percentile FWI (FWI_{95d}) during the reference period (1971-2000), along with the relative changes compared to the reference period at 2 °C and 3 °C GWLs. The top panel displays the climatological distribution of FWI_{95d} during 1971-2000. Here, it is important to note that the spatial distribution of FWI_{95d} during the reference period would be nearly uniform with around 18 days year^{-1} everywhere if FWI were calculated continuously, since the 95th percentile is calculated locally for each grid. However, this is not the case here, as overwintering of the DC interrupts the continuous FWI calculation and only calculates FWI during the fire season, which is defined based on a temperature threshold[1]. Therefore, the latitudinal differences in FWI_{95d} are a natural consequence of this calculation. More days exceed the local 95th percentile at lower latitudes, primarily because the fire season is longer (as defined by Wotton and Flannigan (1993)). In the Iberian Peninsula and some other regions in southern Europe, there are about 18 days year^{-1} of FWI_{95d}, indicating that the fire season defined by the temperature threshold lasts almost the entire year.

The lower panels of Figure 6.1 show the projected percentage changes in FWI_{95d} relative to the reference period at 2 °C and 3 °C GWLs. At 2 °C, changes are mainly confined to southern Europe, with only 25% of the total land area in the domain exhibiting significant and robust signals. In

[1] The fire season begins when the maximum temperature exceeds 12 °C for at least three consecutive days and ends when the maximum temperature drops below 5 °C for at least three consecutive days (Wotton and Flannigan, 1993; Quilcaille et al., 2023).

contrast, at 3 °C, significant and robust signals are projected to extend into central Europe, covering 47% of the total land area. In addition, the strength of the signal becomes much more pronounced at 3 °C, with relative increases exceeding 150% in many regions, such as the Iberian Peninsula, southern France, the Balkans, and Turkey. For example, this would translate to nearly 30 additional days of extreme fire weather conditions in the Iberian Peninsula. Even regions with historically low frequencies of extreme fire weather, such as northern Europe, show increases of up to 50%. However, these increases are not statistically significant or model agreement is not well established due to uncertainty in the signal. In areas where at least 66% of the models agree on the direction and significance of the change, the mean relative increase in FWI_{max} is 91% and 147%, respectively, at 2 °C and 3 °C GWLs. Overall, a general increase in fire weather conditions is projected across Europe, with the magnitude and spatial extent of changes becoming much more pronounced at 3 °C compared to 2 °C. However, robust changes are mostly confined to ares south of 50° latitude even at 3 °C.

Figure 6.1: Number of days per year exceeding the 95th percentile FWI (FWI_{95d}) for the reference period and two GWLs based on the bias-adjusted EURO-CORDEX ensemble simulations. The top panel shows FWI_{95d} during the reference period (1971-2000). The bottom panels show changes in FWI_{95d} at 2 °C and 3 °C GWLs relative to the reference period. Note that the reference period is already 0.46 °C warmer than the preindustrial period. Non-hatched areas indicate where at least 66% of the models show statistically significant changes according to t-test ($p < 0.05$) and agree on the sign of change.

Fire weather season length (FWI_{fwsl}) is another important metric that commonly used in the literature to estimate the impacts of climate change on wildfire danger (e.g., (Jolly et al., 2015; Abatzoglou et al., 2019)). Figure 6.2 shows the FWI_{fwsl} in Europe during the reference period, along with relative changes compared to the reference period at 2 °C and 3 °C GWLs. The top panel displays the climatological FWI_{fwsl} for 1971-2000, which shows longer fire seasons in southern Europe, particularly in the Iberian Peninsula, southern Italy, Greece and Turkey, with more than

60 days year^{-1}. In contrast, central and northern Europe experience shorter fire seasons. Since these values are lower than expected, it is important to distinguish between different methods for calculating the duration of the fire season. As explained above, Wotton and Flannigan (1993) defines the fire season based on a temperature threshold, which often leads to an overestimation of fire season length, especially in southern Europe due to higher temperatures. In contrast, Jolly et al. (2015) define FWI_{fwsl} as the number of days when FWI exceeds its midrange value (the average of maximum and minimum values). Here, the definition of Jolly et al. (2015) is followed, as in many other studies (Abatzoglou et al., 2019; Jones et al., 2022). However, this approach possibly underestimated the actual FWI_{fwsl} in some regions, likely because overwintering the DC reduces the number of days with an available FWI value throughout the year due to the condition of Wotton and Flannigan (1993) during overwintering. Therefore, the focus in this figure should be on the relative changes at 2 °C and 3 °C rather than the absolute values of FWI_{fwsl}.

Figure 6.2: Same as in Figure 6.1, but for fire weather season length (FWI_{fwsl}).

The lower panels of Figure 6.2 illustrate the projected changes in FWI_{fwsl} at 2 °C and 3 °C relative to the reference period. At 2 °C, increases in FWI_{fwsl} are already evident in some regions, with a signal of up to 100% in areas like parts of the Balkans. Similar to Figure 6.1, the increase in FWI_{fwsl} becomes more widespread and intense at 3 °C, particularly in central Europe and southern France, with a relative increase exceeding 150%. There are almost no regions exhibiting a negative change in FWI_{fwsl} at either GWLs (except for a small area in northern Poland). The projected mean relative change in FWI_{fwsl} for the grids where the models agree on both the sign and significance of the change is lower than that for FWI_{95d}: 49% at 2 °C and 90% at 3 °C. Most of this signal is confined to regions south of 50° latitude, with a robust signal simulated in 27% and 49% of the land area, respectively, at 2 °C and 3 °C.

In addition to projections of the frequency of extreme fire weather, as shown in Figures 6.1 and 6.2, it is also important to quantify the projected changes in the magnitude of extreme fire weather. Figure 6.3 shows the climatological annual maximum FWI (FWI_{max}) during the reference period and the projected changes relative to this period. Similar to the frequency metrics, the top panel displays the latitudinal gradient in FWI_{max}, with higher values exceeding 40 observed in southern Europe and lower values, usually below 20, observed in central to northern Europe. Mountainous regions, such as the Alps and Carpathians, exhibit very low FWI_{max} values, reflecting their colder and moister climates compared to the surrounding areas. In southern Europe, regions like the Iberian Peninsula and Turkey have FWI_{max} values greater than 50, indicating that these areas experience extreme fire weather conditions annually.

Figure 6.3: Same as in Figure 6.1, but for annual maximum FWI (FWI_{max}).

The lower panels in Figure 6.3 show the projected changes in FWI_{max} at 2 and 3 °C GWLs relative to the reference period. At 2 °C, the simulated positive changes are relatively small (around 10-20%). Central and northern Europe show spatial variability, including negative changes in some regions (e.g., Poland), although these are not robust signals. Only 8% of the land area shows model agreement on the direction and significance of the change at 2 °C, and these areas are mostly limited to regions with very low climatological FWI_{max} values. In contrast, at 3 °C, the percentage of land area where the majority of models have robust climate change signals increases sharply to 39%. However, these areas are still primarily in regions with low climatological values (e.g., mountainous regions), with the exception of some parts of Southern Europe, such as Italy and the Balkans, where projected increases range from 20% to 40%. Overall, in regions where model agreement on the direction and significance of the change signal is established, the simulated mean increase in FWI_{max} is 25% and 32% relative to the reference period, respectively, at 2 and 3 °C.

As another metric of the magnitude of fire weather conditions, Figure 6.4 shows the annual peak 90-day average FWI (FWI_{fs}) during the reference period and the projected changes relative to it at 2 °C and 3 °C GWLs. The top panel is consistent with the rest of the figures, with high FWI_{fs} values concentrated mainly in southern Europe due to hot and dry summer conditions. In regions such as the Iberian Peninsula, southern Italy, Greece and Turkey FWI_{fs} values exceed 30, approaching the very high fire danger threshold of 38 accepted by EFFIS (see Table 7.1). Since this threshold represents daily conditions, encountering these values in a running mean average indicates that high fire danger conditions are prevalent in these regions.

The lower panels of Figure 6.4 illustrate the projected relative changes in FWI_{fs} under 2 °C and 3 °C GWLs. At 2 °C, most of Europe is projected to experience a relative increase in FWI_{fs}, with the exception of regions such as Poland and northern Scandinavia. However, many areas still lack model agreement on the significance or direction of the change, with only 24% of the land area showing robust signals. At +3 °C, FWI_{fs} becomes more widespread and intense, following the same pattern seen in other metrics. It is projected to increase by more than 50% (with robust signals) not only in southern and eastern Europe, but also in regions that historically exhibited lower fire danger, such as central France and western Germany. The percentage of land area with model agreement also increases to 43% at 3 °C. The spatially averaged relative increase in FWI_{fs} for regions with model agreement on the robustness is also projected to increase as the GWL increases: 23% at 2 °C and 44% at 3 °C.

Figure 6.4: Same as in Figure 6.1, but for annual peak 90-day average FWI (FWI_{fs}).

In summary, fire weather is projected to become more widespread and intense as the mean surface temperature continues to rise. Southern and Eastern Europe are projected to be more susceptible to these changes with robust signals, but central Europe is also projected experience increased

susceptibility, particularly at 3 °C GWL. The next section focuses more closely on regional differences, by summarizing the results over the PRUDENCE regions.

6.2 Projected Changes over PRUDENCE Regions

In Section 6.1, extreme fire weather metrics (FWI_{95d}, FWI_{fwsl}, FWI_{max}, FWI_{fs}) and their projected evolution under climate change are presented in spatial detail at the EURO-CORDEX grid resolution. Figure 6.5 shows the same fire weather metrics, but aggregated and averaged over the PRUDENCE regions highlight differences between the European subregions and show the spread across the model ensemble. The results are displayed as boxplots for each PRUDENCE region during the reference period (1971-2000), at 2 °C and 3 °C GWLs. The regions are ordered by latitude to clarify differences in baseline climatologies.

Across all metrics and regions, a clear upward trend in extreme fire weather is projected as global mean surface temperature increases, albeit with notable regional differences. In general, southern European regions (MED, IP, TR) are projected to experience more intense and prolonged extreme fire weather conditions, consistent with their baseline climatologies of dry and warm summers. However, these changes are not limited to the southern regions; almost all regions are projected to experience worsening fire weather conditions, particularly at 3 °C GWL.

FWI_{95d} shows a quasi-uniform distribution across models in all PRUDENCE regions, due to the definition of the metric (Figure 6.5, top-left panel). FWI_{95d} measures the number of days exceeding the 95th percentile based on the local FWI distribution regardless of the absolute values. Since overwintering of the DC limits FWI calculation to the fire season, the expected value of around 18 days year^{-1} (5% of 365 days) is not observed consistently across regions. Since input temperature fields are bias adjusted, it is reasonable to assume that this adjustment effectively determines the start and end of the fire season (i.e., days above the temperature threshold) and thereby reduces model-to-model differences.

Under both warming scenarios, the median FWI_{95d} is projected to increase across all regions with a stronger signal at 3 °C. In the Iberian Peninsula, for example, FWI_{95d} is projected to increase rapidly from a median of 16.8 days year^{-1} during 1971-2000 to 31 days year^{-1} at 2 °C and 44.7 days year^{-1} at 3 °C (Figure 6.5, top-left panel). A similar trend is projected for France, with the median increasing from 14.5 days year^{-1} during 1971-2000 to almost 23 days year^{-1} at 2 °C and 34.5 days year^{-1} at 3 °C. In some regions, such as Eastern Europe (EA), the model spread is relatively large, with some models projecting a change, and some projecting a very extreme positive change. The model agreement is stronger in southern European regions (MD, IP, TR), where all models project a positive trend under both 2 °C and 3 °C GWLs. In addition, the spread among models increases from 2 °C to 3 °C in all regions, indicating a growing uncertainty with higher levels of warming.

There is a clear regional separation in both the reference period and projected values of FWI_{fwsl}, with southern European regions (MD, IP, TR) showing higher values than the rest of Europe (Figure 6.5, top-right panel). However, a positive change signal is evident across all regions, especially

at 3 °C GWL. In the Alps, a region historically characterized by shorter fire seasons, the median FWI_{fwsl} is projected to more than double: 14.3 days year^{-1} during 1971-2000, to over 21 days year^{-1} at 2 °C, and more than 31 days year^{-1} at 3 °C. The Iberian Peninsula is projected to experience the highest absolute increase in median FWI_{fwsl}, rising from 43.3 days year^{-1} during 1971-2000 to a projected +20 days year^{-1} at 2 °C and almost +35 days year^{-1} at 3 °C.

Figure 6.5: Four FWI metrics (FWI_{95d}, FWI_{fwsl}, FWI_{max}, FWI_{fs}) spatially aggregated and averaged over the PRUDENCE regions during the reference period, +2 °C GWL and +3 °C GWL based on the bias-adjusted EURO-CORDEX ensemble. The whiskers in the boxplots represent the upper and lower extremes (1.5 times the inter-quartile range) of the ensemble and circles denote outliers. The PRUDENCE regions are ordered by latitude. SC: Scandinavia, BI: British Isles, ME: Mid-Europe, EA: Eastern Europe, FR: France, AL: Alps, MD: Mediterranean, IP: Iberian Peninsula, TR: Turkey.

A clear latitudinal gradient is observed in the magnitude of FWI_{max} during the reference period and at both 2 °C and °C GWLs with southern European regions exhibiting higher fire danger due to their warm and dry summer climates in summer (Figure 6.5, bottom-left panel). The main exception to this latitudinal pattern is the Alps, which naturally shows lower values due to its colder and moister climate conditions. Overall, the median FWI_{max} is projected to increase consistently across all regions as the GWL increases. However, the projected relative changes in FWI_{max}, a magnitude-based metric, are not as pronounced as those seen in the frequency-based metrics (FWI_{95d} and FWI_{fwsl}). The Mediterranean, Iberian Peninsula, and Turkey clearly stand out from other regions. For instance, Turkey shows a simulated median FWI_{max} of 49 during 1971-2000, projected to increase to 54 at 2 °C and 58 at 3 °C.

The FWI_{fs} is also projected to follow a similar pattern to FWI_{max} with a clear latitudinal gradient in fire danger (Figure 6.5, bottom-right panel). However, the distribution ranges for FWI_{fs} are narrower than those for FWI_{max}, particularly in northern and central European regions. This is

likely due to the running mean calculation used for FWI_{fs}, which reduces the influence of outlier days. The intensity of prolonged fire weather, as represented by FWI_{fs}, is projected to increase in all regions. For example, the median FWI_{fs} in the Mediterranean is projected to increase from 15 during 1971-2000 to 18 and 21 at 2 °C and 3 °C GWLs, respectively.

In summary, all four fire weather metrics examined in this study are projected to increase as surface temperatures continue to rise, with more pronounced changes at 3 °C GWL compared to 2 °C. Overall, the relative change signals are stronger for the frequency-based metrics (FWI_{95d} and FWI_{fwsl}) than for the magnitude-based metrics (FWI_{max} and FWI_{fs}). A clear latitudinal gradient is also observed, with southern European regions projected to experience more severe and frequent fire weather conditions. Furthermore, the ensemble spread increases from 2 °C to 3 °C GWL, particularly for the frequency-based metrics, indicating greater uncertainty at higher warming levels.

6.3 Decomposition of FWI Projections into Drivers

Extreme fire weather conditions across Europe are projected to become more frequent and intense, as shown in the previous sections. However, the underlying drivers of these changes remain uncertain as the final impact results from the interaction of many factors. To provide insight into this question, the main subcomponents of the FWI system can be examined: BUI, which represents longer-term fuel dryness conditions, and ISI, which reflects short-term variations in fuel moisture and wind speed. Figure 6.6 illustrates the relationship between FWI, ISI and BUI across PRUDENCE regions, based on spatially aggregated fields from the bias-adjusted EURO-CORDEX models. The ISI–BUI pairs correspond to days when FWI exceeds its 99th percentile during the reference period (1971–2000), as well as at 2 °C and 3 °C GWLs. Overlaid contour lines represent theoretical FWI isolines as a function of ISI and BUI, helping to interpret how shifts in these components contribute to changes in extreme fire weather conditions.

As GWL increases, there is a clear projected shift in BUI towards higher values in all regions (Figure 6.6). This shift is particularly evident in the northern and central European regions (top row), where the projected increase in the 99th percentile of FWI is mainly driven by the rising BUI values, indicating increased fuel dryness. In the regions EA, FR and AL (second row), there is also a notable shift in BUI, along with a slight increase in ISI, both of which contribute to the resulting FWI. In particular in France, the median BUI is projected to increase by almost 50% at 3 °C relative to the reference period, while ISI increases only by around 25%. The increase in BUI is also apparent in the southern European regions. However, this does not directly translate into an increase in FWI in those areas. This is because in the FWI calculation, the contribution of BUI saturates at high values, which is consistent with the principle that there is a limit to the amount of fuel that can be used in fires (Van Wagner, 1987). Specifically, FWI reaches 90% of its potential value at a BUI of 160, beyond which further increases in BUI do not strongly influence FWI, which is also evident in Figure 6.6 (Van Wagner, 1987) (see Section 3.2.3 for a detailed explanation). This effect is clearly seen in southern European regions, where BUI values during the reference period

Figure 6.6: FWI as a function of ISI and BUI, with FWI contours overlaid. Circles show ISI and BUI averages on days when FWI exceeds its 99th percentile during the reference period 1971-2000 (blue), at 2 °C GWL (green) and at 3 °C GWL (red). All values are spatially aggregated and averaged over the PRUDENCE regions. Each circle corresponds to a bias adjusted EURO-CORDEX model; crosses indicate ensemble medians. The PRUDENCE regions are ordered by latitude. SC: Scandinavia, BI: British Isles, ME: Mid-Europe, EA: Eastern Europe, FR: France, AL: Alps, MD: Mediterranean, IP: Iberian Peninsula, TR: Turkey.

are already very high. As a result, further increases in BUI do not significantly affect FWI. Instead, in these regions, the projected increase in FWI is driven by a projected increase in ISI values, which may result from increased surface layer dryness (reflected by FFMC) or stronger winds.

To disentangle the contributions of wind speed and fuel dryness, Figure 6.7 shows vapor pressure deficit (VPD) plotted against maximum wind speed across PRUDENCE regions. The VPD-wind speed pairs correspond to days when FWI exceeds its 99th percentile during the reference period (1971–2000), as well as at 2 °C and 3 °C GWLs. The median of maximum wind speeds are projected to either decrease or remain unchanged across all PRUDENCE regions, except in southern Europe, where a very slight increase is projected which is likely negligible. In contrast, the median VPD, which reflects the thermodynamic effects of temperature and relative humidity through atmospheric drying, increases across all regions, with particularly strong increases in central and southern Europe. This suggests that the projected changes in FWI are primarily driven by increased fuel aridity due to thermodynamic drivers rather than by stronger winds. This may also indicate that the projected changes in ISI are largely influenced by increased surface layer fuel dryness (FFMC), rather than wind speed; however, this requires further investigation for confident attribution.

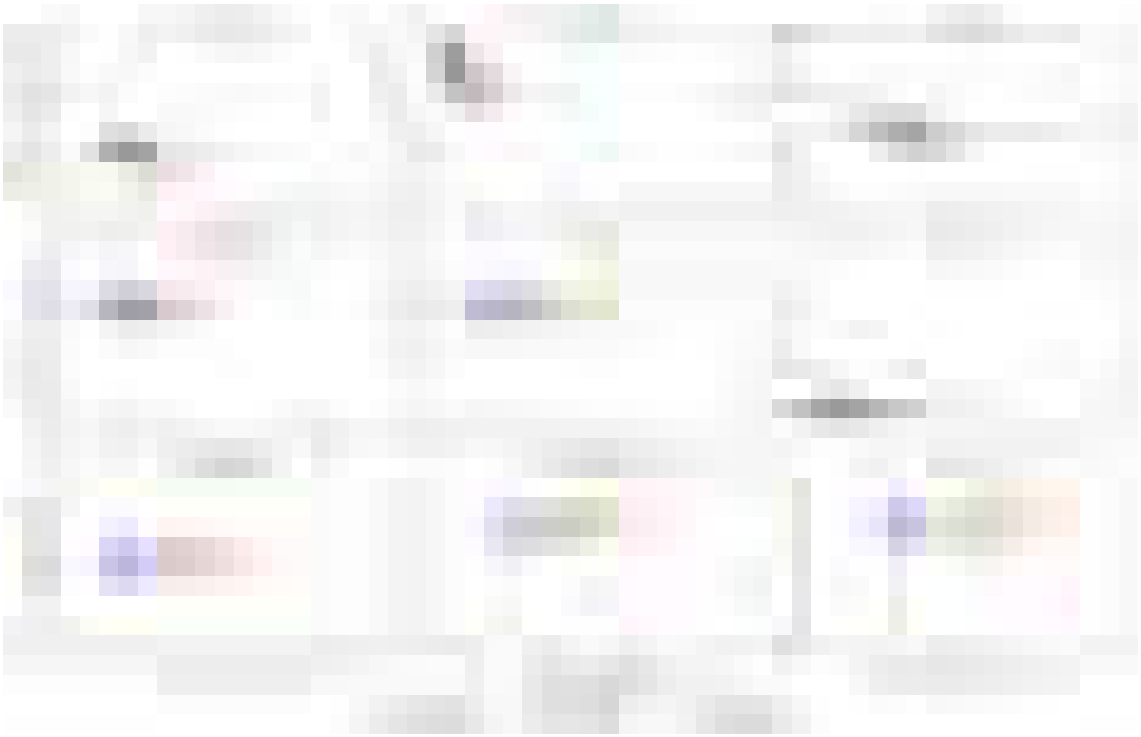

Figure 6.7: VPD (hPa) vs. maximum wind speed (km/h). Circles show VPD and maximum wind speed averages on days when FWI exceeds its 99th percentile during the reference period 1971-2000 (blue), at 2 °C GWL (green) and at 3 °C GWL (red). All values are spatially aggregated and averaged over the PRUDENCE regions. Note that the VPD values are likely overestimated, as they are calculated using maximum temperature and relative humidity. Each circle corresponds to a bias adjusted EURO-CORDEX model; crosses indicate ensemble medians. The PRUDENCE regions are ordered by latitude. SC: Scandinavia, BI: British Isles, ME: Mid-Europe, EA: Eastern Europe, FR: France, AL: Alps, MD: Mediterranean, IP: Iberian Peninsula, TR: Turkey.

7 Discussion and Conclusions

This thesis aims to investigate the impact of climate change on extreme fire weather in Europe under current and projected future conditions. It also evaluates the performance of EURO-CORDEX RCMs and the potential improvements offered by bias adjustment. Chapter 4 analyzes historical trends in the FWI based on ERA5-Land reanalysis data. Chapter 5 evaluates the performance of the EURO-CORDEX ensemble's input fields and FWI, as well as the added value of bias adjustment. Chapter 6 explores projected changes in extreme fire weather at 2 °C and 3 °C GWLs and investigates the potential drivers of these changes. This final chapter addresses the main research questions by synthesizing the key findings from each chapter, followed by a broader discussion of wildfires in a changing climate and concludes with an outlook on future directions.

7.1 Overview of Key Findings

7.1.1 Observed Trends in Extreme Fire Weather

Research Question 1: What is the observed climatology of the frequency and intensity of extreme fire weather across Europe and what are the associated trends since 1950?

In Chapter 4, the most suitable combination of input variables for approximating the original noon-time FWI calculation at daily resolution was first identified, as many RCMs do not provide sub-daily outputs. Maximum temperature, accumulated precipitation, mean relative humidity, and maximum wind speed were selected based on their relatively lower bias in the resulting FWI calculations and broader model availability in the EURO-CORDEX framework. This input combination was used consistently throughout the study FWI computation.

Subsequently, an analysis of the historical climatology based on the ERA5-Land reanalysis data for the period 1950-2023 revealed a notable latitudinal gradient in extreme fire weather danger, with more extreme values occurring in southern Europe. Trend analysis showed that 29% and 37% of the land area exhibited significant trend in FWI_{max} and FWI_{95d}, respectively. Nearly all grid cells with significant trends showed positive changes, except for a few in the Eastern Mediterranean. The majority of the significant trends for both metrics were concentrated in the Iberian Peninsula, Central Europe, and Ukraine.

7.1.2 Evaluation of Model Performance and Bias Adjustment

Research Question 2: To what extent do bias adjustment methods improve model performance and spatial patterns of bias in the input meteorological fields and the FWI within the EURO-CORDEX multi-model ensemble?

In Chapter 5, the spatial patterns of bias in the extreme quantiles of input variables from EURO-CORDEX RCMs were evaluated against ERA5-Land reanalysis. The models exhibited substantial biases, with distinct patterns for each variable. Visual inspection of the GCM-RCM matrix suggested that the choice of RCM had a greater qualitative influence on bias patterns than the driving GCM. Biases in the input fields compounded in the calculation of FWI, with spatial mean absolute relative biases reaching up to 200% for some models, notably higher than those observed for any individual input variable.

Following the application of univariate QDM bias adjustment, biases in the input fields were substantially reduced, at least within the calibration period. Calculating the FWI from these bias-adjusted input fields also yielded significantly improved estimates. Although the biases in the individual input variables were reduced to near-zero levels, the resulting FWI still retained some residual bias. Nevertheless, the spatial mean bias of the ensemble median FWI decreased from 78% to below 9% after QDM adjustment of the input fields.

As a proof of concept, a multivariate bias adjustment method called MBCn was applied to a single model over a smaller subdomain where QDM had underperformed. Compared to QDM, MBCn method produced improved results. However, due to time and computational constraints, and since QDM yielded a sufficiently low bias for the purposes of this study, the QDM-adjusted version of the FWI was used for all future projections. Here, it is important to note that QDM adjustment was applied to the input variables, not directly to the FWI itself.

7.1.3 Extreme Fire Weather in Europe in a Changing Climate

Research Question 3: How do the frequency and intensity of extreme fire weather change at 2 °C and 3 °C GWLs, based on the bias-adjusted EURO-CORDEX multi-model ensemble? What are the potential drivers underlying these changes?

In Chapter 6, projections of the frequency and magnitude of extreme fire weather were assessed using the bias-adjusted EURO-CORDEX models at 2 °C and 3 °C GWLs. Extreme fire weather is projected to become more spatially extensive, more frequent, and more intense with increasing GWL. Relative increases in frequency-based extreme fire weather metrics are larger than those for magnitude-based metrics. The spatial extent of robust signals nearly doubles at 3 °C GWL compared to 2 °C, except for FWI_{max}, for which the area showing robust change increases almost fivefold. Note that robustness is defined using a strict criterion: a projected signal is considered robust only when at least 66% of the models agree on both the sign and the statistical significance of the change.

A latitudinal gradient is evident in both present-day and projected fire weather danger, southern European regions (the Iberian Peninsula, the Mediterranean, and Turkey) expected to experience longer and more intense fire weather conditions. The frequency and magnitude of extreme fire weather are also projected to increase in regions such as France, the Alps, Eastern Europe, and Mid-Europe, particularly at 3 °C GWL. The uncertainty (i.e., model spread) in projected changes increases from 2 °C to 3 °C GWL. It is important to note that projected changes in FWI do not always directly correspond to actual fire danger, as the relationship between FWI and fire occurrence — and the thresholds for what constitutes extreme — can vary regionally.

The subcomponents of the FWI system, namely the BUI and the ISI, were also examined to identify potential drivers of projected changes in FWI. BUI, which represents long-term fuel dryness and the potential amount of fuel available for consumption, is projected to increase with rising GWLs across all PRUDENCE regions. ISI, which estimates the rate of spread of a fire by combining surface fuel dryness with wind speed, is also projected to increase in most regions, except Scandinavia and the British Isles. In regions such as France and Eastern Europe, contribution to the increase in FWI is partitioned between BUI and ISI. However, since the influence of BUI on FWI saturates beyond a certain threshold (due to the principle that there is a limit to the amount of fuel that can be used in fires) and since southern European regions already exhibit very high BUI values, changes in the ISI emerges as the dominant driver of change in those regions. As ISI depends on wind speed and FFMC (proxy for surface fuel dryness), projected changes in VPD and maximum wind speed were also evaluated. The results show that projected changes in wind speed are minimal, if present at all, while VPD is projected to increase across all regions. This indicates that thermodynamic factors, specifically temperature and relative humidity as reflected by VPD, are the primary drivers of changes in extreme fire weather behavior, rather than wind. The contribution of precipitation was not evaluated separately; but is discussed in the following section.

7.2 Discussion

A positive trend in the frequency and magnitude of extreme fire weather has been observed since the 1950s across many regions, consistent with previous studies (Jolly et al., 2015; Abatzoglou et al., 2019; Jones et al., 2022; Hetzer et al., 2024). Significant trends are observed in the Iberian Peninsula, Central Europe, and Ukraine. Similarly, under continued global warming, the frequency, magnitude and spatial extent of extreme fire weather conditions are projected to increase across Europe, findings that align with global assessments (Abatzoglou et al., 2019; Jones et al., 2022; Quilcaille et al., 2023). However, this study provides refined spatial detail because of the use of higher resolution RCMs from the EURO-CORDEX framework. This extensive intensification includes a particularly strong increase in southern Europe and a northward expansion of extreme fire weather into Central Europe, especially at 3 °C GWL. Two recent studies focusing on Europe also report qualitatively similar results based on CMIP6 GCMs (El Garroussi et al., 2024; Hetzer et al., 2024). However, these studies did not explicitly assess model uncertainty or the robustness of projected change signals. The robustness analysis presented in this thesis reveals that the projected change signals are not robust in all areas, which particularly reduces confidence in projections

for some parts of Central Europe. If a more relaxed robustness criterion were applied, such as requiring only agreement on the direction of change rather than statistical significance, the area showing robust change signals would extend across nearly all of Europe at 3 °C GWL. As such, the approach used here can be considered conservative, and the actual extent of robust signals may be broader, especially considering the ongoing debate about the issues with statistical significance testing (see Amrhein et al. (2019)). It should also be noted that this study does not account for temporal and spatial autocorrelation, although peak fire weather conditions are likely to be highly spatially autocorrelated.

The projected increase in extreme fire weather conditions appears to be primarily driven by enhanced fuel dryness resulting from warming-induced increases in atmospheric drying, as represented by VPD across Europe. This finding aligns with a growing body of evidence indicating that increased fuel dryness is a key driver behind both observed and projected increases in fire weather in many regions globally (Williams et al., 2019; Resco de Dios et al., 2021; Jain et al., 2022; Ellis et al., 2022; Clarke et al., 2022). At this point, it is important to clarify the distinction between VPD and relative humidity. For a given relative humidity, VPD increases exponentially with temperature due to the Clausius-Clapeyron relationship. This means that the same relative humidity corresponds to a much higher VPD at higher temperatures than at lower temperatures (Seager et al., 2015). Therefore, the combined and absolute nature of VPD makes it a more holistic indicator of regional water balance and a better predictor of fire incidence than individual variables such as temperature alone (Williams et al., 2014). According to the results of this thesis, projected changes in maximum wind speed are generally negligible except for a weakening in the British Isles. The effects of precipitation change are more uncertain and exhibit strong regional variability. El Garroussi et al. (2024) evaluated the impact of precipitation changes on fire weather using impact response surfaces based on CMIP6 simulations and found that declines in precipitation more strongly affect fire weather in temperate and boreal regions than in Mediterranean areas. This finding aligns with the results presented here, where additional increases in BUI had little effect on FWI in Southern Europe. Given that ISI is projected to increase in these regions while wind speed remains largely stable, it can be hypothesized that surface fuel drying (related to increases in VPD) may become a key factor in shaping extreme wildfire behavior in Southern Europe.

Although extreme fire weather conditions, as represented by the FWI, are projected to intensify in both frequency and magnitude, it is important to emphasize that the FWI is not a direct measure of fire occurrence. Rather, fire weather creates conditions that enhance the susceptibility of landscapes to other key wildfire drivers, namely ignition, drought, and fuel continuity, thereby increasing the likelihood that an ignition will result in a fire and that vegetation will become more flammable due to vegetation stress (Pausas and Keeley, 2021). Together with the continuous availability of fuel, fire weather also plays a critical role in determining the potential size and spread of a fire (Pausas and Keeley, 2021). In general, FWI provides the most meaningful information in regions where fire activity is limited by fuel dryness rather than by vegetation productivity (Jones et al., 2022). The strongest relationships between FWI and burned area are observed in ecosystems with intermediate moisture availability (Jones et al., 2022), including boreal and evergreen forests (Bedia et al., 2015; Abatzoglou et al., 2018), as well as in Mediterranean Europe (Carvalho et al., 2008;

Table 7.1: FWI ranges defining the fire classes in EFFIS. Adapted from San-Miguel-Ayanz et al. (2012).

Fire Danger Class	FWI
Low	< 11.2
Moderate	11.2 - 21.3
High	21.3 - 38.0
Very High	38.0 - 50.0
Extreme	50.0 - 70.0
Very Extreme	> 70.0

Urbieta et al., 2015; Fox et al., 2018; Jones et al., 2022). Notably, nearly 65% of all extreme wildfires between 2002 and 2013 occurred under extreme fire weather conditions, as represented by the FWI (Bowman et al., 2017).

EFFIS uses threshold-based fire danger classes based on absolute FWI values across Europe (Table 7.1) (San-Miguel-Ayanz et al., 2012). According to the results presented in this thesis, if these uniform thresholds were adopted, only certain regions in southern and eastern Europe would be projected to reach extreme fire danger levels, even at 3 °C GWL, when assessed using the annual maximum FWI (FWI_{max}). However, this study employs locally defined FWI metrics, as the relationship between FWI and burned area varies significantly across different biomes and climate types. In warmer and drier climates, higher FWI values (around ∼50) typically indicate high fire danger, while in cooler and moister climates FWI values around ∼25 may already signal extreme danger (Kudláčková et al., 2024). As such, using uniform fire danger thresholds across Europe may lead to underestimation of actual fire danger in regions like Central Europe. This highlights the importance of incorporating regional climate and biome characteristics when interpreting FWI values for fire danger assessments, in order to improve early warning systems and fire mitigation strategies in a changing climate (Kudláčková et al., 2024).

As discussed above, fire activity is not solely determined by fire weather. Other particularly important factors include vegetation productivity and human influences on fire ignition and fuel availability (Jones et al., 2022). These non-climatic drivers can either amplify or offset the influence of fire weather on actual fire activity (Jones et al., 2022). For example, although fire weather season length has increased in parts of the African savannas, the burned area has decreased due to human-induced changes in the environment, such as vegetation fragmentation from agricultural expansion (Andela et al., 2017; Jones et al., 2022). It should also be noted that more than 97% of all fires in the Mediterranean region with a known cause are linked to human activity (Ganteaume et al., 2013). This thesis has focused exclusively on the role of fire weather in influencing fire activity. However, it remains unclear whether other bioclimatic and anthropogenic factors will remain unchanged in Europe in the future. Consequently, the findings presented here, that climate change is projected to increase fire potential by lengthening and intensifying fire weather conditions, are based on the assumption that these other factors remain relatively constant in the future.

The final ecosystem and socioeconomic impacts of a fire depend not only on fire weather, the availability of flammable vegetation, and ignition sources, but also on forest management practices prior to fire events and suppression efforts once a fire has ignited. For instance, mechanical thinning and prescribed burning have been shown to be effective in mitigating fire impacts by reducing fuel loads and fire intensity, thereby making wildfires more controllable when they occur (Rabin et al., 2022; Davis et al., 2024). Fire suppression efforts also play a significant role in determining the total burned area. For example, the burned area in the Mediterranean has shown a declining trend since the 1980s, primarily due to enhanced suppression strategies (Turco et al., 2016), despite increasing trends in fire weather shown in this thesis (e.g., in the Iberian Peninsula) and in previous work (e.g., Giannaros et al. (2021)). However, under increasing pressure from climate change and more extreme fire weather conditions, there may come a point where high-intensity fires overwhelm the suppression capacity (Podur and Wotton, 2010). In response to this growing challenge, international resource sharing has been recognized as both necessary and effective in Europe (Bloem et al., 2022). RescEU represents the collective response of European member states to this growing need for suppression and mitigation capabilities by pooling resources such as firefighting aircraft (Hopkins and Faulkner, 2021). It is also critical to acknowledge the so-called "fire-fighting trap" or "suppression paradox", which suggests that extinguishing all fires at any cost may lead to fires with greater severity in the following years under extreme fire weather conditions, due to fuel accumulation over time (Parisien et al., 2020; Moreira et al., 2020; Kreider et al., 2024). As such, since climate change is projected to further lengthen and intensify extreme fire weather conditions, particularly in Mediterranean-type climates, a paradigm shift is advocated (Moreira et al., 2020). This shift emphasizes the importance of complementing suppression efforts with mitigation measures. In this context, policy effectiveness should not be measured solely by the extent of burned area, but rather by the degree to which socio-ecological damage is avoided (Moreira et al., 2020).

Disasters do not result solely from natural hazards, but rather when hazards meet vulnerability (Raju et al., 2022). In the context of wildfires, the disaster risk framework encompasses the severity of the wildfire (hazard), the exposure of populations, economic assets, and ecological resources, as well as the vulnerability of those exposed elements (Cardona et al., 2012; ClimateData.ca). Fire weather represents only one component of the hazard within this framework; the ultimate impact also depends heavily on exposure and vulnerability (Figure 7.1). Attributing such disasters entirely to climate change can deflect responsibility and overlook the need to address the underlying ecological and societal vulnerabilities (Raju et al., 2022). Therefore, while this study has focused specifically on the influence of climate change on extreme fire weather as a hazard component (specifically climate), it is essential to also consider exposure and vulnerability when designing strategies to mitigate the impacts of wildfires.

7.2.1 Outlook

Based on the results of this thesis, the uncertainty in the projected change signal increases markedly at 3 °C GWL. Moreover, although most models agree on the sign of projected change, there is

Figure 7.1: The relationship between fire weather and wildfire risk. Climate (the long-term statistics of fire weather), ignitions, and vegetation are three key factors that affect fire danger and ultimately wildfire activity – in this case, the hazard of concern. In turn, this hazard can be related to wildfire risk by also considering the vulnerability and exposure of at-risk communities. Fire weather is only one of several components that must be considered to assess overall wildfire risk. Figure and caption are reprinted from ClimateData.ca.

generally no consensus on the statistical significance of these changes in Central and Northern Europe. To reduce this uncertainty, future studies could consider using model ensembles that apply weighting based on performance and independence (Brunner et al., 2020) or constrain projections using historical observations (Ribes et al., 2021). Given that some CMIP6 simulations (Eyring et al., 2016) are known to exhibit unrealistically high equilibrium Equilibrium Climate Sensitivity (ECS) that are not supported by current evidence (Hausfather et al., 2022), future assessments of extreme fire weather in Europe using these models should account for this issue. In addition to model weighting and observational constraints, this challenge can also be addressed by selecting only those models with ECS values within the likely range of 2.5-4 °C (Masson-Delmotte et al., 2021; Hausfather et al., 2022; Bayar et al., 2023). Finally, if the warming trajectory is not particularly important for the study, projected changes can be analyzed at GWLs, as done in this study, which avoids reliance on the realism of the models' warming trajectory.

Another approach to reducing uncertainty is to apply bias adjustment to model outputs rather than relying on raw simulations. This thesis employed a univariate bias adjustment method (QDM) to adjust the marginal distributions of the input variables. However, several studies have shown that multivariate bias adjustment techniques can provide improved performance when applied to compound hazard estimates (Cannon, 2018; Zscheischler et al., 2019). In this thesis, a multivariate method (MBCn) also demonstrated better performance over a region where the univariate approach lacked skill. That said, the multivariate approach used here comes with substantially higher computational cost. MBCn incorporates QDM in an intermediate step to adjust

marginal distributions, but also involves additional matrix operations and iterative convergence, making it theoretically at least N times more computationally expensive than QDM, where N is the number of iterations. Future research should further explore the potential of multivariate bias adjustment to further reduce biases in extreme fire weather projections, particularly in cases where computational resources are not a limiting factor. Nevertheless, it is important to acknowledge that bias adjustment methods reduce the uncertainty without necessarily providing a satisfactory physical justification and may lead to a false sense of confidence in the results (Ehret et al., 2012). As multivariate bias adjustment methods continue to evolve and adjust more aspects of inter-variable dependence, the question of what is preserved of the actual simulation always needs to be considered and the method selection should be considered carefully (François et al., 2020).

The next generation of simulations in the EURO-CORDEX framework, downscaled from CMIP6 GCMs, is currently underway (Katragkou et al., 2024), with some outputs expected to become available by the end of 2025. This new generation of simulations retains the same spatial resolution as their CMIP5 counterparts, but incorporates greenhouse gas forcing scenarios based on the state-of-the-art SSPs instead of RCPs, along with a consistent space- and time-varying aerosol forcing (Katragkou et al., 2024). FWI calculations may offer an opportunity to compare these two generations of models to evaluate improvements, particularly in the representation of multivariate hazard estimates. In addition, policymakers often require high-resolution simulations at the local scale to support more informed decision-making. Therefore, calculating the FWI using convection-permitting simulations, which explicitly resolve convective processes at finer scales and help reduce uncertainty, should also be considered in future assessments (Prein et al., 2015; Lucas-Picher et al., 2021), especially given the uncertainties in precipitation simulations and their influence on extreme fire weather.

Finally, understanding the physical drivers of projected changes in extreme fire weather is essential. This study found that projected increases in extreme fire weather are closely correlated with increases in VPD, but not with wind speeds are projected to remain largely stable. This suggests that thermodynamic processes, particularly those associated with atmospheric drying driven by temperature and relative humidity, may be playing a dominant role in these changes. Storyline simulations offer useful approach to isolate the thermodynamic component of climate change by forcing the wind fields to follow observed winds patterns while altering the thermodynamic background to simulate "what if" scenarios in a colder preindustrial climate or a warmer future world (Shepherd et al., 2018; Athanase et al., 2024). Such simulations provide an opportunity to quantify how the magnitude of extreme fire weather has already changed due to thermodynamic factors like VPD, and how it may evolve under future warming. This approach could complement and elaborate the findings of this thesis by offering a more precise attribution of thermodynamic influences on projected fire weather.

The outcomes of this study may serve as an initial starting point to explore these future directions and contribute to a broader understanding of extreme fire weather in a changing climate.

A Appendix

Figure A.1: FWI time series calculated in this study, compared with two existing products from Vitolo et al. (2020) and McElhinny et al. (2020) for the 2017 wildfires in Portugal.

Figure A.2: FWI time series calculated in this study, compared with two existing products from Vitolo et al. (2020) and McElhinny et al. (2020) for the 2018 wildfires in Monchique.

Figure A.3: FWI time series calculated in this study, compared with the existing product from Vitolo et al. (2020) for the 2023 wildfires in Alexandroupolis.

Figure A.4: FWI time series calculated in this study, compared with the existing product from Vitolo et al. (2020) for the 2017 fire season in Portugal.

Abbreviations

FWI Fire Weather Index

ISI Initial Spread Index

BUI Buildup Index

FFMC Fine Fuel Moisture Code

DMC Duff Moisture Code

DC Droght Code

GCM General Circulation Model

ESM Earth System Model

RCM Regional Climate Model

GWL Global Warming Level

CMIP Coupled Model Intercomparison Project

CORDEX Coordinated Regional Climate Downscaling Experiment

WMO World Meteorological Organization

WCRP World Climate Research Programme

IPCC Intergovernmental Panel on Climate Change

ECMWF European Centre for Medium-Range Weather Forecast

ESGF Earth System Grid Federation

DKRZ German Climate Computing Centre

RCP Representative Concentration Pathway

SSP Shared Socioeconomic Pathway

VPD Vapor Pressure Deficit

QDM Quantile Delta Mapping

CDF Cumulative Distribution Function

SSR Singularity Stochastic Removal

WUI Wildland-Urban Interface

EFFIS The European Forest Fire Information System

ECS Equilibrium Climate Sensitivity

Bibliography

Abatzoglou, J. T., and A. P. Williams, 2016: Impact of anthropogenic climate change on wildfire across western US forests. *Proceedings of the National Academy of Sciences*, **113 (42)**, 11 770–11 775, https://doi.org/10.1073/pnas.1607171113.

Abatzoglou, J. T., A. P. Williams, and R. Barbero, 2019: Global Emergence of Anthropogenic Climate Change in Fire Weather Indices. *Geophysical Research Letters*, **46 (1)**, 326–336, https://doi.org/10.1029/2018GL080959.

Abatzoglou, J. T., A. P. Williams, L. Boschetti, M. Zubkova, and C. A. Kolden, 2018: Global patterns of interannual climate–fire relationships. *Global Change Biology*, **24 (11)**, 5164–5175, https://doi.org/10.1111/gcb.14405.

Abram, N. J., and Coauthors, 2021: Connections of climate change and variability to large and extreme forest fires in southeast Australia. *Communications Earth & Environment*, **2 (1)**, 1–17, https://doi.org/10.1038/s43247-020-00065-8.

Alduchov, O. A., and R. E. Eskridge, 1996: Improved Magnus Form Approximation of Saturation Vapor Pressure. *Journal of Applied Meteorology and Climatology*, **35 (4)**, 601–609, https://doi.org/10.1175/1520-0450(1996)035<0601:IMFAOS>2.0.CO;2.

Aldy, J. E., M. Auffhammer, M. Cropper, A. Fraas, and R. Morgenstern, 2022: Looking Back at 50 Years of the Clean Air Act. *Journal of Economic Literature*, **60 (1)**, 179–232, https://doi.org/10.1257/jel.20201626.

Alifdini, I., J. Moemken, A. M. Ramos, and J. G. Pinto, 2025: Future Changes of European Windstorm Losses in EURO-CORDEX Simulations. *Tellus A: Dynamic Meteorology and Oceanography*, **77 (1)**, https://doi.org/10.16993/tellusa.4094.

Amrhein, V., S. Greenland, and B. McShane, 2019: Scientists rise up against statistical significance. *Nature*, **567 (7748)**, 305–307, https://doi.org/10.1038/d41586-019-00857-9.

Andela, N., and Coauthors, 2017: A human-driven decline in global burned area. *Science*, **356 (6345)**, 1356–1362, https://doi.org/10.1126/science.aal4108.

Argüeso, D., J. P. Evans, and L. Fita, 2013: Precipitation bias correction of very high resolution regional climate models. *Hydrology and Earth System Sciences*, **17 (11)**, 4379–4388, https://doi.org/10.5194/hess-17-4379-2013.

Athanase, M., A. Sánchez-Benítez, E. Monfort, T. Jung, and H. F. Goessling, 2024: How climate change intensified storm Boris' extreme rainfall, revealed by near-real-time storylines. *Communications Earth & Environment*, **5 (1)**, 676, https://doi.org/10.1038/s43247-024-01847-0.

Baars, H., and Coauthors, 2021: Californian Wildfire Smoke Over Europe: A First Example of the Aerosol Observing Capabilities of Aeolus Compared to Ground-Based Lidar. *Geophysical Research Letters*, **48 (8)**, e2020GL092 194, https://doi.org/10.1029/2020GL092194.

Balch, J. K., B. A. Bradley, J. T. Abatzoglou, R. C. Nagy, E. J. Fusco, and A. L. Mahood, 2017: Human-started wildfires expand the fire niche across the United States. *Proceedings of the National Academy of Sciences*, **114 (11)**, 2946–2951, https://doi.org/10.1073/pnas.1617394114.

Barbero, R., J. T. Abatzoglou, N. K. Larkin, C. A. Kolden, and B. Stocks, 2015: Climate change presents increased potential for very large fires in the contiguous United States. *International Journal of Wildland Fire*, **24 (7)**, 892–899, https://doi.org/10.1071/WF15083, publisher: CSIRO PUBLISHING.

Barbero, R., J. T. Abatzoglou, F. Pimont, J. Ruffault, and T. Curt, 2020: Attributing Increases in Fire Weather to Anthropogenic Climate Change Over France. *Frontiers in Earth Science*, **8**, https://doi.org/10.3389/feart.2020.00104.

Bayar, A. S., M. T. Yilmaz, I. Yucel, and P. Dirmeyer, 2023: CMIP6 Earth System Models Project Greater Acceleration of Climate Zone Change Due To Stronger Warming Rates. *Earth's Future*, **11 (4)**, e2022EF002 972, https://doi.org/10.1029/2022EF002972.

Bedia, J., S. Herrera, J. M. Gutiérrez, A. Benali, S. Brands, B. Mota, and J. M. Moreno, 2015: Global patterns in the sensitivity of burned area to fire-weather: Implications for climate change. *Agricultural and Forest Meteorology*, **214-215**, 369–379, https://doi.org/10.1016/j.agrformet.2015.09.002.

Bedia, J., S. Herrera, J. M. Gutiérrez, G. Zavala, I. R. Urbieta, and J. M. Moreno, 2012: Sensitivity of fire weather index to different reanalysis products in the Iberian Peninsula. *Natural Hazards and Earth System Sciences*, **12 (3)**, 699–708, https://doi.org/10.5194/nhess-12-699-2012.

Belcher, C. M., J. M. Yearsley, R. M. Hadden, J. C. McElwain, and G. Rein, 2010: Baseline intrinsic flammability of Earth's ecosystems estimated from paleoatmospheric oxygen over the past 350 million years. *Proceedings of the National Academy of Sciences*, **107 (52)**, 22 448–22 453, https://doi.org/10.1073/pnas.1011974107.

Bellprat, O., S. Kotlarski, D. Lüthi, and C. Schär, 2012: Objective calibration of regional climate models. *Journal of Geophysical Research: Atmospheres*, **117 (D23)**, https://doi.org/10.1029/2012JD018262.

Bento, V. A., and Coauthors, 2023: The future of extreme meteorological fire danger under climate change scenarios for Iberia. *Weather and Climate Extremes*, **42**, 100 623, https://doi.org/10.1016/j.wace.2023.100623.

Bloem, S., A. C. Cullen, L. O. Mearns, and J. T. Abatzoglou, 2022: The Role of International Resource Sharing Arrangements in Managing Fire in the Face of Climate Change. *Fire*, **5 (4)**, 88, https://doi.org/10.3390/fire5040088.

Bond, W. J., F. I. Woodward, and G. F. Midgley, 2005: The global distribution of ecosystems in a world without fire. *New Phytologist*, **165 (2)**, 525–538, https://doi.org/10.1111/j.1469-8137.2004.01252.x.

Bourgault, P., and Coauthors, 2023: xclim: xarray-based climate data analytics. *Journal of Open Source Software*, **8 (85)**, 5415, https://doi.org/10.21105/joss.05415.

Bowman, D., G. Williamson, M. Yebra, J. Lizundia-Loiola, M. L. Pettinari, S. Shah, R. Bradstock, and E. Chuvieco, 2020a: Wildfires: Australia needs national monitoring agency. *Nature*, **584 (7820)**, 188–191, https://doi.org/10.1038/d41586-020-02306-4.

Bowman, D. M. J. S., C. A. Kolden, J. T. Abatzoglou, F. H. Johnston, G. R. van der Werf, and M. Flannigan, 2020b: Vegetation fires in the Anthropocene. *Nature Reviews Earth & Environment*, **1 (10)**, 500–515, https://doi.org/10.1038/s43017-020-0085-3.

Bowman, D. M. J. S., G. J. Williamson, J. T. Abatzoglou, C. A. Kolden, M. A. Cochrane, and A. M. S. Smith, 2017: Human exposure and sensitivity to globally extreme wildfire events. *Nature Ecology & Evolution*, **1 (3)**, 1–6, https://doi.org/10.1038/s41559-016-0058.

Bowman, D. M. J. S., and Coauthors, 2009: Fire in the Earth System. *Science*, https://doi.org/10.1126/science.1163886.

Brunner, L., A. G. Pendergrass, F. Lehner, A. L. Merrifield, R. Lorenz, and R. Knutti, 2020: Reduced global warming from CMIP6 projections when weighting models by performance and independence. *Earth System Dynamics*, **11 (4)**, 995–1012, https://doi.org/10.5194/esd-11-995-2020.

Burke, M., M. L. Childs, B. de la Cuesta, M. Qiu, J. Li, C. F. Gould, S. Heft-Neal, and M. Wara, 2023: The contribution of wildfire to PM2.5 trends in the USA. *Nature*, **622 (7984)**, 761–766, https://doi.org/10.1038/s41586-023-06522-6.

Burton, C., and Coauthors, 2024: Global burned area increasingly explained by climate change. *Nature Climate Change*, **14 (11)**, 1186–1192, https://doi.org/10.1038/s41558-024-02140-w.

Byrne, B., and Coauthors, 2024: Carbon emissions from the 2023 Canadian wildfires. *Nature*, **633 (8031)**, 835–839, https://doi.org/10.1038/s41586-024-07878-z.

Cannon, A. J., 2018: Multivariate quantile mapping bias correction: an N-dimensional probability density function transform for climate model simulations of multiple variables. *Climate Dynamics*, **50 (1)**, 31–49, https://doi.org/10.1007/s00382-017-3580-6.

Cannon, A. J., S. R. Sobie, and T. Q. Murdock, 2015: Bias Correction of GCM Precipitation by Quantile Mapping: How Well Do Methods Preserve Changes in Quantiles and Extremes? *Journal of Climate*, **28 (17)**, 6938–6959, https://doi.org/10.1175/JCLI-D-14-00754.1.

Capua, G. D., and S. Rahmstorf, 2023: Extreme weather in a changing climate. *Environmental Research Letters*, **18 (10)**, 102 001, https://doi.org/10.1088/1748-9326/acfb23.

Cardona, O.-D., and Coauthors, 2012: Determinants of Risk: Exposure and Vulnerability. *Managing the Risks of Extreme Events and Disasters to Advance Climate Change Adaptation*, C. B. Field, V. Barros, T. F. Stocker, and Q. Dahe, Eds., 1st ed., Cambridge University Press, 65–108, https://doi.org/10.1017/CBO9781139177245.005, URL https://www.cambridge.org/core/product/identifier/CBO9781139177245A021/type/book_part.

Carnicer, J., and Coauthors, 2022: Global warming is shifting the relationships between fire weather and realized fire-induced CO2 emissions in Europe. *Scientific Reports*, **12 (1)**, 10 365, https://doi.org/10.1038/s41598-022-14480-8.

Carvalho, A., M. D. Flannigan, K. Logan, A. I. Miranda, and C. Borrego, 2008: Fire activity in Portugal and its relationship to weather and the Canadian Fire Weather Index System. *International Journal of Wildland Fire*, **17 (3)**, 328–338, https://doi.org/10.1071/WF07014.

Casanueva, A., S. Herrera, M. Iturbide, S. Lange, M. Jury, A. Dosio, D. Maraun, and J. M. Gutiérrez, 2020: Testing bias adjustment methods for regional climate change applications under observational uncertainty and resolution mismatch. *Atmospheric Science Letters*, **21 (7)**, e978, https://doi.org/10.1002/asl.978, _eprint: https://onlinelibrary.wiley.com/doi/pdf/10.1002/asl.978.

Cattau, M. E., C. Wessman, A. Mahood, and J. K. Balch, 2020: Anthropogenic and lightning-started fires are becoming larger and more frequent over a longer season length in the U.S.A. *Global Ecology and Biogeography*, **29 (4)**, 668–681, https://doi.org/10.1111/geb.13058, _eprint: https://onlinelibrary.wiley.com/doi/pdf/10.1111/geb.13058.

Chen, J., R. Arsenault, F. P. Brissette, and S. Zhang, 2021a: Climate Change Impact Studies: Should We Bias Correct Climate Model Outputs or Post-Process Impact Model Outputs? *Water Resources Research*, **57 (5)**, e2020WR028 638, https://doi.org/10.1029/2020WR028638.

Chen, Y., D. M. Romps, J. T. Seeley, S. Veraverbeke, W. J. Riley, Z. A. Mekonnen, and J. T. Randerson, 2021b: Future increases in Arctic lightning and fire risk for permafrost carbon. *Nature Climate Change*, **11 (5)**, 404–410, https://doi.org/10.1038/s41558-021-01011-y.

Christensen, J. H., and O. B. Christensen, 2007: A summary of the PRUDENCE model projections of changes in European climate by the end of this century. *Climatic Change*, **81 (1)**, 7–30, https://doi.org/10.1007/s10584-006-9210-7.

Chuvieco, E., and Coauthors, 2018: Generation and analysis of a new global burned area product based on MODIS 250 m reflectance bands and thermal anomalies. *Earth System Science Data*, **10 (4)**, 2015–2031, https://doi.org/10.5194/essd-10-2015-2018.

Clarke, H., R. Gibson, B. Cirulis, R. A. Bradstock, and T. D. Penman, 2019: Developing and testing models of the drivers of anthropogenic and lightning-caused wildfire ignitions in south-eastern Australia. *Journal of Environmental Management*, **235**, 34–41, https://doi.org/10.1016/j.jenvman.

2019.01.055.

Clarke, H., R. H. Nolan, V. R. De Dios, R. Bradstock, A. Griebel, S. Khanal, and M. M. Boer, 2022: Forest fire threatens global carbon sinks and population centres under rising atmospheric water demand. *Nature Communications*, **13 (1)**, 7161, https://doi.org/10.1038/s41467-022-34966-3.

ClimateData.ca, ????: Understanding Fire Weather and Climate Change Basics. URL https://climatedata.ca/resource/understanding-fire-weather-and-climate-change-basics/.

Copernicus Climate Change Service (C3S), 2025: European State of the Climate 2024. Tech. rep., Copernicus Climate Change Service (C3S).

Cunningham, C. X., G. J. Williamson, and D. M. J. S. Bowman, 2024: Increasing frequency and intensity of the most extreme wildfires on Earth. *Nature Ecology & Evolution*, **8 (8)**, 1420–1425, https://doi.org/10.1038/s41559-024-02452-2.

Curt, T., and T. Frejaville, 2018: Wildfire Policy in Mediterranean France: How Far is it Efficient and Sustainable? *Risk Analysis*, **38 (3)**, 472–488, https://doi.org/10.1111/risa.12855, URL https://onlinelibrary.wiley.com/doi/abs/10.1111/risa.12855.

Damany-Pearce, L., B. Johnson, A. Wells, M. Osborne, J. Allan, C. Belcher, A. Jones, and J. Haywood, 2022: Australian wildfires cause the largest stratospheric warming since Pinatubo and extends the lifetime of the Antarctic ozone hole. *Scientific Reports*, **12 (1)**, 12 665, https://doi.org/10.1038/s41598-022-15794-3.

Davis, K. T., J. Peeler, J. Fargione, R. D. Haugo, K. L. Metlen, M. D. Robles, and T. Woolley, 2024: Tamm review: A meta-analysis of thinning, prescribed fire, and wildfire effects on subsequent wildfire severity in conifer dominated forests of the Western US. *Forest Ecology and Management*, **561**, 121 885, https://doi.org/10.1016/j.foreco.2024.121885.

de Rigo, D., G. Libertà, T. Houston Durrant, T. A. Vivancos, J. San-Miguel-Ayanz, and P. O. o. t. E. Union, 2017: Forest fire danger extremes in Europe under climate change: variability and uncertainty. Research Report, Publications Office of the European Union.

Descals, A., D. L. A. Gaveau, A. Verger, D. Sheil, D. Naito, and J. Peñuelas, 2022: Unprecedented fire activity above the Arctic Circle linked to rising temperatures. *Science*, https://doi.org/10.1126/science.abn9768.

Dosio, A., and P. Paruolo, 2011: Bias correction of the ENSEMBLES high-resolution climate change projections for use by impact models: Evaluation on the present climate. *Journal of Geophysical Research: Atmospheres*, **116 (D16)**, https://doi.org/10.1029/2011JD015934, URL https://onlinelibrary.wiley.com/doi/abs/10.1029/2011JD015934.

Dowdy, A. J., G. A. Mills, K. Finkele, and W. de Groot, 2010: Index sensitivity analysis applied to the Canadian Forest Fire Weather Index and the McArthur Forest Fire Danger Index. *Meteorological Applications*, **17 (3)**, 298–312, https://doi.org/10.1002/met.170.

Edwards, P. N., 2011: History of climate modeling. *WIREs Climate Change*, **2 (1)**, 128–139, https://doi.org/10.1002/wcc.95.

Ehret, U., E. Zehe, V. Wulfmeyer, K. Warrach-Sagi, and J. Liebert, 2012: HESS Opinions "Should we apply bias correction to global and regional climate model data?". *Hydrology and Earth System Sciences*, **16 (9)**, 3391–3404, https://doi.org/10.5194/hess-16-3391-2012.

El Garroussi, S., F. Di Giuseppe, C. Barnard, and F. Wetterhall, 2024: Europe faces up to tenfold increase in extreme fires in a warming climate. *npj Climate and Atmospheric Science*, **7 (1)**, 30, https://doi.org/10.1038/s41612-024-00575-8.

Ellis, T. M., D. M. J. S. Bowman, P. Jain, M. D. Flannigan, and G. J. Williamson, 2022: Global increase in wildfire risk due to climate-driven declines in fuel moisture. *Global Change Biology*, **28 (4)**, 1544–1559, https://doi.org/10.1111/gcb.16006.

Enright, N. J., J. B. Fontaine, D. M. Bowman, R. A. Bradstock, and R. J. Williams, 2015: Interval squeeze: altered fire regimes and demographic responses interact to threaten woody species persistence as climate changes. *Frontiers in Ecology and the Environment*, **13 (5)**, 265–272, https://doi.org/10.1890/140231.

Eyring, V., S. Bony, G. A. Meehl, C. A. Senior, B. Stevens, R. J. Stouffer, and K. E. Taylor, 2016: Overview of the Coupled Model Intercomparison Project Phase 6 (CMIP6) experimental design and organization. *Geoscientific Model Development*, **9 (5)**, 1937–1958, https://doi.org/10.5194/gmd-9-1937-2016.

Fargeon, H., F. Pimont, N. Martin-StPaul, M. De Caceres, J. Ruffault, R. Barbero, and J.-L. Dupuy, 2020: Projections of fire danger under climate change over France: where do the greatest uncertainties lie? *Climatic Change*, **160 (3)**, 479–493, https://doi.org/10.1007/s10584-019-02629-w, URL https://doi.org/10.1007/s10584-019-02629-w.

Feng, S., J. Zscheischler, Z. Hao, and E. Bevacqua, 2025: Growing human-induced climate change fingerprint in regional weekly fire extremes. *npj Climate and Atmospheric Science*, **8 (1)**, 1–11, https://doi.org/10.1038/s41612-025-01021-z.

Filkov, A. I., T. Ngo, S. Matthews, S. Telfer, and T. D. Penman, 2020: Impact of Australia's catastrophic 2019/20 bushfire season on communities and environment. Retrospective analysis and current trends. *Journal of Safety Science and Resilience*, **1 (1)**, 44–56, https://doi.org/10.1016/j.jnlssr.2020.06.009.

Finney, D. L., R. M. Doherty, O. Wild, D. S. Stevenson, I. A. MacKenzie, and A. M. Blyth, 2018: A projected decrease in lightning under climate change. *Nature Climate Change*, **8 (3)**, 210–213, https://doi.org/10.1038/s41558-018-0072-6.

Fischer, E. M., and R. Knutti, 2015: Anthropogenic contribution to global occurrence of heavy-precipitation and high-temperature extremes. *Nature Climate Change*, **5 (6)**, 560–564, https://doi.org/10.1038/nclimate2617.

Fosberg, M. A., 1978: Weather in wildland fire management: the fire weather index. *Conference on Sierra Nevada meteorology, June*, **19-21, 1978, S Lake Tahoe, California**, 1–4, URL https://eurekamag.com/research/001/033/001033296.php.

Fox, D. M., P. Carrega, Y. Ren, P. Caillouet, C. Bouillon, and S. Robert, 2018: How wildfire risk is related to urban planning and Fire Weather Index in SE France (1990–2013). *Science of The Total Environment*, **621**, 120–129, https://doi.org/10.1016/j.scitotenv.2017.11.174.

François, B., M. Vrac, A. J. Cannon, Y. Robin, and D. Allard, 2020: Multivariate bias corrections of climate simulations: which benefits for which losses? *Earth System Dynamics*, **11 (2)**, 537–562, https://doi.org/10.5194/esd-11-537-2020.

Friedlingstein, P., and Coauthors, 2025: Global Carbon Budget 2024. *Earth System Science Data*, **17 (3)**, 965–1039, https://doi.org/10.5194/essd-17-965-2025.

Fromm, M., R. Servranckx, B. J. Stocks, and D. A. Peterson, 2022: Understanding the critical elements of the pyrocumulonimbus storm sparked by high-intensity wildland fire. *Communications Earth & Environment*, **3 (1)**, 1–7, https://doi.org/10.1038/s43247-022-00566-8.

Galizia, L. F., R. Barbero, M. Rodrigues, J. Ruffault, F. Pimont, and T. Curt, 2023: Global Warming Reshapes European Pyroregions. *Earth's Future*, **11 (5)**, e2022EF003 182, https://doi.org/10.1029/2022EF003182.

Ganteaume, A., A. Camia, M. Jappiot, J. San-Miguel-Ayanz, M. Long-Fournel, and C. Lampin, 2013: A Review of the Main Driving Factors of Forest Fire Ignition Over Europe. *Environmental Management*, **51 (3)**, 651–662, https://doi.org/10.1007/s00267-012-9961-z.

Giannaros, T. M., V. Kotroni, and K. Lagouvardos, 2021: Climatology and trend analysis (1987–2016) of fire weather in the Euro-Mediterranean. *International Journal of Climatology*, **41 (S1)**, E491–E508, https://doi.org/10.1002/joc.6701, _eprint: https://rmets.onlinelibrary.wiley.com/doi/pdf/10.1002/joc.6701.

Gillett, N. P., F. W. Zwiers, A. J. Weaver, and P. A. Stott, 2003: Detection of human influence on sea-level pressure. *Nature*, **422 (6929)**, 292–294, https://doi.org/10.1038/nature01487.

Giorgi, F., 2019: Thirty Years of Regional Climate Modeling: Where Are We and Where Are We Going next? *Journal of Geophysical Research: Atmospheres*, **124 (11)**, 5696–5723, https://doi.org/10.1029/2018JD030094.

Giorgi, F., C. Jones, and G. R. Asrar, 2009: Addressing climate information needs at the regional level: the CORDEX framework. *WMO Bulletin*, **58 (3)**, 175–183.

Giorgi, F., and W. J. G. Jr, 2015: Regional Dynamical Downscaling and the CORDEX Initiative. *Annual Review of Environment and Resources*, **40 (Volume 40, 2015)**, 467–490, https://doi.org/10.1146/annurev-environ-102014-021217.

Gumus, B., S. Oruc, I. Yucel, and M. T. Yilmaz, 2023: Impacts of Climate Change on Extreme Climate Indices in Türkiye Driven by High-Resolution Downscaled CMIP6 Climate Models. *Sustainability*, **15 (9)**, 7202, https://doi.org/10.3390/su15097202.

Gutowski, W. J., S. G. Decker, R. A. Donavon, Z. Pan, R. W. Arritt, and E. S. Takle, 2003: Temporal–Spatial Scales of Observed and Simulated Precipitation in Central U.S. Climate. *Journal of Climate*, **16 (22)**.

Haerter, J. O., S. Hagemann, C. Moseley, and C. Piani, 2011: Climate model bias correction and the role of timescales. *Hydrology and Earth System Sciences*, **15 (3)**, 1065–1079, https://doi.org/10.5194/hess-15-1065-2011.

Hakala, K., N. Addor, and J. Seibert, 2018: Hydrological Modeling to Evaluate Climate Model Simulations and Their Bias Correction. *Journal of Hydrometeorology*, **19 (8)**, https://doi.org/10.1175/JHM-D-17-0189.1, section: Journal of Hydrometeorology.

Hausfather, Z., K. Marvel, G. A. Schmidt, J. W. Nielsen-Gammon, and M. Zelinka, 2022: Climate simulations: recognize the 'hot model' problem. *Nature*, **605 (7908)**, 26–29, URL https://www.nature.com/articles/d41586-022-01192-2.

Hawkins, L. R., J. T. Abatzoglou, S. Li, and D. E. Rupp, 2022: Anthropogenic Influence on Recent Severe Autumn Fire Weather in the West Coast of the United States. *Geophysical Research Letters*, **49 (4)**, e2021GL095 496, https://doi.org/10.1029/2021GL095496.

He, Q., A. P. Williams, M. R. Johnston, C. S. Juang, and B. Wang, 2025: Influence of Time-Averaging of Climate Data on Estimates of Atmospheric Vapor Pressure Deficit and Inferred Relationships With Wildfire Area in the Western United States. *Geophysical Research Letters*, **52 (7)**, e2024GL113 708, https://doi.org/10.1029/2024GL113708, URL https://onlinelibrary.wiley.com/doi/abs/10.1029/2024GL113708.

He, T., B. B. Lamont, and J. G. Pausas, 2019: Fire as a key driver of Earth's biodiversity. *Biological Reviews*, **94 (6)**, 1983–2010, https://doi.org/10.1111/brv.12544.

Herold, N., S. M. Downes, M. H. Gross, F. Ji, N. Nishant, I. Macadam, N. N. Ridder, and K. Beyer, 2021: Projected changes in the frequency of climate extremes over southeast Australia. *Environmental Research Communications*, **3 (1)**, 011 001, https://doi.org/10.1088/2515-7620/abe6b1.

Hetzer, J., M. Forrest, J. Ribalaygua, C. Prado-López, and T. Hickler, 2024: The fire weather in Europe: large-scale trends towards higher danger. *Environmental Research Letters*, **19 (8)**, 084 017, https://doi.org/10.1088/1748-9326/ad5b09.

Hopkins, W. J., and H. Faulkner, 2021: To The RescEU? Disaster Response As A Driver For European Integration. *University of Canterbury*, https://doi.org/10.26021/12400, URL https://hdl.handle.net/10092/103298, publisher: University of Canterbury.

Hundhausen, M., H. Feldmann, R. Kohlhepp, and J. G. Pinto, 2024: Climate change signals of extreme precipitation return levels for Germany in a transient convection-permitting simulation ensemble. *International Journal of Climatology*, **44 (5)**, 1454–1471, https://doi.org/10.1002/joc.8393.

Iles, C. E., R. Vautard, J. Strachan, S. Joussaume, B. R. Eggen, and C. D. Hewitt, 2020: The benefits of increasing resolution in global and regional climate simulations for European climate extremes. *Geoscientific Model Development*, **13 (11)**, 5583–5607, https://doi.org/10.5194/gmd-13-5583-2020.

Jacob, D., and Coauthors, 2014: EURO-CORDEX: new high-resolution climate change projections for European impact research. *Regional Environmental Change*, **14 (2)**, 563–578, https://doi.org/10.1007/s10113-013-0499-2, URL https://doi.org/10.1007/s10113-013-0499-2.

Jain, P., D. Castellanos-Acuna, S. C. P. Coogan, J. T. Abatzoglou, and M. D. Flannigan, 2022: Observed increases in extreme fire weather driven by atmospheric humidity and temperature. *Nature Climate Change*, **12 (1)**, 63–70, https://doi.org/10.1038/s41558-021-01224-1.

Jain, P., and Coauthors, 2024: Drivers and Impacts of the Record-Breaking 2023 Wildfire Season in Canada. *Nature Communications*, **15 (1)**, 6764, https://doi.org/10.1038/s41467-024-51154-7.

James, R., R. Washington, C.-F. Schleussner, J. Rogelj, and D. Conway, 2017: Characterizing half-a-degree difference: a review of methods for identifying regional climate responses to global warming targets. *WIREs Climate Change*, **8 (2)**, e457, https://doi.org/10.1002/wcc.457.

Janssen, T. A. J., M. W. Jones, D. Finney, G. R. van der Werf, D. van Wees, W. Xu, and S. Veraverbeke, 2023: Extratropical forests increasingly at risk due to lightning fires. *Nature Geoscience*, **16 (12)**, 1136–1144, https://doi.org/10.1038/s41561-023-01322-z.

Johnston, F. H., and Coauthors, 2012: Estimated Global Mortality Attributable to Smoke from Landscape Fires. *Environmental Health Perspectives*, **120 (5)**, 695–701, https://doi.org/10.1289/ehp.1104422.

Jolly, W. M., M. A. Cochrane, P. H. Freeborn, Z. A. Holden, T. J. Brown, G. J. Williamson, and D. M. J. S. Bowman, 2015: Climate-induced variations in global wildfire danger from 1979 to 2013. *Nature Communications*, **6 (1)**, 7537, https://doi.org/10.1038/ncomms8537.

Jones, M. W., and Coauthors, 2022: Global and Regional Trends and Drivers of Fire Under Climate Change. *Reviews of Geophysics*, **60 (3)**, e2020RG000726, https://doi.org/10.1029/2020RG000726.

Jones, M. W., and Coauthors, 2024: Global rise in forest fire emissions linked to climate change in the extratropics. *Science*, https://doi.org/10.1126/science.adl5889.

Jones, P. W., 1999: First- and Second-Order Conservative Remapping Schemes for Grids in Spherical Coordinates. *Monthly Weather Review*, **127 (9)**, 2204–2210.

Katragkou, E., and Coauthors, 2024: Delivering an Improved Framework for the New Generation of CMIP6-Driven EURO-CORDEX Regional Climate Simulations. *Bulletin of the American Meteorological Society*, **105 (6)**, E962–E974, https://doi.org/10.1175/BAMS-D-23-0131.1.

Keeley, J. E., and C. J. Fotheringham, 2000: Role of fire in regeneration from seed. *Seeds: the ecology of regeneration in plant communities*, Seeds: the ecology of regeneration in plant communities, CABI Publishing, 311–330.

Keeley, J. E., J. G. Pausas, P. W. Rundel, W. J. Bond, and R. A. Bradstock, 2011: Fire as an evolutionary pressure shaping plant traits. *Trends in Plant Science*, **16 (8)**, 406–411, https://doi.org/10.1016/j.tplants.2011.04.002.

Kendall, M. G., 1955: *Rank correlation methods.* Griffin.

Keuler, K., K. Radtke, S. Kotlarski, and D. Lüthi, 2016: Regional climate change over Europe in COSMO-CLM: Influence of emission scenario and driving global model. *Meteorologische Zeitschrift*, 121–136, https://doi.org/10.1127/metz/2016/0662.

Kharuk, V. I., K. J. Ranson, M. L. Dvinskaya, and S. T. Im, 2011: Wildfires in northern Siberian larch dominated communities. *Environmental Research Letters*, **6 (4)**, 045 208, https://doi.org/10.1088/1748-9326/6/4/045208.

Kirchmeier-Young, M. C., N. P. Gillett, F. W. Zwiers, A. J. Cannon, and F. S. Anslow, 2019: Attribution of the Influence of Human-Induced Climate Change on an Extreme Fire Season. *Earth's Future*, **7 (1)**, 2–10, https://doi.org/10.1029/2018EF001050.

Kreider, M. R., P. E. Higuera, S. A. Parks, W. L. Rice, N. White, and A. J. Larson, 2024: Fire suppression makes wildfires more severe and accentuates impacts of climate change and fuel accumulation. *Nature Communications*, **15 (1)**, 2412, https://doi.org/10.1038/s41467-024-46702-0.

Kudláčková, L., and Coauthors, 2024: Assessing fire danger classes and extreme thresholds of the Canadian Fire Weather Index across global environmental zones: a review. *Environmental Research Letters*, **20 (1)**, 013 001, https://doi.org/10.1088/1748-9326/ad97cf, publisher: IOP Publishing.

Lehner, F., I. Nadeem, and H. Formayer, 2023: Evaluating skills and issues of quantile-based bias adjustment for climate change scenarios. *Advances in Statistical Climatology, Meteorology and Oceanography*, **9 (1)**, 29–44, https://doi.org/10.5194/ascmo-9-29-2023.

Liu, Z., A. P. Ballantyne, and L. A. Cooper, 2019: Biophysical feedback of global forest fires on surface temperature. *Nature Communications*, **10 (1)**, 214, https://doi.org/10.1038/s41467-018-08237-z.

Liu, Z., J. M. Eden, B. Dieppois, and M. Blackett, 2022: A global view of observed changes in fire weather extremes: uncertainties and attribution to climate change. *Climatic Change*, **173 (1)**, 14, https://doi.org/10.1007/s10584-022-03409-9.

Lucas-Picher, P., D. Argüeso, E. Brisson, Y. Tramblay, P. Berg, A. Lemonsu, S. Kotlarski, and C. Caillaud, 2021: Convection-permitting modeling with regional climate models: Latest developments and next steps. *WIREs Climate Change*, **12 (6)**, e731, https://doi.org/10.1002/wcc.731.

Manabe, S., and K. Bryan, 1969: Climate Calculations with a Combined Ocean-Atmosphere Model. *Journal of the Atmospheric Sciences*, **26 (4)**, 786–789.

Mann, H. B., 1945: Nonparametric Tests Against Trend. *Econometrica*, **13 (3)**, 245–259, https://doi.org/10.2307/1907187.

Maraun, D., 2016: Bias Correcting Climate Change Simulations - a Critical Review. *Current Climate Change Reports*, **2 (4)**, 211–220, https://doi.org/10.1007/s40641-016-0050-x.

Maraun, D., and M. Widmann, 2018: Cross-validation of bias-corrected climate simulations is misleading. *Hydrology and Earth System Sciences*, **22 (9)**, 4867–4873, https://doi.org/10.5194/hess-22-4867-2018.

Maraun, D., and Coauthors, 2017: Towards process-informed bias correction of climate change simulations. *Nature Climate Change*, **7 (11)**, 764–773, https://doi.org/10.1038/nclimate3418.

Marris, E., 2023: Hawaii wildfires: did scientists expect Maui to burn? *Nature*, **620 (7975)**, 708–709, https://doi.org/10.1038/d41586-023-02571-z, URL https://www.nature.com/articles/d41586-023-02571-z, bandiera_abtest: a Cg_type: News Explainer Publisher: Nature Publishing Group Subject_term: Climate change, Agriculture, Climate sciences, Environmental sciences.

Masson-Delmotte, V., and Coauthors, Eds., 2021: *Climate Change 2021: The Physical Science Basis. Contribution of Working Group I to the Sixth Assessment Report of the Intergovernmental Panel on Climate Change*. Cambridge University Press, Cambridge, United Kingdom and New York, NY, USA, https://doi.org/10.1017/9781009157896.

McElhinny, M., J. F. Beckers, C. Hanes, M. Flannigan, and P. Jain, 2020: A high-resolution reanalysis of global fire weather from 1979 to 2018 – overwintering the Drought Code. *Earth System Science Data*, **12 (3)**, 1823–1833, https://doi.org/10.5194/essd-12-1823-2020.

Miller, J., A. Böhnisch, R. Ludwig, and M. I. Brunner, 2024: Climate change impacts on regional fire weather in heterogeneous landscapes of central Europe. *Natural Hazards and Earth System Sciences*, **24 (2)**, 411–428, https://doi.org/10.5194/nhess-24-411-2024.

Moemken, J., B. Koerner, F. Ehmele, H. Feldmann, and J. G. Pinto, 2022: Recurrence of Drought Events Over Iberia. Part II: Future Changes Using Regional Climate Projections. *Tellus A: Dynamic Meteorology and Oceanography*, **74 (1)**, https://doi.org/10.16993/tellusa.52.

Moreira, B., and J. G. Pausas, 2012: Tanned or Burned: The Role of Fire in Shaping Physical Seed Dormancy. *PLOS ONE*, **7 (12)**, e51 523, https://doi.org/10.1371/journal.pone.0051523.

Moreira, F., and Coauthors, 2020: Wildfire management in Mediterranean-type regions: paradigm change needed. *Environmental Research Letters*, **15 (1)**, 011 001, https://doi.org/10.1088/1748-9326/ab541e.

Mozny, M., M. Trnka, and R. Brázdil, 2021: Climate change driven changes of vegetation fires in the Czech Republic. *Theoretical and Applied Climatology*, **143 (1)**, 691–699, https://doi.org/10.1007/s00704-020-03443-6.

Muerth, M. J., and Coauthors, 2013: On the need for bias correction in regional climate scenarios to assess climate change impacts on river runoff. *Hydrology and Earth System Sciences*, **17 (3)**, 1189–1204, https://doi.org/10.5194/hess-17-1189-2013.

Murray, L. T., 2018: An uncertain future for lightning. *Nature Climate Change*, **8 (3)**, 191–192, https://doi.org/10.1038/s41558-018-0094-0.

Muñoz-Sabater, J., and Coauthors, 2021: ERA5-Land: a state-of-the-art global reanalysis dataset for land applications. *Earth System Science Data*, **13 (9)**, 4349–4383, https://doi.org/10.5194/essd-13-4349-2021.

Nesterov, V. G., 1949: Combustibility of the forest and methods for its determination. USSR State Industry Press.

Noble, I. R., A. M. Gill, and G. a. V. Bary, 1980: McArthur's fire-danger meters expressed as equations. *Australian Journal of Ecology*, **5 (2)**, 201–203, https://doi.org/10.1111/j.1442-9993.1980.tb01243.x.

Parisien, M.-A., Q. E. Barber, K. G. Hirsch, C. A. Stockdale, S. Erni, X. Wang, D. Arseneault, and S. A. Parks, 2020: Fire deficit increases wildfire risk for many communities in the Canadian boreal forest. *Nature Communications*, **11 (1)**, 2121, https://doi.org/10.1038/s41467-020-15961-y, URL https://www.nature.com/articles/s41467-020-15961-y.

Pausas, J. G., and S. Fernández-Muñoz, 2012: Fire regime changes in the Western Mediterranean Basin: from fuel-limited to drought-driven fire regime. *Climatic Change*, **110 (1)**, 215–226, https://doi.org/10.1007/s10584-011-0060-6.

Pausas, J. G., and J. E. Keeley, 2021: Wildfires and global change. *Frontiers in Ecology and the Environment*, **19 (7)**, 387–395, https://doi.org/10.1002/fee.2359.

Perkins-Kirkpatrick, S. E., and S. C. Lewis, 2020: Increasing trends in regional heatwaves. *Nature Communications*, **11 (1)**, 3357, https://doi.org/10.1038/s41467-020-16970-7.

Peterson, D. A., J. R. Campbell, E. J. Hyer, M. D. Fromm, G. P. Kablick, J. H. Cossuth, and M. T. DeLand, 2018: Wildfire-driven thunderstorms cause a volcano-like stratospheric injection of smoke. *npj Climate and Atmospheric Science*, **1 (1)**, 1–8, https://doi.org/10.1038/s41612-018-0039-3.

Phillips, N. A., 1956: The general circulation of the atmosphere: A numerical experiment. *Quarterly Journal of the Royal Meteorological Society*, **82 (352)**, 123–164, https://doi.org/10.1002/qj.

49708235202.

Pitié, F., A. C. Kokaram, and R. Dahyot, 2007: Automated colour grading using colour distribution transfer. *Computer Vision and Image Understanding*, **107 (1)**, 123–137, https://doi.org/10.1016/j.cviu.2006.11.011.

Podur, J., and M. Wotton, 2010: Will climate change overwhelm fire management capacity? *Ecological Modelling*, **221 (9)**, 1301–1309, https://doi.org/10.1016/j.ecolmodel.2010.01.013.

Prein, A. F., and Coauthors, 2015: A review on regional convection-permitting climate modeling: Demonstrations, prospects, and challenges. *Reviews of Geophysics*, **53 (2)**, 323–361, https://doi.org/10.1002/2014RG000475.

Qiu, M., D. Chen, M. Kelp, J. Li, G. Huang, and M. D. Yazdi, 2025: The rising threats of wildland-urban interface fires in the era of climate change: The Los Angeles 2025 fires. *The Innovation*, **6 (5)**, publisher: Elsevier.

Quilcaille, Y., F. Batibeniz, A. F. S. Ribeiro, R. S. Padrón, and S. I. Seneviratne, 2023: Fire weather index data under historical and shared socioeconomic pathway projections in the 6th phase of the Coupled Model Intercomparison Project from 1850 to 2100. *Earth System Science Data*, **15 (5)**, 2153–2177, https://doi.org/10.5194/essd-15-2153-2023.

Rabin, S. S., F. N. Gérard, and A. Arneth, 2022: The influence of thinning and prescribed burning on future forest fires in fire-prone regions of Europe. *Environmental Research Letters*, **17 (5)**, 055 010, https://doi.org/10.1088/1748-9326/ac6312.

Radeloff, V. C., and Coauthors, 2018: Rapid growth of the US wildland-urban interface raises wildfire risk. *Proceedings of the National Academy of Sciences*, **115 (13)**, 3314–3319, https://doi.org/10.1073/pnas.1718850115.

Raju, E., E. Boyd, and F. Otto, 2022: Stop blaming the climate for disasters. *Communications Earth & Environment*, **3 (1)**, 1, https://doi.org/10.1038/s43247-021-00332-2.

Ramos, A. M., and Coauthors, 2023: The compound event that triggered the destructive fires of October 2017 in Portugal. *iScience*, **26 (3)**, 106 141, https://doi.org/10.1016/j.isci.2023.106141.

Resco de Dios, V., and Coauthors, 2021: Climate change induced declines in fuel moisture may turn currently fire-free Pyrenean mountain forests into fire-prone ecosystems. *Science of The Total Environment*, **797**, 149 104, https://doi.org/10.1016/j.scitotenv.2021.149104.

Riahi, K., and Coauthors, 2017: The Shared Socioeconomic Pathways and their energy, land use, and greenhouse gas emissions implications: An overview. *Global Environmental Change*, **42**, 153–168, https://doi.org/10.1016/j.gloenvcha.2016.05.009, URL https://www.sciencedirect.com/science/article/pii/S0959378016300681.

Ribes, A., S. Qasmi, and N. P. Gillett, 2021: Making climate projections conditional on historical observations. *Science Advances*, **7 (4)**, eabc0671, https://doi.org/10.1126/sciadv.abc0671.

Robinson, A., J. Lehmann, D. Barriopedro, S. Rahmstorf, and D. Coumou, 2021: Increasing heat and rainfall extremes now far outside the historical climate. *npj Climate and Atmospheric Science*, **4 (1)**, 1–4, https://doi.org/10.1038/s41612-021-00202-w.

Romps, D. M., 2019: Evaluating the Future of Lightning in Cloud-Resolving Models. *Geophysical Research Letters*, **46 (24)**, 14 863–14 871, https://doi.org/10.1029/2019GL085748, URL https://onlinelibrary.wiley.com/doi/abs/10.1029/2019GL085748.

Romps, D. M., J. T. Seeley, D. Vollaro, and J. Molinari, 2014: Projected increase in lightning strikes in the United States due to global warming. *Science*, **346 (6211)**, 851–854, https://doi.org/10.1126/science.1259100.

Rovithakis, A., M. G. Grillakis, K. D. Seiradakis, C. Giannakopoulos, A. Karali, R. Field, M. Lazaridis, and A. Voulgarakis, 2022: Future climate change impact on wildfire danger over the Mediterranean: the case of Greece. *Environmental Research Letters*, **17 (4)**, 045 022, https://doi.org/10.1088/1748-9326/ac5f94.

Ruffault, J., and Coauthors, 2020: Increased likelihood of heat-induced large wildfires in the Mediterranean Basin. *Scientific Reports*, **10 (1)**, 13 790, https://doi.org/10.1038/s41598-020-70069-z.

San-Miguel-Ayanz, J., and Coauthors, 2012: Comprehensive Monitoring of Wildfires in Europe: The European Forest Fire Information System (EFFIS). *Approaches to Managing Disaster - Assessing Hazards, Emergencies and Disaster Impacts*, IntechOpen.

Schwertfeger, B. T., G. Lohmann, and H. Lipskoch, 2023: Introduction of the BiasAdjustCXX command-line tool for the application of fast and efficient bias corrections in climatic research. *SoftwareX*, **22**, 101 379, https://doi.org/10.1016/j.softx.2023.101379.

Scott, A. C., and I. J. Glasspool, 2006: The diversification of Paleozoic fire systems and fluctuations in atmospheric oxygen concentration. *Proceedings of the National Academy of Sciences*, **103 (29)**, 10 861–10 865, https://doi.org/10.1073/pnas.0604090103.

Seager, R., A. Hooks, A. P. Williams, B. Cook, J. Nakamura, and N. Henderson, 2015: Climatology, Variability, and Trends in the U.S. Vapor Pressure Deficit, an Important Fire-Related Meteorological Quantity. *Journal of Applied Meteorology and Climatology*, **54 (6)**, 1121–1141, https://doi.org/10.1175/JAMC-D-14-0321.1.

Sen, P. K., 1968: Estimates of the Regression Coefficient Based on Kendall's Tau. *Journal of the American Statistical Association*, **63 (324)**, 1379–1389, https://doi.org/10.1080/01621459.1968.10480934, publisher: ASA Website.

Shaw, T. A., and Coauthors, 2016: Storm track processes and the opposing influences of climate change. *Nature Geoscience*, **9 (9)**, 656–664, https://doi.org/10.1038/ngeo2783.

Shepherd, T. G., 2014: Atmospheric circulation as a source of uncertainty in climate change projections. *Nature Geoscience*, **7 (10)**, 703–708, https://doi.org/10.1038/ngeo2253.

Shepherd, T. G., and Coauthors, 2018: Storylines: an alternative approach to representing uncertainty in physical aspects of climate change. *Climatic Change*, **151 (3)**, 555–571, https://doi.org/10.1007/s10584-018-2317-9.

Silva, J. M. N., M. V. Moreno, Y. Le Page, D. Oom, I. Bistinas, and J. M. C. Pereira, 2019: Spatiotemporal trends of area burnt in the Iberian Peninsula, 1975–2013. *Regional Environmental Change*, **19 (2)**, 515–527, https://doi.org/10.1007/s10113-018-1415-6.

Solomon, S., Intergovernmental Panel on Climate Change, and Intergovernmental Panel on Climate Change, Eds., 2007: *Climate change 2007: the physical science basis: contribution of Working Group I to the Fourth Assessment Report of the Intergovernmental Panel on Climate Change*. Cambridge University Press, Cambridge ; New York.

Stroeve, J., M. M. Holland, W. Meier, T. Scambos, and M. Serreze, 2007: Arctic sea ice decline: Faster than forecast. *Geophysical Research Letters*, **34 (9)**, https://doi.org/10.1029/2007GL029703.

Taylor, K. E., R. J. Stouffer, and G. A. Meehl, 2012: An Overview of CMIP5 and the Experiment Design. *Bulletin of the American Meteorological Society*, **93 (4)**, https://doi.org/10.1175/BAMS-D-11-00094.1.

Teichmann, C., K. Bülow, J. Otto, S. Pfeifer, D. Rechid, K. Sieck, and D. Jacob, 2018: Avoiding Extremes: Benefits of Staying below +1.5 °C Compared to +2.0 °C and +3.0 °C Global Warming. *Atmosphere*, **9 (4)**, 115, https://doi.org/10.3390/atmos9040115.

Teutschbein, C., and J. Seibert, 2012: Bias correction of regional climate model simulations for hydrological climate-change impact studies: Review and evaluation of different methods. *Journal of Hydrology*, **456-457**, 12–29, https://doi.org/10.1016/j.jhydrol.2012.05.052.

Theil, H., 1950: A Rank-Invariant Method of Linear and Polynomial Regression Analysis. *Henri Theil's Contributions to Economics and Econometrics: Econometric Theory and Methodology*, B. Raj, and J. Koerts, Eds., Springer Netherlands, Dordrecht, 345–381.

Tian, C., and Coauthors, 2022: Fire–climate interactions through the aerosol radiative effect in a global chemistry–climate–vegetation model. *Atmospheric Chemistry and Physics*, **22 (18)**, 12 353–12 366, https://doi.org/10.5194/acp-22-12353-2022.

Tong, Y., X. Gao, Z. Han, Y. Xu, Y. Xu, and F. Giorgi, 2021: Bias correction of temperature and precipitation over China for RCM simulations using the QM and QDM methods. *Climate Dynamics*, **57 (5)**, 1425–1443, https://doi.org/10.1007/s00382-020-05447-4.

Torma, C., F. Giorgi, and E. Coppola, 2015: Added value of regional climate modeling over areas characterized by complex terrain—Precipitation over the Alps. *Journal of Geophysical Research: Atmospheres*, **120 (9)**, 3957–3972, https://doi.org/10.1002/2014JD022781, _eprint: https://agupubs.onlinelibrary.wiley.com/doi/pdf/10.1002/2014JD022781.

Turco, M., and Coauthors, 2016: Decreasing Fires in Mediterranean Europe. *PLOS ONE*, **11 (3)**, e0150 663, https://doi.org/10.1371/journal.pone.0150663.

Urbieta, I. R., M. Franquesa, O. Viedma, and J. M. Moreno, 2019: Fire activity and burned forest lands decreased during the last three decades in Spain. *Annals of Forest Science*, **76 (3)**, 1–13, https://doi.org/10.1007/s13595-019-0874-3.

Urbieta, I. R., G. Zavala, J. Bedia, J. M. Gutiérrez, J. S. Miguel-Ayanz, A. Camia, J. E. Keeley, and J. M. Moreno, 2015: Fire activity as a function of fire–weather seasonal severity and antecedent climate across spatial scales in southern Europe and Pacific western USA. *Environmental Research Letters*, **10 (11)**, 114 013, https://doi.org/10.1088/1748-9326/10/11/114013.

Van de Velde, J., M. Demuzere, B. De Baets, and N. E. C. Verhoest, 2021: Exploring the Effect of Occurrence-Bias-Adjustment Assumptions on Hydrological Impact Modeling. *Water*, **13 (11)**, 1573, https://doi.org/10.3390/w13111573.

van der Werf, G. R., and Coauthors, 2017: Global fire emissions estimates during 1997–2016. *Earth System Science Data*, **9 (2)**, 697–720, https://doi.org/10.5194/essd-9-697-2017.

van Oldenborgh, G. J., and Coauthors, 2021: Attribution of the Australian bushfire risk to anthropogenic climate change. *Natural Hazards and Earth System Sciences*, **21 (3)**, 941–960, https://doi.org/10.5194/nhess-21-941-2021.

van Vuuren, D. P., and Coauthors, 2011: The representative concentration pathways: an overview. *Climatic Change*, **109 (1)**, 5, https://doi.org/10.1007/s10584-011-0148-z.

Van Wagner, C., 1987: Development and structure of the Canadian Forest Fire Weather Index System. Tech. Rep. 35, The Canadian Forestry Service, Ottawa.

Varela, V., D. Vlachogiannis, A. Sfetsos, S. Karozis, N. Politi, and F. Giroud, 2019: Projection of Forest Fire Danger due to Climate Change in the French Mediterranean Region. *Sustainability*, **11 (16)**, 4284, https://doi.org/10.3390/su11164284, URL https://www.mdpi.com/2071-1050/11/16/4284, number: 16 Publisher: Multidisciplinary Digital Publishing Institute.

Vautard, R., and Coauthors, 2014: The European climate under a 2 °C global warming. *Environmental Research Letters*, **9 (3)**, 034 006, https://doi.org/10.1088/1748-9326/9/3/034006.

Vautard, R., and Coauthors, 2021: Evaluation of the Large EURO-CORDEX Regional Climate Model Ensemble. *Journal of Geophysical Research: Atmospheres*, **126 (17)**, e2019JD032 344, https://doi.org/10.1029/2019JD032344.

Veraverbeke, S., B. M. Rogers, M. L. Goulden, R. R. Jandt, C. E. Miller, E. B. Wiggins, and J. T. Randerson, 2017: Lightning as a major driver of recent large fire years in North American boreal forests. *Nature Climate Change*, **7 (7)**, 529–534, https://doi.org/10.1038/nclimate3329.

Viegas, D. X., G. Bovio, A. Ferreira, A. Nosenzo, and B. Sol, 1999: Comparative study of various methods of fire danger evaluation in southern Europe. *International Journal of Wildland Fire*,

9 (4), 235–246, https://doi.org/10.1071/wf00015.

Vitolo, C., F. Di Giuseppe, C. Barnard, R. Coughlan, J. San-Miguel-Ayanz, G. Libertá, and B. Krzeminski, 2020: ERA5-based global meteorological wildfire danger maps. *Scientific Data*, **7 (1)**, 216, https://doi.org/10.1038/s41597-020-0554-z.

Vrac, M., T. Noël, and R. Vautard, 2016: Bias correction of precipitation through Singularity Stochastic Removal: Because occurrences matter. *Journal of Geophysical Research: Atmospheres*, **121 (10)**, 5237–5258, https://doi.org/10.1002/2015JD024511.

Walker, X. J., and Coauthors, 2019: Increasing wildfires threaten historic carbon sink of boreal forest soils. *Nature*, **572 (7770)**, 520–523, https://doi.org/10.1038/s41586-019-1474-y.

Wang, X., D. K. Thompson, G. A. Marshall, C. Tymstra, R. Carr, and M. D. Flannigan, 2015: Increasing frequency of extreme fire weather in Canada with climate change. *Climatic Change*, **130 (4)**, 573–586, https://doi.org/10.1007/s10584-015-1375-5.

Wang, Z., and Coauthors, 2024: Severe Global Environmental Issues Caused by Canada's Record-Breaking Wildfires in 2023. *Advances in Atmospheric Sciences*, **41 (4)**, 565–571, https://doi.org/10.1007/s00376-023-3241-0.

Wehrli, K., B. P. Guillod, M. Hauser, M. Leclair, and S. I. Seneviratne, 2018: Assessing the Dynamic Versus Thermodynamic Origin of Climate Model Biases. *Geophysical Research Letters*, **45 (16)**, 8471–8479, https://doi.org/10.1029/2018GL079220, _eprint: https://onlinelibrary.wiley.com/doi/pdf/10.1029/2018GL079220.

Williams, A. P., J. T. Abatzoglou, A. Gershunov, J. Guzman-Morales, D. A. Bishop, J. K. Balch, and D. P. Lettenmaier, 2019: Observed Impacts of Anthropogenic Climate Change on Wildfire in California. *Earth's Future*, **7 (8)**, 892–910, https://doi.org/10.1029/2019EF001210.

Williams, A. P., and Coauthors, 2014: Correlations between components of the water balance and burned area reveal new insights for predicting forest fire area in the southwest United States. *International Journal of Wildland Fire*, **24 (1)**, 14–26, https://doi.org/10.1071/WF14023.

Wotton, B. M., 2009: Interpreting and using outputs from the Canadian Forest Fire Danger Rating System in research applications. *Environmental and Ecological Statistics*, **16 (2)**, 107–131, https://doi.org/10.1007/s10651-007-0084-2.

Wotton, B. M., and M. D. Flannigan, 1993: Length of the fire season in a changing climate. *The Forestry Chronicle*, **69 (2)**, 187–192, https://doi.org/10.5558/tfc69187-2.

Xavier, A. C. F., L. L. Martins, A. P. Rudke, M. V. B. de Morais, J. A. Martins, and G. C. Blain, 2022: Evaluation of Quantile Delta Mapping as a bias-correction method in maximum rainfall dataset from downscaled models in São Paulo state (Brazil). *International Journal of Climatology*, **42 (1)**, 175–190, https://doi.org/10.1002/joc.7238.

Zhang, X., H. Wan, F. W. Zwiers, G. C. Hegerl, and S.-K. Min, 2013: Attributing intensification of precipitation extremes to human influence. *Geophysical Research Letters*, **40 (19)**, 5252–5257, https://doi.org/10.1002/grl.51010.

Zhang, X., F. W. Zwiers, G. C. Hegerl, F. H. Lambert, N. P. Gillett, S. Solomon, P. A. Stott, and T. Nozawa, 2007: Detection of human influence on twentieth-century precipitation trends. *Nature*, **448 (7152)**, 461–465, https://doi.org/10.1038/nature06025.

Zheng, B., P. Ciais, F. Chevallier, E. Chuvieco, Y. Chen, and H. Yang, 2021: Increasing forest fire emissions despite the decline in global burned area. *Science Advances*, https://doi.org/10.1126/sciadv.abh2646.

Zscheischler, J., E. M. Fischer, and S. Lange, 2019: The effect of univariate bias adjustment on multivariate hazard estimates. *Earth System Dynamics*, **10 (1)**, 31–43, https://doi.org/10.5194/esd-10-31-2019.

Zscheischler, J., and Coauthors, 2020: A typology of compound weather and climate events. *Nature Reviews Earth & Environment*, **1 (7)**, 333–347, https://doi.org/10.1038/s43017-020-0060-z.

Zubkova, M., M. L. Humber, and L. Giglio, 2023: Is global burned area declining due to cropland expansion? How much do we know based on remotely sensed data? *International Journal of Remote Sensing*, **44 (4)**.

Acknowledgments

I would like to begin by sincerely thanking Prof. Dr. Joaquim Pinto for his invaluable guidance, supervision, support, and advice not only throughout my thesis, but also regarding my future career and life. I have learned so much from you, both academically and personally.

From the bottom of my heart, I would like to thank Dr. Alexandre Ramos for his supervision, guidance, and continuous feedback from beginning to end. You always encouraged and supported me, even when things felt difficult to resolve within a limited time. I am grateful to you not only for supervising me, but also for being a friend with whom I could talk about many things.

I would like to thank Prof. Dr. Andreas Fink for his valuable input following my midterm presentation. I also wish to extend special thanks to Dr. Célia Gouveia for our fruitful discussions during the early stages of my thesis.

My sincere thanks go to Dr. Hendrik Feldmann and Dr. Florian Ehmele for the long and insightful conversations about bias adjustment and EURO-CORDEX simulations.

I would like to thank Annabell for her constant emotional support, encouragement, and many helpful discussions, as well as for providing feedback on the German abstract. I also want to thank my fellow students Iason, Gayatri and Ariane for their presence and friendship since we first started our degree programs. My thanks also go to the members of our research group "Regional Climate and Weather Hazards" for their support, especially to Soner, whose support crossed borders.

I want to extend my somewhat belated thanks to Prof. Dr. Tugrul Yilmaz for introducing me to the world of climate data analysis. I learned so much under your guidance before I left my engineering background behind.

I am deeply grateful to my family for always supporting and believing in me through this rather late journey and major career shift. I know it has not been easy for you.

Above all, I would like to thank Berfin for being in my life. You believed in me even when I could not believe in myself. You saw through me even when I felt lost and did not know what to do. Thank you for helping me discover my passion for science and for encouraging me to follow this path. This work would not have been possible without you from the very beginning. Although we were far apart for most of this thesis, I always felt your presence. I am incredibly lucky to have grown up with you.

Erklärung

Ich versichere wahrheitsgemäß, die Arbeit selbstständig verfasst, alle benutzten Hilfsmittel vollständig und genau angegeben und alles kenntlich gemacht zu haben, was aus Arbeiten anderer unverändert oder mit Abänderungen entnommen wurde sowie die Satzung des KIT zur Sicherung guter wissenschaftlicher Praxis in der jeweils gültigen Fassung beachtet zu haben.

Karlsruhe, den 15.07.2025

(Ali Serkan Bayar)